PROBING IRON ACCUMULATION IN *SACCHROMYCES CEREVISIAE* USING INTEGRATIVE BIOPHYSICAL AND BIOCHEMICAL TECHNIQUES

A Dissertation

by

REN MIAO

Submitted to the Office of Graduate Studies of
Texas A&M University
in partial fulfillment of the requirements for the degree of

DOCTOR OF PHILOSOPHY

December 2010

Major Subject: Chemistry

PROBING IRON ACCUMULATION IN *SACCHROMYCES CEREVISIAE* USING INTEGRATIVE BIOPHYSICAL AND BIOCHEMICAL TECHNIQUES

A Dissertation

by

REN MIAO

Submitted to the Office of Graduate Studies of
Texas A&M University
in partial fulfillment of the requirements for the degree of

DOCTOR OF PHILOSOPHY

Approved by:

Chair of Committee,	Paul A. Lindahl
Committee Members,	David P. Barondeau
	Tadhg P. Begley
	Frank M. Raushel
Head of Department,	David H. Russell

December 2010

Major Subject: Chemistry

ABSTRACT

Probing Iron Accumulation in *Sacchromyces cerevisiae* Using Integrative Biophysical and Biochemical Techniques. (December 2010)

Ren Miao, B.S, Nanjing University, China;

M.S., Nanjing University, China

Chair of Advisory Committee: Dr. Paul A. Lindahl

Iron is an essential element for life. It is involved in a number of biological processes, including iron sulfur (Fe/S) cluster assembly and heme biosynthesis. However it is also potentially toxic due to its ability to induce formation of reactive oxygen species (ROS) via Fenton chemistry. Therefore its uptake, trafficking and utilization must be regulated to avoid its toxicological effect. It has been recently discovered that Fe/S cluster biosynthesis machinery plays a key role in the cellular iron regulation and its disruption leads to impaired iron regulation and iron accumulation within mitochondria.

The iron accumulation resulted from impaired Fe/S cluster assembly in the eukaryotic model organism *Saccharomyces cerevisiae* (baker's yeast) was studied. Various biophysical (e.g. Mössbauer, EPR, UV-vis spectroscopy) and biochemical (e.g. Western blots, PCR, enzyme activity assay, etc.) techniques were used to characterize the iron content in yeast mitochondria isolated from several mutants strains. In these mutants one of the proteins involved in Fe/S cluster biosynthesis (Yah1p and Atm1p) is mutated

and iron regulation and metabolism are disrupted. By integrating the results obtained from these different methods, it was determined that excess iron accumulates in the mutant mitochondria as inorganic phosphate Fe(III) nano-particles exhibiting superparamagnetic behaviors. Oxygen is required for iron accumulation and nanoparticle formation. The Fe(III) nano-particles can be chemically reduced to Fe(II) then largely exported from the mitochondria.

These biophysical and biochemical methods were also used to examine the iron distribution in whole yeast cells of the Aft1-1up strain in which iron regulon genes are constitutively activated and compared to that of Yah1p-depleted and wild type yeast. Constitutive activation of iron regulon genes does not alter the cellular iron distribution significantly. However disruption of Fe/S cluster assembly by Yah1p depletion causes dramatic cellular iron redistribution: the vacuolar iron is largely evacuated and most of the cellular iron probably precipitates in mitochondria as Fe(III) nanoparticles. The results provide novel insights into iron trafficking and possible signal communications between organelles within cells.

DEDICATION

I dedicate this work to my family and friends. My parents, my wife, Jun, and my son, William (Ruize), have always provided me with the encouragement, love and support one needs to become successful in daily life and professional pursuit.

ACKNOWLEDGEMENTS

I owe my deepest gratitude to those who have helped me during my research and the preparation for this dissertation. I am heartily thankful to my advisor, Dr. Paul A. Lindahl, whose continuous and generous encouragement, guidance and support from the beginning to the final level enabled me to successfully complete the projects and this dissertation. I also would like to thank my committee members: Dr. Frank M. Raushel, Dr. David P. Barondeau and Dr. Tadhg P. Begley for their time and professional advices.

I am grateful to all Dr. Lindahl's lab members, past and present: Brandon, Jessica, Greg, Sean, Jinkyu, Nema, Allison, Marco, Wolfgang, Ivan and Dr. Tan for their kind help, encouragement and discussion.

I also wish to thank our collaborators: Dr. Roland Lill for his generous gifts of yeast strains and helpful discussion; Dr. Eckard Münck, Dr. Yisong Guo and Dr. Marlène Martinho for their help with collecting and analyzing Mössbauer spectra; Dr. Hendrich for help with analyzing EPR spectra; Hansoo Kim and E. Ann Ellis for preparing and running electron microscopy samples; Dr. Robert A. Scott and Dr. Uma Mahendra Kumar Koppolu for collecting and analyzing XAS spectra. I am also indebted to Dr. Jerry Kaplan for sending us yeast strains and Dr. Laurie A. Davidson for help with designing and running RT-PCR.

I would like to end with special thanks to my parents, my wife, Jun and my son, William (Ruize) for their love, understanding and abiding patience during the past years. Without their support I would not have succeeded.

TABLE OF CONTENTS

Page

CHAPTER Page

CHAPTER Page

CHAPTER Page

LIST OF FIGURES

LIST OF FIGURES (CONTINUED)

LIST OF FIGURES (CONTINUED)

LIST OF TABLES

NOMENCLATURE

Ar,	Argon
Buffer 1 × SH,	0.6 M sorbitol, 20 mM HEPES-KOH, pH 7.4
BPS,	Bathophenanthroline disulfonate
BVS,	Bond valence sum
CD,	Central doublet
CIA,	Cytosolic iron sulfur assembly
DNPH,	2,4-Dinitrophenylhydrazine
E/D,	Electron paramagnetic resonance rhombicity parameter
EDX,	Energy dispersive x-ray
EGTA,	Glycol-bis(2-aminoethylether)-N,N,N',N'-tetraacetic acid
EM,	Electron microscopy
EPR,	Electron paramagnetic resonance
E_Q,	Quadrupole splitting
EXAFS,	Extended X-ray absorption fine structure

Gal-ATM1/Gal/O_2,	Gal-ATM1 cells grown on minimal media with galactose as a carbon source and under O_2
Gal-ATM1/Glu/O_2,	Same but with glucose as a carbon source
Gal-ATM1/Glu/Ar,	Same as Gal-ATM1/Glu/O_2 but under an argon atmosphere
HAADF,	High angle annular dark field
HS,	High-spin
ICP-MS,	Inductively coupled plasma emission mass spectrometry
IM,	Inner mitochondrial membrane
ISC,	Fe/S cluster assembly machinery
LS,	Low-spin
NHHS,	Nonheme high-spin
OD,	Optical density
PVDF,	Polyvinylidene fluoride
ROS,	Reactive oxygen species
STEM,	Scanning transmission electron microscope
TEM,	Transmission electron microscope
T_B,	Blocking temperature

TBS buffer,	20 mM Tris, 0.9% NaCl, pH 7.5
WT,	Wild-type
W303/Gal/O_2,	W303 cells grown on minimal media with galactose as a carbon source and under O_2
W303/Glu/O_2,	Same but with glucose as a carbon source
W303/Glu/Ar,	Same as W303/Glu/O_2 but under an argon atmosphere
XANES,	X-ray absorption near edge structure
XAS,	X-ray absorption spectroscopy
YPD,	Yeast peptone dextrose yeast growth media
YPGal,	Same as YPD but with galactose replacing dextrose
Yah1p-depleted/O_2,	Gal-*YAH1* cells grown on YPD under O_2
Yah1p-replete/O_2,	Gal-*YAH1* cells grown on YPGal under O_2
Yah1p-depleted/Ar,	Gal-*YAH1* cells grown under YPD under argon
δ,	Isomer shift

CHAPTER I

INTRODUCTION

Iron is an essential element for life. In cells it is used for synthesis of various cofactors such as iron-sulfur (Fe/S) clusters and heme centers (*1*). Fe-S cluster containing proteins are involved in respiration, electron transfer, DNA replication and transcription while hemes are found in myoglobin, hemoglobin and cytochromes (*2*).

Iron can also be toxic to life. Free ferrous iron can induce the Fenton reaction and produce reactive oxygen species (ROS) that can readily damage proteins or DNA (*3*). Therefore the uptake, trafficking and utilization of iron must be tightly regulated to maintain homeostasis and minimize toxicity.

Iron homeostasis is highly important for human health. When iron regulation goes awry in humans, iron-disorder diseases can develop. Many such diseases involve the accumulation of iron. For example in the degenerative disease Friedreich's ataxia (FRDA) where the human protein Frataxin is mutated, excess iron accumulates in mitochondria of the affected tissue (*2*) (*4*). Iron accumulation has been suggested to induce elevated ROS levels and worsen the symptoms.

Iron uptake and homeostasis regulation has been studied in many systems but the

---

This dissertation follows the style and format of *Biochemistry*.

yeast *Sacchromyces serevisiae* is perhaps the most well-understood eukaryotic model organism. The major components involved in cellular iron uptake in yeast have been identified. As shown in Figure 1-1, there are three major iron uptake pathways, mediated by: 1) ferroxidase-permease complexes; 2) ferrous iron transporters; and 3) siderophores (*5*). Extracellular iron generally exists as ferric complexes that are not readily utilizable by cells. Membrane proteins Fre1-3p reduce these ferric complexes (including siderophores) to produce labile Fe^{2+} species. These species serve as substrates for the ferroxidase-permease complex mediated and ferrous iron transporter mediated trafficking pathways.

The ferroxidase-permease mediated pathway is used for high-affinity Fe transport and is generally the dominant mechanism by which yeast uptakes iron from the environment under regular aerobic growth conditions. This system consists of two proteins located on the plasma membrane: a multicopper oxidase (Fet3p) that catalyzes the oxidation of Fe^{2+} to Fe^{3+} and an iron permease (Ftr1p) that transports the ferroxidase-generated Fe^{3+} across the plasma membrane. The second uptake pathway is through the ferrous iron transporter Fet4p. Fet4p is a low affinity transporter of ferrous iron across the plasma membrane. It serves as a minor uptake pathway under regular aerobic growth condition. Under *anaerobic* growth condition, the Fet3p-Ftr1p system is transcriptionally

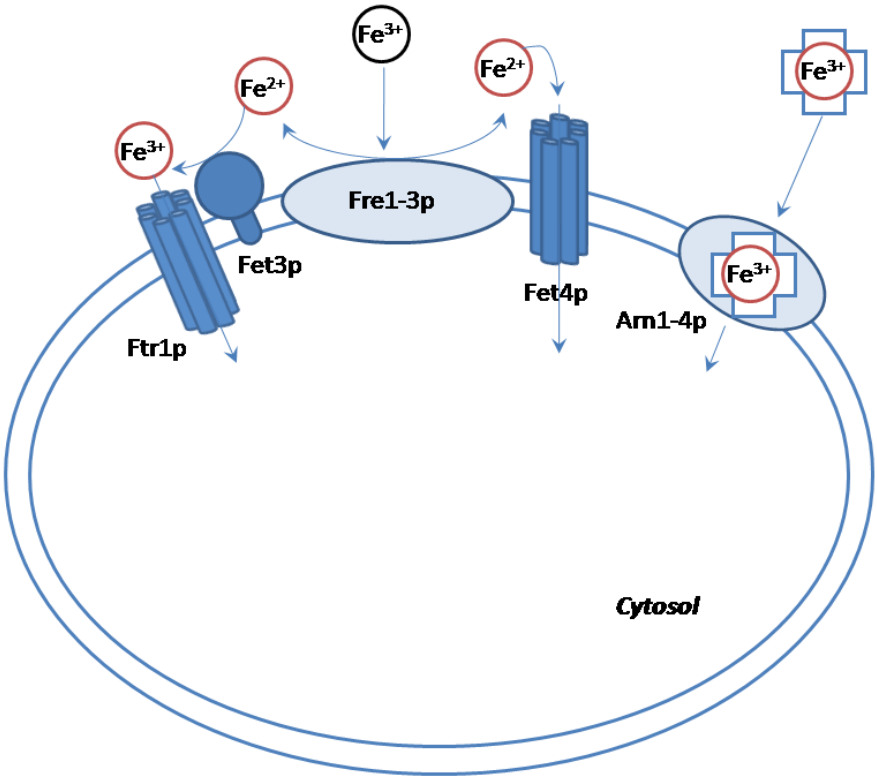

Figure 1-1: The three major iron uptake pathways in yeast *Saccharomyces cerevisiae*. Modified from: Kwok, E., and Kosman, D. J. (2005) Iron in yeast: mechanisms involved in homeostasis. *Top. Curr. Genet.* 14:59-99.

repressed whereas FET4 gene transcription is activated and responsible for most of cellular iron uptake (*6*).

Saccharomyces cerevisiae does not produce siderophores itself but it can uptake these molecules with high efficiency and utilize the iron once internalized. Siderophore receptors include Arn1-4p.

Iron homeostasis is transcriptionally regulated by Aft1p and Aft2p, with Aft1p generally considered as the major regulator. When medium iron concentration is low, Aft1p (and possibly Aft2p) enters the nucleus, binds the promoter regions of > 20 genes (collectively termed as ***iron regulon***) and activates their transcription. The iron regulon genes include FET3, FTR1 and other cellular iron uptake genes. This binding will lead to an elevated cellular iron uptake capacity. On the contrary, when medium iron is high, Aft1/2p move out of nucleus, shutting off the iron regulon, and decreasing cellular iron uptake capacity. Although Aft1/2p play very important roles in iron homeostasis, the mechanism by which they sense iron remains unclear (*7*).

Recently new insights connecting Iron-Sulfur Cluster (ISC) biosynthesis and the regulation of cellular iron homeostasis has been revealed (*7*) (*8*). In eukaryotes more than 20 proteins are involved in ISC biosynthesis (*1*). In yeast mitochondrion is the major site for ISC biosynthesis and mitochondrial ISC machinery is indispensible for cellular ISC biosynthesis. The major proteins involved in yeast mitochondrial ISC

assembly have been identified and their proposed roles are shown in Figure 1-2. Iron is believed to be imported into mitochondria at the ferrous oxidation state through the high affinity transporters Mrs3p/Mrs4p (and possibly several other low-affinity transporters). Once imported, it may form an iron pool providing feedstock for ISC assembly and heme biosynthesis (*9*). Iron is delivered to scaffold proteins Isu1/2p by the chaperone protein Yfh1p. Sulfur is provided by Nfs1p which catalyzes the reaction where cysteine is converted to alanine. The sulfur atom produced in this reaction needs two electrons to be reduced to sulfide for ISC assembly and these electrons are proposed to come from NADH via an electron transfer chain involving Arh1p and Yah1p.

Once assembled, Fe-S clusters are inserted into various apoproteins. This process requires aids from several chaperone proteins including Ssq1p, Jac1p, Mge1p and Grx5p. Some unknown product of Fe-S biosynthesis machinery (perhaps a precursor of Fe-S clusters) is exported via an ATP binding cassette (ABC) transporter Atm1p which is located on the inner mitochondrial membrane. This unknown product is required for cytosolic ISC biosynthesis and may also serve as the signal molecule relaying the iron status within mitochondria to other parts of the cell. It has been observed as a common phenotype that upon disruption of ISC biosynthesis (by deleting or depleting proteins involved in ISC assembly), the Aft1/2-controlled iron regulon genes are constitutively activated. This leads to elevated cellular iron uptake rate and the accumulation of iron

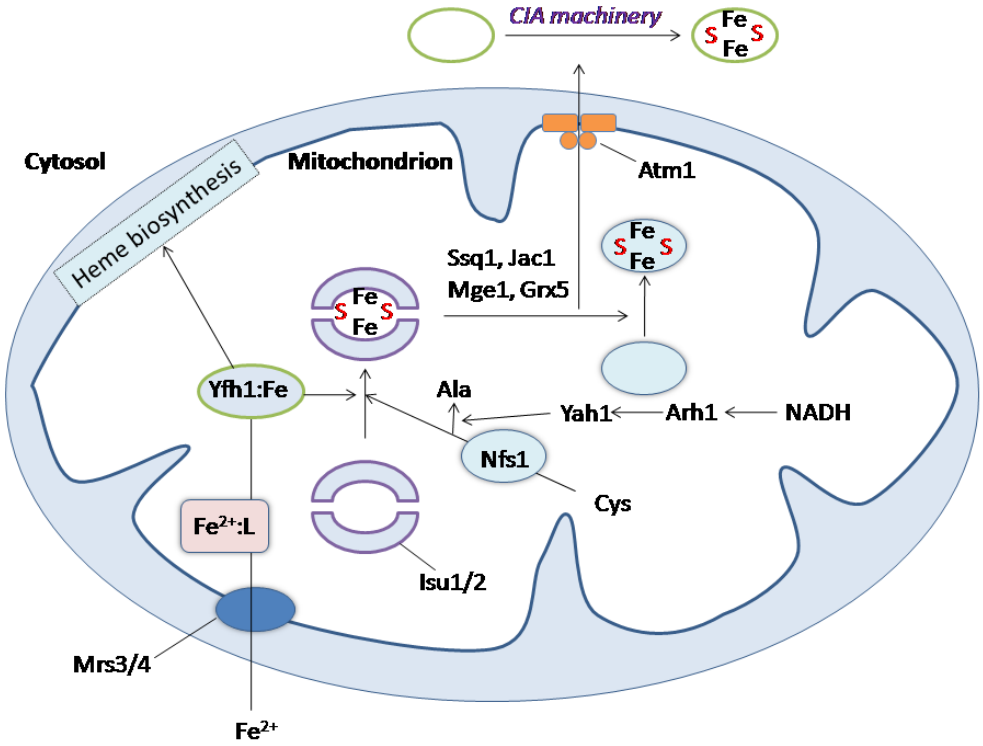

Figure 1-2. A working model for Fe/S biosynthesis in yeast.

within mitochondria. For example, upon deletion or depletion of Yfh1p, Yah1p or Atm1p, more than 10-fold increase in mitochondrial iron content has been reported (*10*) (*11*) (*12*). In humans, defects in Fe-S cluster assembly can result in different iron disorders involving iron accumulation in affected tissues (*2*).

Vacuoles also play very important roles in yeast iron metabolism and homeostasis. These organelles are the major site of iron storage in yeast. Disruption of its role in iron trafficking can lead to decreased fitness and even the inability to grow under certain conditions (*13*).

CCC1 is the only known vacuolar iron import protein. Deletion of this gene leads to diminished iron levels in vacuoles and an increased sensitivity toward high medium iron. Iron exporters include the divalent metal iron transporter Smf3p and the Fet5p/Fth1p complex. This Fet5p/Fth1p complex is paralogous to the plasma membrane ferroxidase-permease complex (Fet3p/Ftr1p). Deletion of these exporters leads to iron accumulation in vacuoles (*5*).

Vacuoles and mitochondria have tight connections. Alteration of iron trafficking of one can often affect the other. Excess amount of iron accumulates in *Δyfh1* mitochondria, whereas the over-expression of CCC1 can repress iron accumulation in mitochondria of Yfh1p-deleted cells likely by limiting iron availability to mitochondria (*14*). Deletion of mitochondria iron importers Mrs3/4p leads to decreased iron import to mitochondria;

this increases the activity of Ccc1p and iron accumulation in vacuoles up to 6-fold (*15*).

Iron accumulation is an important symptom for iron overload diseases and this can be well mimicked in yeast models. Understanding iron accumulation in terms of cellular distribution, the chemical nature and the detailed mechanism of formation would be of great importance. In recent years advances have been made toward this goal using newly developed biophysical approaches. For example, laser ablation inductively coupled plasma mass spectrometry (LA-ICP-MS) has been used to image element (including iron) distribution in mice brain tissues. Brain tissues from normal and some disease model mice were investigated and iron deposits are found at some tissue locations (*16*).

The traditional chemical analysis methods, including Mössbauer, EPR, x-ray absorption spectroscopy and electron microscopy, have proved to be effective in characterizing the relatively simple and homogeneous iron-containing species. Attempts to apply these chemical techniques to study iron in more complicated cell biology systems have been reported (*17, 18*). These methods can sometimes provide detailed insights into the chemical nature of the biological iron that will be otherwise very difficult to obtain by traditional cell biology techniques. However, these techniques have their own strengths and limitation for studying biological iron.

Mössbauer spectroscopy is one of the most powerful techniques for probing iron. A more informative name for the technique is *nuclear gamma-ray absorption* spectroscopy.

This method measures energy transitions of ^{57}Fe (natural abundance of ^{57}Fe is 2.2%) nuclei between the ground spin state I = 1/2 and the first excited spin state I = 3/2. The 14.4 keV gamma rays used in this technique are emitted during the decay of a ^{57}Co source. The energy of emitted photons is modulated by the Doppler Effect (the source is mounted on a motor that moves backward and forward with defined velocity) and the absorption spectrum is collected. The isomer shift, quadruple splitting and other magnetic interactions evidenced in Mössbauer spectra can provide detailed information regarding iron redox states and ligand environments. Mössbauer spectroscopy is a non-destructive method that does not disrupt biological membranes; this is advantageous since biological samples can be maintained in their original *in vivo* states. This can also eliminate the risk of altering the chemical properties during cell disruption. All ^{57}Fe-containing species are visible by Mössbauer spectroscopy and the extinction coefficient for each species is similar. Therefore Mössbauer spectroscopy can be used to detect the major iron species and determine the percentage of each iron species in the sample. Its major disadvantage is its low sensitivity. Thus, for biological studies ^{57}Fe enrichment is often necessary and some minor species are difficult to detect even samples are ^{57}Fe enriched (the detection limit is estimated to be 10 - 50 μM ^{57}Fe depending on the nature of the signal).

EPR (Electron Paramagnetic Resonance) spectroscopy is also commonly used for

characterize iron-containing species. EPR measures the transition energy of unpaired electrons in the presence of an externally applied magnetic field. EPR spectroscopy has been used extensively to study Fe-S cluster containing proteins. It has the potential to provide information regarding the electron spin state, redox state and ligand environment of the iron. It is a sensitive technique that is able to detect species at micromolar levels. It is also a non-destructive technique that allows measurement of intact biological samples. It major disadvantage is that it can only detect the species containing unpaired electron, such as Fe^{3+} ions, $[Fe_2S_2]^{+}$ clusters and $[Fe_4S_4]^{+}$ clusters. Thus some species such as Fe^{2+} ions, $[Fe_2S_2]^{2+}$ clusters and $[Fe_4S_4]^{2+}$ clusters are invisible by this technique.

X-ray absorption spectroscopy is useful for studying the structure of metal ions in biological systems. Utilizing the high flux and broad energy range of X-rays supplied by synchrotron light sources, it is possible to excite selectively core electronic transitions in each metal. Spectroscopic signals from such transitions can be used to probe the chemical architecture of metal ions (e.g. iron) in the biological samples. Moreover, this technique is non-destructive. The major limitation of the technique is that it inherently averages the coordination structure and electronic properties of heterogeneous biological samples thus limiting spectral resolution.

Scanning transmission electron microscopy (STEM) has been widely applied in studying biological samples. STEM is a type of transmission electron microscopy

(TEM), but it is different from conventional TEM in that the electron beams are focused into a narrow spot which is scanned over the sample in a raster pattern. The STEM technique has higher contrast imaging ability than the conventional TEM and allows imaging of biological samples without staining. Due to the raster nature of the electron beam, STEM is suitable for analysis techniques such element mapping by Energy Dispersive X-ray (EDX) spectroscopy. Therefore this technique, when samples are carefully prepared, can be used to determine the metal element compartmentalization in biological samples. However, due to the relatively low sensitivity of EDX, high local element concentrations are generally required. In biological samples where metal concentrations are often low compared to the EDX detection limit, the metal may only be detected in an aggregated state.

All these chemical analysis techniques discussed above have strengths and limitations such that they can provide complementary structural or electronic information. Therefore, one can obtain a more complete understanding of an iron-containing biological sample by examining it with these different biophysical techniques and interpreting the results integratively.

As described in this dissertation, the objective of my research has been to apply various biophysical and biochemical techniques to probe the iron accumulation in the model organism yeast *Saccharomyces cerevisiae*. Along with our collaborators, we have

determined the chemical nature of iron accumulation in mitochondria isolated from several mutant strains (Yah1p-depleted, Atm1p-depleted, and Aft1p-1up strains). We studied the chemical reactivity of the accumulated iron as well as the conditions that are required for its formation. We further studied the mechanism by which Yah1p-depletion alters the cellular iron distribution. We compared the distribution of Fe in these cells to that in the Aft1-1up strain where the iron regulon genes are also constitutively activated due to a mutation in Aft1p. Our results provide insights into how disruption of Fe-S cluster biosynthesis (e.g. by depletion of Yah1p and Atm1p) alters mitochondrial Fe metabolism as well as the iron distribution at the whole cell level.

CHAPTER II

METHODOLOGY AND PROTOCOLS

Materials

All reagents and chemicals, unless otherwise noted, were purchased from Fisher Scientific, Sigma Aldrich and MP Biomedicals. Deionized water was used for preparing medium or buffer. ^{57}Fe metal (95% purity) was purchased from Cambridge Isotope Laboratories. Ar, N_2, O_2 and air gas cylinders were purchased from Praxair through the Texas A&M University Department of Chemistry Stockroom.

Yeast Strains

Saccharomyces cerevisiae strain W303 (*MATα, ura3-1, ade2-1, trp1-1, his3-11,15, leu2-3,112*) was purchased from American Type Culture Collection (ATCC) and served as wild type control. Gal-YAH1 (described in (*10*)) and Gal-ATM1 (described in (*19*)) are both derivatives of W303 in which the wild-type YAH1 and ATM1 promoter has been exchanged for a galactose-inducible promoter. Both strains were generous gifts from Dr. Roland Lill at University of Marburg, Germany. Aft1-1up (*MATα, trp1-63, leu2-3,112, gcn4-101, his3-609, FRE1-HIS3::URA3, AFT1-1^{up}*), Δccc1 (*MATa, ura3-52, leu2-3,112, trp1-1, his3-11, ade2-1, can1-100, ⊿ccc1::HIS3*), CCC1-overexpression

strains (WT strain transformed with a multicopy plasmid that contains CCC1 gene under its own native promoter) were gifts from Dr. Jerry Kaplan at the University of Utah.

Media and Cell Growth

Standard rich medium was used for the Gal-YAH1 study. This medium contains 1% yeast extract, 2% peptone and supplemented with the required carbon source (2% glucose for YPD or 2% galactose for YPGal). Gal-YAH1 cells were cultivated in YPD or YPGal medium until the OD (600) reached 0.7-1.1. To prevent foaming, 100 ppm silicone antifoam B (JT Baker) was added to the media. To enrich samples with ^{57}Fe, a 10-fold molar excess of sodium citrate was added to $^{57}Fe^{3+}$ ions in acid (final pH ~ 5.5) and this solution was added to the media to obtain a final ^{57}Fe concentration of ~40 μM.

Minimal medium was used for Gal-ATM1 study. Gal-ATM1 cells were grown in minimal medium supplemented with required amino acid nutrients (100 mg/L leucine, 40 mg/L adenine sulfate, 20 mg/L uracil, 20 mg/L histidine, and 50 mg/L tryptophan) and containing either 2% (w/v) glucose or galactose. Minimal medium does not form significant amounts of foam thus addition of antifoam is not necessary. To enhance the enrichment of ^{57}Fe for Mössbauer samples, a modified yeast nitrogen base (MP Bio) which lacks copper and iron salts (Cat # 4027-112) was used. Copper and iron were added back as copper sulfate (1 μM final concentration) and $^{57}Fe(III)$ citrate (20 μM

final concentration).

Complete minimal medium containing glucose (2%, w/v) was used for the Aft1-1up study. Complete medium was used because the *gcn4* background of Aft1-1up strain makes it unable to activate amino acid biosynthesis pathways; thus this strain grows slowly on non-complete medium. A complete supplement mixture (MP Bio) was used to provide the whole spectrum of amino acids. The modified yeast nitrogen base (MP Bio) lacking copper and iron used in Gal-ATM1 study was used. Copper and iron were added back as copper sulfate (10 μM final concentration) and ^{57}Fe(III) citrate (various concentration, see results). Standard rich medium containing glucose (2%, w/v) (YPD) was also used in some experiments.

Cell Growth and Harvesting Conditions for Mitochondria Isolation

For mitochondria isolation, cells were grown in large quantity (in a 25 L glass fermenter) at 30 °C, as described (*20*). For aerobic growth, pure O_2 was bubbled through the media at a flow rate of ~2 L/min. For anaerobic growth, the media was supplemented with 20 mg/L ergosterol (Acros Organics) and 1.0 mL/L Tween-80 (Acros Organics) dissolved in 1.0 mL/L ethanol, which was sterilized by heating for 10 min in boiling water. Research-grade (99.998% pure) argon (Botco Co., TX, USA) was used for anaerobic cell growth to maintain anaerobiosis. For this growth, media was vigorously

deaerated by bubbling with Ar for 1 h before inoculation; thereafter the Ar flow rate was set at ~2 L/min. Approximately 50 mL of aerobically cultured cells at OD (600) ~ 1 was used as the inoculum, requiring cells to undergo 8-10 mass doublings before harvesting (when OD (600) = 0.7-1.1) to ensure complete anaerobic adaptation.

Aerobically grown cells were harvested by centrifugation (5 min at 5000×g) and then transferred to an Ar-atmosphere glovebox (MBraun) maintained at ~5 °C and ~1 ppm of O_2. Anaerobically grown cells were transferred (through PharMed tubing driven by a peristaltic pump) into an Ar atmosphere glovebox (Vacuum Atmospheres Inc., O_2 < 3 ppm) while the culture in the fermenter was continuously bubbled with Ar at a flow rate > 15 L/min. The suspension culture was transferred into sealed centrifuge bottles, removed from the box and centrifuged as above. The bottles were then returned to the box, and the process was repeated. Thus, anaerobically grown cells were not exposed to significant O_2 during either growth or harvesting.

Mitochondria Isolation Procedures and Treatments

Mitochondria were isolated following the protocols described in (*20*). Lyticase (Sigma; 300 units/g wet weight cells) was used to form spheroplasts within 1 hour. Spheroplasts were gently ruptured in a glass Dounce homogenizer (tight fitting, 20-40 strokes). Cell debris was removed at 1500×g for 5 min, and the soluble mitochondria

fraction was pelleted at 12000×g for 10 min. Resulting crude mitochondria were further purified using a discontinuous 16 - 22% Nycodenz (Sigma) gradient at 150000×g for 1 hour. As determined by electron microscopy (EM), the interface of the two layers contained mitochondria. This layer was collected and will be referred to as intact mitochondria in the as-isolated state. Portions of as-isolated mitochondrial samples were packed by centrifugation at 15000×g for 1 h into EPR or Mössbauer holders and then frozen in liquid N_2 for subsequent analysis. There was some batch-to-batch variation in the extent of ^{57}Fe incorporation into mitochondria. Prior to packing, some aliquots of as-isolated mitochondria were incubated for 1 hour with 5 mM sodium dithionite in a buffer containing 0.6 M sorbitol, 100 mM Tris (pH 8.5) supplemented with or without 1 mM EGTA. Other aliquots were incubated with 1 atm O_2 for 30 min before packing and freezing.

Cell Growth and Harvesting Conditions for Whole Cell Sample Preparation

Cells were grown in 1000 mL culture flasks to OD (600) ~ 1 and harvested by centrifugation at 5000×g for 5 min. To remove metal ions loosely bound to the cell walls, cells were washed with deionized H_2O, then with 100 μM EDTA and then again with deionized H_2O. To prepare Mössbauer and EPR samples, washed cells were packed into Mössbauer cups or custom-designed EPR tubes at 6000×g for 10 min. Packed cells were

frozen and stored in liquid N_2 for subsequent Mössbauer and EPR analysis.

Western Blot Procedures

Cellular extracts were prepared as described in (*21*). Cells were resuspended in 100 µl distilled water followed by the addition of 100 µl of 0.2 M NaOH. The suspension was incubated for 5 min at room temperature and then spun by centrifugation. The pellet was resuspended in 50 µl SDS sample buffer, boiled for 3 min, cooled on ice and centrifuged again and the supernatant was used for electrophoresis. Mitochondria extracts were prepared by directly boiling mitochondrial samples in SDS sample buffer for 3 min. 20 μL soluble portions of either cell extracts or mitochondria were separated by SDS-PAGE and transferred onto polyvinylidene fluoride (PVDF) membranes (Bio-Rad). Membranes were blocked by nonfat milk (5%) in TBS buffer (20 mM Tris, 0.9% NaCl, pH 7.5) and 0.1% Tween 20 before protein detection. An ECL Western blotting detection kit (Amersham Biosciences) was used to detect corresponding antisera as visualized using a Fujifilm LAS-4000 mini imaging system.

Oxyblot Procedures

The assay was performed using an Oxyblot kit (Millipore, USA) following manufacturer's procedures. Isolated mitochondria were solubilized with 12% SDS

solution, derivatized with 2, 4-dinitrophenylhydrazine (DNPH) and separated on a 4-20% SDS-PAGE gel. The primary antibody used for the Western blot was raised against DNPH.

Protein and Metal Analysis

Protein concentrations were determined by the Biuret (*22*) and Bradford methods (*23*). Metal analysis was performed using either a DRCII ICP-MS spectrometer (Perkin-Elmer) or a colorometric method based on detecting Fe(II) bathophenanthrolinesulfonate (BPS, Sigma). For ICP-MS analysis, typically three volumes (50 μL, 75 μL and 100 μL) of mitochondrial suspensions were digested overnight in sealed plastic tubes in 100 μL of 70% trace-metal grade nitric acid (Fisher Scientific) at 95° C. Digested samples were diluted with deionized and distilled H_2O to a final HNO_3 concentration of 0.2 M before measurement. For the BPS method, the protocol of Tamarit et al. (*24*) was followed. Packed mitochondria or whole cells were diluted in 2 - 3 volumes of deionized water, and 50 or 100 μL suspensions were digested in 500 μL of 30% trace-metal grade nitric acid (Fisher Scientific) at 95-100 °C overnight. Digested samples (100 μL) were mixed with 200 μL of 6.4 M ammonium acetate (Sigma), 100 μL of 0.2 M sodium ascorbate (Acros Organics), 100 μL of 10 mM BPS, and 500 μL of deionized H_2O. The concentration of $Fe(BPS)_3$ was determined from the absorbance at 535 nm assuming a

molar extinction coefficient of 22167 M^{-1} cm^{-1}.

Electron Microscopy

Mitochondrial pellets were fixed in 3% (vol/vol) glutaraldehyde in isolation medium, washed with isolation buffer (1XSH buffer) and treated overnight at 4 °C with 1% para-phenylenediamine (w/v) in 1XSH buffer followed by dehydration in a graded methanol series to propylene oxide. Pellets were then infiltrated and embedded in epoxy resin followed by polymerization overnight at 60 °C. Ultrathin sections (100 nm) were cut with an ultramicrotome and picked up on copper grids. Grids were stabilized with a 10 nm deposit of carbon before examination in the transmission electron microscope. Elemental analysis was performed on a TECNAI F20 (scanning) transmission electron microscope (TEM/STEM) fitted with a Schottky field emission gun, a high angle annular dark field (HAADF) detector, and an Oxford instruments ultrathin window energy dispersive X-ray spectroscopy (EDX) detector. The combination of STEM and EDX allows direct imaging of a nanoscale area and *in situ* identification of component elements. An EDX spectrum at each spot in the area of interest was collected at a 200 kV accelerating voltage and a ~15° tilting angle with a stationary electron probe in STEM mode. An elemental map was then acquired after choosing a proper energy window for an element specific transition along with STEM-HAADF images. Above procedures

were carried out by Hansoo Kim and E. Ann Ellis at Microscopy and Imaging Center, Texas A&M University.

Mössbauer and EPR Spectroscopy

Some Mössbauer spectra were collected at Carnegie Mellon University, with two spectrometers, using Janis Research Super-Varitemp dewars that allowed studies in applied magnetic fields up to 8.0 T in the temperature range from 1.5 to 200 K. The remaining Mössbauer spectra were collected at Texas A&M University using a model MS4 WRC spectrometer (WEB Research, Edina, MN) with a 4.5 to 300 K closed-cycle helium refrigerated system and a W106 temperature controller. Data from both instruments were analyzed using the WMOSS software package (WEB Research, Edina, MN). Isomer shifts are quoted relative to Fe metal at 298 K. EPR spectra were recorded on an X-band Bruker EMS spectrometer with an Oxford ESR900 liquid He cryostat. Quantitative analysis of EPR spectra used *SpinCount* software (developed by Dr. Michael Hendrich at Carnegie Mellon University) with Cu-EDTA as the spin standard. Spectra were recorded with a modulation amplitude of 1 mT at 100 kHz, and if used for concentration determination, under nonsaturating microwave power conditions.

Preparation of Mitochondria for UV-Vis Spectroscopy

Mitochondria were solubilized in a buffer containing 50 mM Tris (pH 8.0), 100 mM NaCl, and 1% (w/v) sodium deoxycholate. The resulting solution had a protein concentration of 5 mg/mL. Potassium ferricyanide (Acros Organics) and sodium dithionite (Sigma), at final concentrations of 12 mM each, were used respectively to oxidize and reduce cytochromes. Spectra were recorded using a 2 mm path length quartz cuvette (NSG Precision Cells, Inc.) on a Hitachi U-3010 UV-vis spectrometer with a Head-On photo multiplier tube.

Enzyme Assays

Aconitase assays were performed according to a published protocol (*25*). Mitochondria were solubilized in a buffer containing 20 mM Tris (pH 7.4) and 0.5% (v/v) Triton X-100. Solubilized samples (20 μL) were mixed with 40 μL of 0.1 M Tris (pH 7.4), 40 μL of 0.5 M NaCl, and 80 μL of deionized H_2O in a 1 mm path length quartz cuvette. The reaction was initiated by the addition of 20 μL of 10 mM sodium cis-aconitate (Sigma). The consumption of aconitate was monitored by a decline of absorbance at 240 nm and quantified assuming a molar extinction coefficient of 3.6 mM^{-1} cm^{-1}. Reaction rates were calculated from the initial linear portion of the slopes. Activities were expressed as units per milligram of protein (1 unit is defined as 1 nmol

of aconitate converted per minute).

Leu1p assays were performed according to a published protocol (*26*). Cells were grown on minimal medium (leucine concentration was lowered to 30 mg/L to increase expression of Leu1p) and harvested when OD (600) reached ~0.7. The pellet obtained by centrifuging 30 mL of cell culture was washed with ice-cold deionized water and resuspended in 0.3 mL of lysis buffer (20 mM KH_2PO_4 buffer, pH 7.2, 50 mM NaCl, 1 mM EDTA, 0.5 mM PMSF). Approximately 0.3 mL of glass beads (Biospec Inc.; 0.5 mm diameter) was added. The mixture was vortexed at highest speed for 30 s followed by 30 s on ice. This cycle was repeated five to six times. Unbroken cells and glass beads were removed by centrifugation at 10000×g for 5 min. Immediately thereafter, 50 μL of the supernatant cell extract was mixed with 50 μL of 0.2 M KH_2PO_4 (pH 7.0) buffer, 395 μL of deionized water, and 5 μL of 0.1 M sodium citraconate (Sigma). The decline in absorbance at 235 nm was monitored for 3 min. Activity was expressed as units per milligram of protein (1 unit is defined as 1 nmol of citraconate converted per minute). Note: Leu1p assay should be performed as soon as possible after cell lysis by glass beads. The enzyme activity decreases rapidly in air, likely due to inactivation by oxygen. Within 30 min after lysis, > 90% of original enzyme activity was detected.

Succinate dehydrogenase assays were performed following a published procedure (*27*). The reaction mixture contained 100 mM Tris (pH ~ 8.3), 0.5 mM EDTA, 2 mM

KCN, 2 mM iodonitrotetrazolium chloride (INT, Sigma), 12 g Cremophor EL (Sigma) and 20 mM succinate (pH ~ 7.4). The reaction was started by mixing 990 μL of the reagent mixture mentioned above with 10 μL of mitochondria suspension (note: a suspension of intact mitochondria, not solubilized mitochondria extract, is used here; when mitochondria were solubilized with Triton X-100 first, lower activities were obtained). The formation of INT-formazan was monitored under room temperature at 500 nm for 5 min. Blanks were measured in the absence of the substrate succinate added and the obtained blank rate was subtracted from the sample rates. The activity was expressed as units per milligram of protein (1 unit is defined as 1 nmol of INT-formazan formed per minute).

X-ray Absorption Spectroscopy

Fluorescence excitation Fe K-edge XAS data were collected directly from packed mitochondria in Mössbauer cups, held inside our standard liquid He continuous flow cryostat with a custom-designed sample holder. Data were collected on beamline 9-3 of the Stanford Synchrotron Radiation Light source with SPEAR3 running at 3.0 G eV and 80-100 mA beam current. Harmonic rejection was achieved by the focusing mirror being configured to a nominal 10 k eV cutoff. We used a 30-element intrinsic Ge solid-state detector and Z-1 fluorescence filter with Soller slits to record the XAS fluorescence

signal from samples. XAS data reduction was carried out using the EXAFSPAK program (http://www-ssrl.slac.stanford.edu/exafspak.html). The photon energy was calibrated using an internal Fe foil with the first inflection point at 7111.2 eV; E0 was defined as 7120 eV. The Atm1p data set was the average of seven individual sweeps, each of 21 min duration. Preedge subtraction used a Gaussain model, and the EXAFS were extracted using a spline with three regions, each of polynomical order 4. Curve fitting was performed using the theoretical phase and amplitude functions calculated by FEFF 8.0 (*28*). The procedures described in this section were performed by Dr. Robert A. Scott and his lab members.

RNA Extraction and Real-time PCR

Aft1-1up and WT (W303) strains were grown to a high density (OD (600) = 3 – 4) in complete minimal medium lacking iron and copper salt. Cells were harvested by centrifugation and diluted into fresh medium for additional 4 hour growth. The fresh medium contained either 100 μM BPS (iron deficient); or 10 μM copper sulfate and 40 μM Fe(III)-citrate (iron rich). Cells were again harvested, then washed once with ice-cold de-ionized water and frozen in liquid N_2 for future RNA extraction.

Total RNA was extracted using the hot-phenol method (*29*). Thawed cells were resuspended in AE buffer (50mM sodium acetate, pH 5.3, 10mM EDTA). Cells were

lysed by the addition of SDS to a final concentration of 1% and an equal volume of AE buffer-equilibrated phenol was added. The mixture was incubated at 65° C for 10 min and vortexed briefly every minute. After incubation, the mixture was rapidly chilled in a dry-ice/ethanol bath and then centrifuged at the maximum speed using a benchtop centrifuge at room temperature (RT) for 5 min. The aqueous phase was extracted with an equal volume of a mixture of phenol:chloroform:isoamyl alcohol (volume ratio 25:24:1) and followed by centrifugation. The aqueous phase was again extracted with an equal volume of a mixture of chloroform:isoamyl alcohol (volume ratio 24:1) and followed by centrifugation. To the resulting aqueous phase was added 0.3 M sodium acetate, pH 5.3, after which 2.5 volumes of ethanol were added to precipitate RNA. After washing with 80% ethanol, RNA was air-dried and resuspended in sterile water and kept frozen at -80° C until use. Total RNA was quantified by OD_{260} readings. Residual contaminating DNA was removed by treating RNA samples with DNA-free reagent (Ambion) following manufacturer's instruction. RNA integrity was confirmed using 1% agarose gel and Bioanalyzer (Agilent). Super Script Vilo cDNA synthesis kit (Applied Biosystems) was used to synthesize cDNA from RNA. qRT - PCR was carried out on the synthesized cDNA using an ABI 7900 Real Time PCR machine (Applied Biosystems). Samples were prepared using Power SYBR green PCR master mix (Applied Biosystems) and primer pairs specific for different genes (See Table 2-1 for primer pairs used in this study).

Table 2-1. Primer pairs for different genes used in qRT – PCR experiments.

	Forward Primer	Reverse Primer
ACT1	GGATTCCGGTGATGGTGTTACT	TGGCGTGAGGTAGAGAGAAACC
FET3	TGGGAAGTCCAGCCCGATA	AAACGAACCCACCCACGTT
FRE1	GGCTGGATGGGTTGGATTT	AATCCTGCAGAATCTATCAAAGCA

CHAPTER III

CHARACTERIZATION OF IRON IN MITOCHONDRIA ISOLATED FROM YEAST UNDER DIFFERENT METABOLIC CONDITIONS*

Introduction

Mitochondria are cellular organelles that play critical roles in cellular physiology. Respiration and oxidative phosphorylation occur in these organelles, as do heme biosynthesis and iron-sulfur cluster assembly. As such, mitochondria are "hubs" of cellular iron trafficking (*30*). The Fe^{II} ions used for these processes are imported by Mrs3p and Mrs4p, high-affinity transporters on the inner membrane (IM) (*30*). Once in the matrix, these ions are delivered to Fe/S scaffold proteins and ferrochelatase (*30*). Many of these centers are inserted into respiratory complexes.

*****This chapter is reproduced in part with permission from: "Characterization of Iron in Mitochondria Isolated from Respiring and Fermenting Yeast" by Jessica Garber-Morales, Gregory P. Holmes-Hampton, Ren Miao, Yisong Guo, Eckard Münck, and Paul A. Lindahl, 2010, *Biochemistry*, 49, 5436-5444, copyright 2010 American Chemical Society and "A Nonheme High-Spin Ferrous Pool in Mitochondria Isolated from Fermenting *Saccharomyces cerevisiae*" by Gregory P. Holmes-Hampton, Ren Miao, Jessica Garber-Morales, Yisong Guo, Eckard Münck, Paul A. Lindahl, 2010, *Biochemistry*, 49, 4227-4234, copyright 2010 American Chemical Society.
My contributions to these studies were to isolate the yeast mitochondria from galactose-containing medium, to prepare whole cell Mössbauer sample, and perform the Mössbauer, EPR and ICP-MS studies. Analysis was done in collaboration with Dr. Eckard Münck and Dr. Yisong Guo at Carnegie Mellon University.

Mitochondrial dysfunction is associated with various diseases, including aging, cancer, heart disease, anemia and neurodegeneration (*31*, *32*). As cells age, there is a decline in iron-sulfur cluster biogenesis and mitochondrial membrane potential, leading with higher probability to a cellular crisis associated with loss of mitochondrial DNA, the instability and hypermutability of nuclear DNA, and cancer (*33*). Aged cells exhibit signs of iron starvation (*33*). Reactive Oxygen Species (ROS) generated by Fe centers within the mitochondria may damage the DNA and other cellular components, and which may initiate apoptosis (*34*). Ferrous ions are particularly adept at producing ROS via Fenton Chemistry (*3*). In Friedrich's Ataxia, the yeast frataxin homolog (Yfh1p) is mutated causing a build-up of Fe nanoparticles (*4*, *18*). Patients with Sideroblastic anemia accumulate Fe that cannot incorporate into hemoglobin (*2*).

Much progress in understanding cellular function has been made by "omics"-level studies in which entire subsets of cellular components are measured simultaneously and analyzed as a system (*35*). We have developed an integrative biophysical approach centered on Mössbauer spectroscopy to study the "*ironome*" of cells and organelles (*20*). ^{57}Fe Mössbauer spectroscopy detects ***all*** Fe species in a sample, with spectral intensities proportional to relative concentrations. In complex systems, Mössbauer cannot resolve *individual* Fe species, but it can identify *groups*. The resolution of mitochondrial Fe species can be enhanced by EPR, which can detect paramagnetic species, UV-vis

spectroscopy, which can quantify heme chromophores, and ICP-MS, which can quantify the overall Fe concentration. The *ironome* is obtained by integrating the results of these techniques.

In this study, we employed the integrative biophysical approach to assess the Fe content of mitochondria isolated from wild type yeast grown under different metabolic conditions (fermenting, respiro-fermenting and respiring conditions). Mitochondria play a dominant role in respiration but not fermentation; however, they are essential for cell viability regardless of metabolic growth mode. Fermenting cells produce fewer mitochondria than respiring cells. Early in exponential growth phase, fermenting cells are largely devoid of mitochondria; in later stages, the organelle occupies ~3% of cell volume. Under respiration, mitochondria represent ~10% of cell volume (*36*). Mitochondria in yeast are present as a large tubular network (*37*); the network from fermenting cells is thinner and less branched.

We report here that respiration-related Fe-containing proteins and other $[Fe_4S_4]^{2+}$ cluster-containing proteins dominate the ironome of mitochondria from respiring and respiro-fermenting cells. Under fermention, the concentrations of these species decline while those of nonheme high-spin (NHHS) Fe^{II} ions, mononuclear high spin (HS) Fe^{III} ions and Fe^{III} nanoparticles increase significantly. These changes can be rationalized by assuming that the NHHS Fe^{II} ions are a pool used for Fe/S cluster and heme biosynthesis.

We also investigated the contribution of mitochondrial iron to iron contents of whole yeast cell.

Results

Respiro-Fermenting Mitochondria

Metal concentrations of mitochondria isolated from respiro-fermenting cells were determined by ICP-MS (Table 3-1). Low-field Mössbauer spectra of respiro-fermenting mitochondria were dominated by the *central doublet* (Figure 3-1). This doublet (~50% of Fe, Table 3-1) has $\delta \approx 0.45$ mm/s and $\Delta E_Q \approx 1.15$ mm/s, parameters characteristic of both S = 0 $[Fe_4S_4]^{2+}$ clusters and low spin (LS) Fe^{II} hemes. A minor contribution of S = 0 $[Fe_2S_2]^{2+}$ clusters to the central spectral region could not be excluded; fits for the 0.05 T spectra, but not the 8.0 T spectra were improved by assuming that ~ 5% of total Fe was in this form (with $\delta = 0.27$ mm/s, $\Delta E_Q = 0.55$ mm/s). A minor contribution of NHHS Fe^{II} (~3% of total iron) was assessed using the 100 K spectrum of Figure 3-1B. The presence of unassigned species is evident from the mismatch of the spectrum and simulation (Figure 3-1B) at ~ 0 mm/s. The 8.0 T spectrum reveals the presence of mononuclear HS Fe^{III} ions (Figure 3-1C, cyan line, ~5% of total iron). The black line in Figure 3-1C is a simulation of the diamagnetic Fe associated with the central doublet at low-field, together with a generic S = ½ $[Fe_2S_2]^{1+}$ cluster.

Table 3-1. Analytical properties of isolated mitochondria isolated from different metabolic conditions.

	Respiring	Respiro-fermenting	Fermenting
Protein (mg/mL)	170 ± 61 (5)	200 ± 60 (2)	110 ± 30 (11)
Fe (μM)	720 ± 210 (5)	840 ± 120 (2)	770 ± 320 (11)
Cu (μM)	210 ± 170 (5)	160 ± 80 (2)	50 ± 37 (11)
Mn (μM)	35 ± 20 (5)	12 ± 4 (2)	15 ± 12 (11)
Zn (μM)	290 ± 160 (5)	230 ± 150 (2)	290 ± 210 (11)
Central Doublet	60 ± 2% (2)	50% (1)	25 ± 4% (5)
HS Fe^{II} heme	7 ± 1% (2)	4% (1)	4 ± 1% (5)
NHHS Fe^{II}	2 ± 1% (2)	3% (1)	20 ± 5% (5)
HS Fe^{III}	0 (2)	5% (1)	15 ± 3% (3)
S = ½ $[Fe_2S_2]^{1+}$	13 ± 2% (2)	10% (1)	~ 0% (5)
$[Fe_2S_2]^{2+}$	< 5% (2)	< 5% (1)	~ 0% (5)
Fe^{III} nanoparticles	< 5% (2)	< 5% (1)	33 ± 7% (5)
unassigned Fe	~20%	~25%	~5% (5)
Fe^{II} Heme *a*(μM)	51 ± 8 (4)	61 (1)	14 ± 1 (4)
Fe^{II} Heme *b*(μM)	52 ± 8 (4)	55 (1)	27 ± 5 (4)
Fe^{II} Heme *c*(μM)	120 ± 10 (4)	160 (1)	73 ± 15 (4)
g_{ave} = 1.94 (μM)	1 – 10 (3)	13 ± 4 (2)	1 - 3 (2)
g_{ave} = 1.90 (μM)	13 ± 3 (3)	29 ± 18 (2)	6 ± 2 (2)
g = 2.01 (μM)	0 – 1 (3)	1 - 2 (2)	0 (2)
g = 2.00 (μM)	0 – 2 (3)	0 – 6 (2)	0 – 1 (2)
g = 2.04 (μM)	1 – 3 (3)	3 ± 1 (2)	1 - 2 (2)
g = 4.3 (μM)	5 – 45 (3)	2 – 14 (2)	3 (1)
g = 5.8 (μM)	1 - 2 (3)	0 - 2 (2)	~ 0 (1)
g = 6.4, 5.3(μM)	1 - 4 (3)	0 - 5 (2)	1 (1)
Cytochrome c oxidase	30	35	8
Succinate dehydrogenase	5	10	2
Cytochrome bc_1	10	20	6
Cytochrome *c*	100	140	60
Other HS heme *b*	20	Minor	minor
Other LS hemes combined	180	230	100
Other $[Fe_4S_4]^{2+}$ only	55	36	13
Other $[Fe_4S_4]^{2+}$ + $[Fe_2S_2]^{+}$	Minor	Minor	minor
Other $[Fe_2S_2]^{2+}$ only	Minor	Minor	minor
Cu^{I} Pool	120	60	30

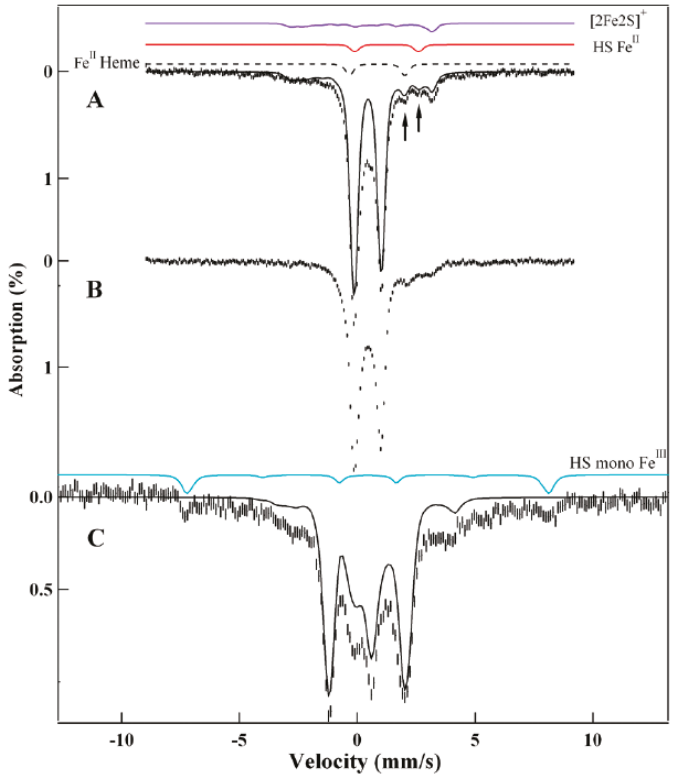

Figure 3-1: Mössbauer spectra of packed mitochondria from respiro-fermenting cells. (A) Spectrum measured at ~5 K with a 0.05 T field applied parallel to the γ radiation. The black line is a simulation for the central doublet, HS Fe^{II} hemes, NHHS Fe^{II}, and S=1/2 $[Fe_2S_2]^{1+}$ clusters. The lines above the spectrum are simulations for S=1/2 $[Fe_2S_2]^{1+}$ (purple), non-heme HS Fe^{II} (red), and HS Fe^{II} heme (black dashed line). (B) Same as panel A but at 100 K. (C) Same as panel A but at 8.0T and 4.2K. The black line is a simulation for the central doublet and S=1/2 $[Fe_2S_2]^{1+}$ clusters. The cyan line above is a simulation for HS mononuclear Fe^{III} species. See Table 3-1 for the concentrations of various species.

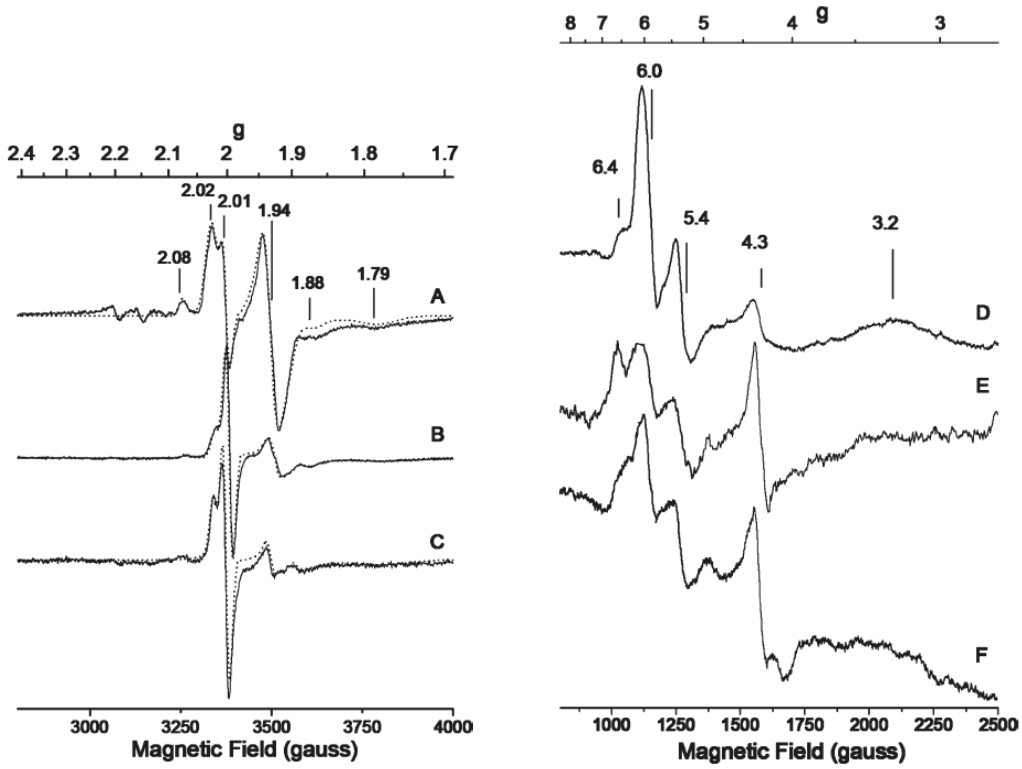

Figure 3-2: EPR spectra (10 K) of mitochondria from respiring (A), respiro-fermenting (B), and fermenting (C) cells. Spectra A and C were recorded at 0.05 mW, and spectrum B was recorded at 0.2 mW. Dashed lines are simulations, with batch-averaged parameters given in Table 1. Spectra D-F show the low-field regions of spectra A-C, respectively.

Respiro-fermenting mitochondria exhibited a quadrupole doublet with $\delta \approx 0.83$ mm/s, $\Delta E_Q \approx 2.4$ mm/s, typical of HS Fe^{II} hemes (*38*) (Figure 3-1A, dash line simulation). The spectrum also contains paramagnetic feature besides the heme and central doublets. The absorption features at ~ +3.1 mm/s and ~ -2.7 mm/s suggest S = ½ $[Fe_2S_2]^{1+}$ clusters (due to the Rieske center in the bc_1 complex and the center in succinate dehydrogenase) (Figure 3-1A, purple line simulation, ~ 10% of total iron). At 100 K (Figure 3-1B) the spin relaxation of the $[Fe_2S_2]^{1+}$ clusters is sufficiently fast to collapse the magnetic pattern observed at 4.5 K, revealing that ~ 3% of spectral intensity arises from NHHS Fe^{II} species ($\Delta E_Q \approx 3.0$ mm/s, $\delta \approx 1.3$ mm/s). The black line on the 8.0 T data of Figure 3-1C simulates the central doublet and S = ½ $[Fe_2S_2]^{1+}$ clusters. After subtracting the above-mentioned spectral features, some unresolved absorption remains at the center of the spectrum which could not be assigned unequivocally (a part may be due to Fe^{III} nanoparticles).

EPR spectra of respiro-fermenting mitochondria revealed additional details of the paramagnetic species observed by Mössbauer spectroscopy. The low-field region (Figure 3-2E) was dominated by EPR signals at $g \approx 6.0$ (E/D = 0) and at g = 6.4 and 5.4 (E/D ≈ 0.021); average spin concentrations are listed in Table 3-1. We assign these signals to the {a_3:Cu_b} center of cytochrome *c* oxidase (*39*) in which heme a_3 is Fe^{III} and Cu_b is Cu^{I}. The signal at g = 4.3 is due to Fe^{III} species. The g = 2 region (Figure 3-2B) was

dominated by signals with g_{ave} = 1.95 (2.03, 1.93, 1.91), g_{ave} = 1.90 (2.02, 1.90, 1.78), g_{ave} = 2.02 (2.08, 1.99, 1.97), and a nearly isotropic signal with g_{ave} = 2.01 (perhaps combined with another signal at g = 2.00) (*40*) .The g_{ave} = 1.95 and 1.90 signals, respectively, have been assigned to the $[Fe_2S_2]^{1+}$ clusters in succinate dehydrogenase (*40*) and the Rieske protein of cytochrome bc_1 (*40*). EPR analysis yielded a spin concentration of ~ 57 μM for the sum of the g_{ave} = 1.95 and 1.90 signals, suggesting that ca. 15% of the Fe belongs to $[Fe_2S_2]^{1+}$ clusters. This value is a bit higher than suggested by the Mössbauer data, but differences are within the uncertainties. The g_{ave} = 2.01 signal may originate from an S = ½ $[Fe_3S_4]^{1+}$ cluster, arising perhaps from the cluster in succinate dehydrogenase. The signal at g = 2.00 probably arises from an organic-based radical. The g_{ave} = 2.02 feature may arise from ET flavoprotein-ubiquinone oxidoreductase (*41*). The bulk of the spin concentration in the g = 2 region belongs to $[Fe_2S_2]^{1+}$ clusters that are most evident in Mössbauer spectra.

Respiring Mitochondria

The metal content of respiring mitochondria samples was determined by ICP-MS and similar to respiro-fermenting mitochondria, except that the Mn concentration was ~3-fold higher (Table 3-1). Mössbauer spectra of respiring mitochondria were also similar. Compared to respiro-fermenting mitochondria, the proportion of Fe present as

the central doublet, HS Fe^{II} hemes, and magnetic Fe in respiring mitochondria increased slightly, while the percentages of NHHS Fe^{II}, HS Fe^{III} and the unassigned absorption in the center of the spectra declined slightly.

Fermenting Mitochondria

Protein and Fe concentrations for fermenting mitochondria (Tables 3-1) were again similar to those of respiring and respiro-fermenting mitochondria. The Mn concentration was similar to that in respiro-fermenting mitochondria while the Cu concentration was lower. Mössbauer spectra of fermenting mitochondria differed substantially from those of respiring or respiro-fermenting mitochondria in that there was a substantial decline in the fraction of central doublet and an increase in the proportion of NHHS Fe^{II} and Fe^{III} nanoparticles (δ = 0.52 mm/s, ΔE_Q = 0.63 mm/s). EPR spectra of fermenting mitochondria (Figure 3-2, C and F) were qualitatively similar to those of respiring and respiro-fermenting mitochondria, but with lower spin concentrations (Table 3-1).

Whole Cell Mössbauer Spectra of Yeast

Mitochondria are considered as "hubs" for iron metabolism and we investigated the contribution of mitochondrial iron to iron contents of whole yeast cell. ^{57}Fe-enriched whole yeast cells under fermenting condition exhibited 5 K Mössbauer spectra

dominated by features indicating magnetically non-interacting mononuclear HS Fe^{III} components (Figure 3-3). These components have vanishingly small spin-dipolar interactions with other paramagnetic Fe sites. At 0.05 T (Figure 3-3A), they display paramagnetic hyperfine structure (a quadrupole doublet would be expected if spin-dipolar interactions were effective or if the Fe^{III} component belonged to nanoparticles with a T_B of << 4 K). At 8.0 T (Figure 3-3C), such species exhibited patterns characteristic of magnetically non-interacting Fe^{III}. This behavior implies that these components should be EPR active.

The red lines in Figure 3-3 are the sums of simulations for three mononuclear HS Fe^{III} species, collectively representing ~70% of the spectral intensity; the actual number of species contributing to these features remains undetermined. Individual differences among the HS Fe^{III} species are lost at 8.0 T. The difference spectrum (Figure 3-3B) obtained by subtraction of the low-field simulation for HS Fe^{III} species (red line in Figure 3-3A) from the spectrum of Figure 3-3A is similar to that obtained for isolated mitochondria (on page 39 in Figure 3-3B the blue line is the spectrum of fermenting mitochondria).

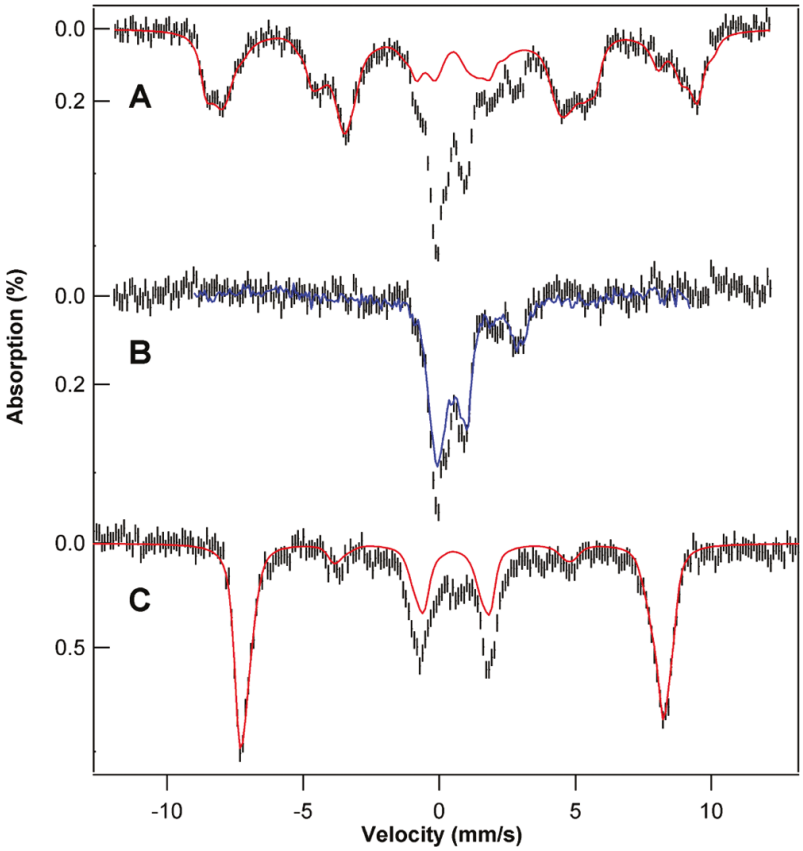

Figure 3-3: Mössbauer spectra (~ 5 K) of whole fermenting yeast cells grown on ^{57}Fe-enriched minimal medium. (A) Applied field of 0.05 T. The red line is a simulation with A values ranging from-21 to -23.5 T. (B) Spectrum obtained after subtraction of the simulation in part A from the data. The blue line is the spectrum of isolated fermenting mitochondria. (C) Same as part A, but at an applied field of 8.0 T. The red line is a simulation with A values ranging from -21.5 to -22.5 T.

A detailed analysis of the iron content of entire yeast cells will require a separate analysis, but our current analysis is sufficient for us to draw two major conclusions. First, most of the magnetically non-interacting mononuclear HS Fe^{III} species (whose contribution was removed from the spectrum of Figure 3-3A) are not located in mitochondria. Second, the majority of Fe in fermenting yeast cells can be divided into two major groups: these non-mitochondrial mononuclear Fe^{III} species and mitochondrial Fe species.

Discussion

The main objective of this study was to characterize the distribution of the major Fe species in mitochondria isolated from respiring, respiro-fermenting, and fermenting yeast cells. The analyzed results are summarized in Figure 3-4. In general, the total Fe concentration was similar regardless of metabolic mode. Also, the overall distribution of Fe in respiro-fermenting mitochondria was similar to that in respiring mitochondria. In contrast, the Fe distribution in fermenting mitochondria was dramatically different. This suggests that the ***repression of respiration*** by glucose, rather than the occurrence of fermentation ***per se***, is responsible for the major shifts observed in Fe distribution.

Viewed in the respiration **à** fermentation direction, cytochrome *c* oxidase ↓ (declined) 4×, succinate dehydrogenase ↓ 3.8×, cytochrome bc_1 ↓ 2.5×, cytochrome *c*

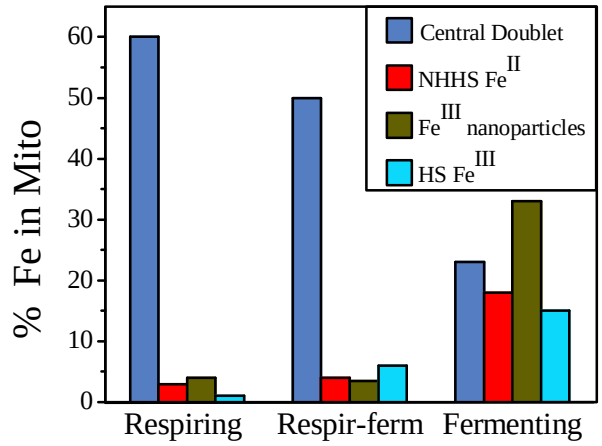

Figure 3-4. Bar graph showing the major forms of Fe present in respiring, respiro-fermenting and fermenting mitochondria. Color-coding is matched to simulated features in previous Mössbauer figures.

↓ 2×, LS hemes generally ↓ 2× and $[Fe_4S_4]^{2+}$ containing proteins ↓ 3.5×. The Cu^{I} pool decreased ↓ 3×. These species in respiro-fermenting mitochondria generally have similar or slightly high concentration than that in respiring condition. In terms of Fe pools, the NHHS Fe^{II} pool, the mononuclear HS Fe^{III} pool and the Fe^{III} nanoparticles went from nearly undetectable in respiring mitochondria to representing ~ 75% of the Fe in the fermenting organelle. These dramatic changes reflect major differences in the way that Fe is handled by the cell, depending on metabolic mode.

The chemical nature of Fe in these pools is unknown. Due to the size of NHHS Fe^{II} pool (especially in fermenting mitochondria which has ~ 150 μM NHHS Fe^{II}), protein bound Fe^{II} is insufficient to account for the overall Fe concentration and it is likely that the NHHS Fe^{II} pool is dominated by non-proteinaceous low-molecular weight complexes.

The Fe used to synthesize mitochondrial Fe/S clusters and hemes is imported into the organelle as Fe^{II} (*1*). Neither the structure nor composition of the imported complex(es) are known but they are probably of low molecular weight as they must pass through transporters in the IM. *We propose that the nonheme HS Fe^{II} ions present in fermenting mitochondria are these imported ions and that they serve in this capacity.* The simple model of Figure 3-5 assumes this role and can rationalize the observed changes in the level of this pool. During respiration, the size of the Fe^{II} pool is small

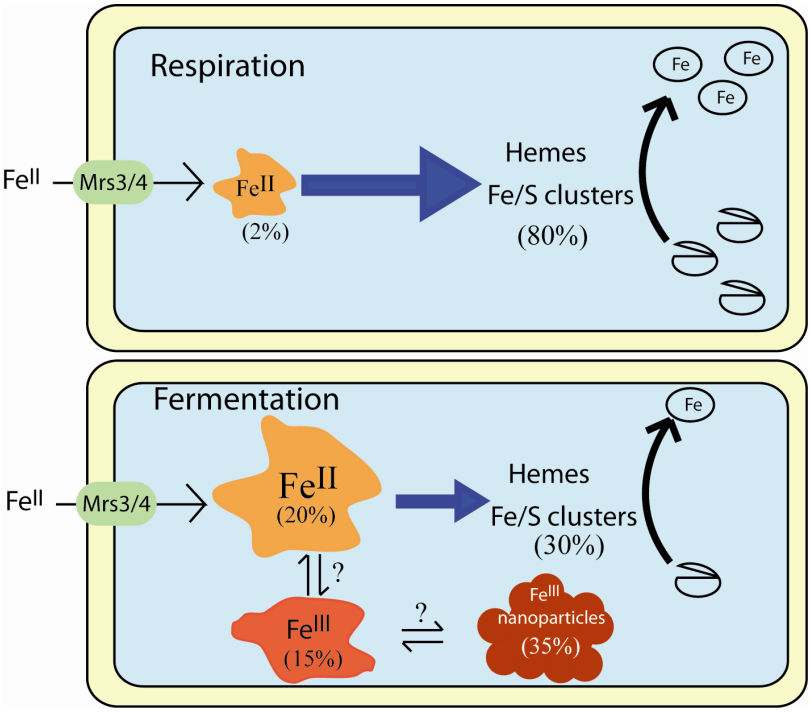

Figure 3-5: Model describing the shift in the iron content of mitochondria with metabolic growth mode. The size of the NHHS Fe^{II} pool is dictated by the balance of input and output fluxes. During respiration, the pool is small (~15 μM). When cells ferment, the rate of Fe-S cluster and heme biosynthesis declines, causing the pool to enlarge (~150 μM). The rate of import of Fe^{II} from the cytosol is not significantly affected by the change in metabolism. Under fermenting conditions, a portion of the NHHS Fe^{II} pool may become oxidized to mononuclear non-heme HS Fe^{III}, a subset of which may precipitate as Fe^{III} nanoparticles.

since the biosynthesis rates of Fe/S clusters and hemes are elevated. During fermentation, the pool increases because the rate of Fe/S cluster and heme biosynthesis is diminished. Consistent with the nearly invariant Fe concentrations in respiring and fermenting mitochondria, the overall rate of Fe^{II} import appears to be unaffected by changes in metabolic growth mode; i.e. the cell does not seem to regulate the rate of Fe^{II} import into mitochondria according to metabolic growth mode. How the other pools of Fe in fermenting mitochondria, including Fe^{III} nanoparticles, mononuclear HS Fe^{III} ions, and the central unresolved material, are related to the NHHS Fe^{II} pool remains uncertain. These pools may exist in a dynamic equilibrium with each other or they might represent independent pools (e.g. imported by different IM transporters). Also uncertain is the cellular ***function*** of these other pools. They certainly ***store*** Fe in fermenting mitochondria, and the absence of these pools during respiration suggests that they can be utilized under respiratory growth conditions. However, whether this is a cellular ***strategy*** for storing Fe, analogous to mitoferrin in human mitochondria (*42*), is uncertain. These pools may result from what might better be characterized as a "malfunction", due perhaps to an insufficient concentration of a coordinating ligand in the matrix or to a shift of either pH or oxidation status in fermenting mitochondria. We favor this characterization especially for the Fe^{III} nanoparticle pool, in that the ligands coordinating these ions are probably not protein bound and thus not under the direct genetic control of the cell. Nevertheless,

this pool may indirectly impact cellular function, e.g. by generating reactive oxygen species during its formation.

We have also observed a pool of Fe in fermenting yeast cells, namely mononuclear HS Fe^{III} ions located in a non-mitochondrial region of the cell. The concentration of this pool is high, representing ~70% of all the Fe in the whole yeast cell. Vacuole has been shown to be the iron storage organelle (*13*). A large part of these Fe^{III} species is likely located within vacuole as Fe storage.

CHAPTER IV

EPR AND MÖSSBAUER SPECTROSCOPY OF INTACT MITOCHONDRIA ISOLATED FROM YAH1P-DEPLETED *SACCHAROMYCES CEREVISIAE**

Introduction

A substantial portion of cellular Fe metabolism occurs in mitochondria. This includes the import of Fe ions from the cytosol, the assembly of iron-sulfur (Fe/S) clusters, the biosynthesis of hemes, the insertion of these Fe prosthetic groups into mitochondrial apo-proteins, and the regulation of these processes. The past decade has witnessed substantial advances in understanding the biochemical players involved in these processes (*43-46*).

Cytosolic Fe^{2+} ions are transported into the matrix compartment of the mitochondria via inner membrane (IM) transporters, including (but probably not limited to) Mrs3p and Mrs4p (*47*). Once in the matrix, the yeast frataxin homolog 1 (Yfh1p) accepts Fe^{2+} ions either directly from these transporters or from unknown intermediary Fe-donors (*43*). Yfh1p delivers Fe^{2+} ions to scaffold proteins Isu1p/Isu2p in the matrix

---

*****This chapter is reproduced with permission from: "EPR and Mössbauer Spectroscopy of Intact Mitochondria Isolated from Yah1p-depleted *Saccharomyces cerevisiae*" by Ren Miao, Marlene Martinho, Jessica Garber-Morales, Hansoo Kim, E. Ann Ellis, Roland Lill, Michael P. Hendrich, Eckard Münck and Paul A. Lindahl, ***Biochemistry*** 2008, 47, 9888-9899, copyright 2008 American Chemical Society.

for subsequent Fe/S cluster assembly. Yfh1p also delivers Fe^{2+} ions to isolated ferrochelatase for heme biosynthesis (*44*) but the physiological meaning of this remains in debate (*48, 49*). After Fe/S clusters are assembled on Isu1p/Isu2p, chaperone proteins Jac1p and Ssq1p, and the monothiol glutaredoxin Grx5p (*50*) facilitate the transfer of Fe/S clusters to mitochondrial Fe/S apo-proteins. The Fe/S cluster (ISC) assembly machinery further assists in the synthesis of an unknown species that is exported to the cytosol via the ABC type IM transporter Atm1p, where it serves to mature cytosolic Fe/S proteins.

In 1999, Barros and Nobrega (*51*) identified open reading frame *YPL252C* in *Saccharomyces cerevisiae* as the homolog to human adrenodoxin and named it *Yeast Adrenodoxin Homolog 1 (Yah1)*. Human adrenodoxin is an $[Fe_2S_2]$-cluster-containing protein that works with ferredoxin reductase to transfer electrons from NADPH to a mitochondrial P450 involved in the synthesis of pregnenolone (*51*).

Lange *et al*. (*10*) discovered that Yah1p localizes to the mitochondrial matrix and is required for mitochondrial ISC assembly. By exchanging the natural promoter of *YAH1* with a galactose-inducible promoter, *YAH1* expression levels in the strain Gal-*YAH1* could be controlled according to carbon source. When Gal-*YAH1* cells are grown on glucose, Yah1p is depleted, ISC biosynthesis is diminished significantly, and Fe accumulates. Yah1p and Arh1p may function together to provide electrons for ISC

assembly, but this has not been established. Yah1p may also function to maintain Fe in the Fe^{2+} oxidation state (*50*). The extent of Fe accumulation is time-dependent (*10*), suggesting that Yah1p-depleted cells cannot regulate Fe in mitochondria as well as wild type (WT) cells.

Yah1p is involved in the assembly of the respiratory complexes. Barros *et al.* (*52, 53*) found that Yah1p is involved in heme *a* biosynthesis. They identified a hydroxylation reaction catalyzed by the monoxygenase Cox15p, using electrons donated byYah1p and Arh1p.

Iron also accumulates in other strains of *S. cerevisiae* that lack various proteins involved in mitochondrial ISC metabolism, most notably Yfh1p (*54*). Based on Mössbauer spectroscopy and chemical analysis, Lesuisse *et al.* assigned the Fe that accumulates in mitochondria from *yfh1D* cells to ferric phosphate nanoparticles (*18*). The accumulated Fe may render these organelles hypersensitive to oxidants and promote formation of reactive oxygen species (*55*).

In humans, a deficiency of frataxin causes the neurodegenerative disease Friedreich's Ataxia (*4, 56*). Current therapy includes ingesting Fe^{3+} chelators, but this has met with only modest success (*57*). The pathogenesis of the disease has received considerable attention, and a general though not universal consensus has emerged. Frataxin might be a matrix-bound Fe carrier, accepting Fe^{2+} ions from IM transporters

and donating them to proteins that serve as entry points for Fe/S protein biosynthesis. Thus, a deficiency of this protein inhibits this transport, leading to the absence of Fe/S prosthetic groups (*4, 18*). Iron probably accumulates because feedstock Fe^{2+} ions continue to be delivered into the matrix in the absence of frataxin.

Depletion of Yah1p causes Fe to accumulate in mitochondria and it impairs Fe/S cluster (*10*) and heme *a* (*52*) biosynthesis. Since a biophysical characterization of the Fe accumulating in Yah1p-depleted strains has been lacking, we report here on the use of EPR and Mössbauer spectroscopy to establish that the Fe which accumulates in the Gal-*YAH1* mutant is aggregated as high-spin Fe^{3+} nanoparticles. We found that Fe/S cluster synthesis is significantly reduced in Yah1p-depleted mitochondria while our results regarding heme biosynthesis are less certain. We qualitatively assess the conditions responsible for Fe accumulation, determine how much Fe accumulates, evaluate the oxidation state and magnetic properties of the accumulated Fe, and show that the accumulated Fe is not chemically inert but can be reduced to the Fe^{2+} state by dithionite. Electron microscopy is employed to visualize these particles, and mechanistic chemical models are presented to help explain their formation.

Results

S. cerevisiae Gal-YAH1 cells allow the expression of *YAH1* to be controlled by the carbon source used in the growth media. Cells grown under standard fermenting conditions, using glucose as a carbon source (YPD media) and with O_2 bubbling through the media, will be called ***Yah1p-depleted/O_2***. Such conditions repress the synthesis of Yah1p. Cells grown equivalently but using galactose as a carbon source will be called ***Yah1p-replete/O_2***. These cells synthesize Yah1p and serve as the control for our experiments. Western Blot analysis (Figure 4-1, top panel) indicates that Yah1p is effectively absent in Yah1p-depleted/O_2 cell extracts (right) but is present in Yah1p-replete/O_2 (left) extracts. Cells grown on glucose (YPD media) but anaerobically under an Ar atmosphere will be called ***Yah1p-depleted/Ar***.

Analytical Characterization

Mitochondria were isolated anaerobically as described in ***Chapter II Methodology and Protocols***, with 1mM EGTA included in all buffers. EM images (Figure 4-1, lower panel) confirmed the purity of the isolated mitochondria. Mitochondria isolated from Yah1p-replete/O_2 cells consumed O_2 at a rate (Table 4-1) corresponding to 5 - 10% of that observed using mitochondria isolated from WT yeast cells grown under respiratory conditions This reduced activity may have arisen because the strain used here (W303)

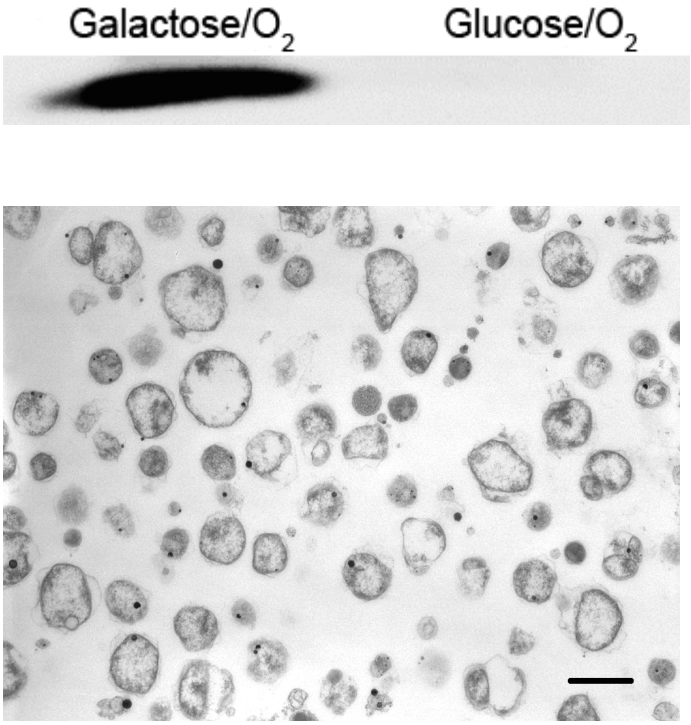

Figure 4-1: Image characterization of mitochondria. Top panel: Western blot of *S. cerevisiae* Gal-YAH1 crude extract; left, Yah1p-replete/O_2; right, Yah1p-depleted/O_2. Bottom panel: Electron micrographs of Yah1p-replete/O_2 mitochondria collected from a Nycodenz gradient. Sections were post stained with uranyl acetate and lead citrate. Bar = 1 μm.

Table 4-1: Analytical characterization of mitochondria isolated from *S. cerevisiae* Gal-*YAH1* cells. Metal and protein values are for packed samples in which the volume due to external solvent (assumed to be 90% (*58*)) has been removed, and corrections due to turbidity effects were included. For O_2 consumption, the estimated relative error was 20%.

	Fe (μM)	Cu (μM)	Mn (μM)	Zn (μM)	O_2 consumption (nmol O_2/min/mg protein)	Protein (mg/mL)
Yah1p-replete/O_2	1190 ± 100	110 ± 30	35 ± 5	240 ± 15	11	81 ± 10
Yah1p-depleted/O_2	7400 ± 400	50 ± 15	70 ± 10	480 ± 35	3	90 ± 6
Yah1p-depleted/Ar	1250 ± 350	40 ± 5	10 ± 5	540 ± 70	ND[a]	83 ± 8

[a], ND: Not Determined.

differed from that used by Hudder *et al.* (*58*), (D273-10B) (*59*). Cells grown on galactose are in a mixed respiration-fermentation mode (*60*) (respiro-fermenting mode) whereas cells grown on lactate, the carbon source used by Hudder *et al.* (*58*), are entirely in respiration mode. These differences are likely to have lowered the relative rate of O_2 consumption in the Yah1p-replete/O_2 mitochondria used in this study.

The rate of O_2 consumption for Yah1p-depleted/O_2 mitochondria (Table 4-1) was lower still. The rate could have been higher with galactose because it is a de-repressing sugar, i.e., it induces respiration. The reduced rate of O_2 consumption for Yah1p-depleted/O_2 mitochondria is consistent with previous results (*10*) showing that Fe/S cluster assembly is impaired when Yah1p is depleted such that respiratory complexes should be largely absent or inoperative.

Metal and protein concentrations of these tightly packed samples were determined (Table 4-1). Fe concentrations in mitochondria isolated from Yah1p-replete/O_2 and Yah1p-depleted/Ar cells were the same within the uncertainties of the measurements (~ 1.2 ± 0.3 mM). This is either equivalent to, or somewhat higher than, the average Fe concentration in mitochondria from WT respiring cells (0.8 ± 0.2 mM) (*58*). In contrast, the Fe concentration in mitochondria isolated from Yah1p-depleted/O_2 cells was far higher (namely 7.4 ± 0.4 mM), indicating significant Fe accumulation. Assuming that Fe

is regulated within the mitochondria, the regulatory mechanism seems to malfunction in the absence of Yah1p, but only when Yah1p-depleted cells are grown under O_2.

Depleting cells of Yah1p had little effect on protein concentration in the mitochondria, but doing so did influence mitochondrial Cu, Mn, and Zn concentrations, lowering [Cu] ~ 2-fold, and raising [Mn] and [Zn] ~ 2-fold (Table 4-1). Growing Yah1p-deleted cells anaerobically had little effect on [Cu] or [Zn], relative to the equivalent cells grown aerobically, but [Mn] was reduced ~ 7-fold under these conditions. The majority of Mn ions in the mitochondria appear to be bound to Sod2p; the expression of *sod2* has been reported to be reduced by a similar factor under anaerobic growth conditions (*61*).

Mössbauer and EPR Spectroscopy of Yah1p-Replete/O_2 Mitochondria

Isolated intact mitochondria were either packed directly into Mössbauer and EPR sample holders (yielding the ***as-isolated*** state), or packed after treatment with a reductant (sodium dithionite at pH 8.5 for ~1 hour) or an oxidant (1 atm pure O_2 for ~ 30 min exposure). These latter states will be called ***dithionite-treated*** and ***O_2-treated,*** respectively.

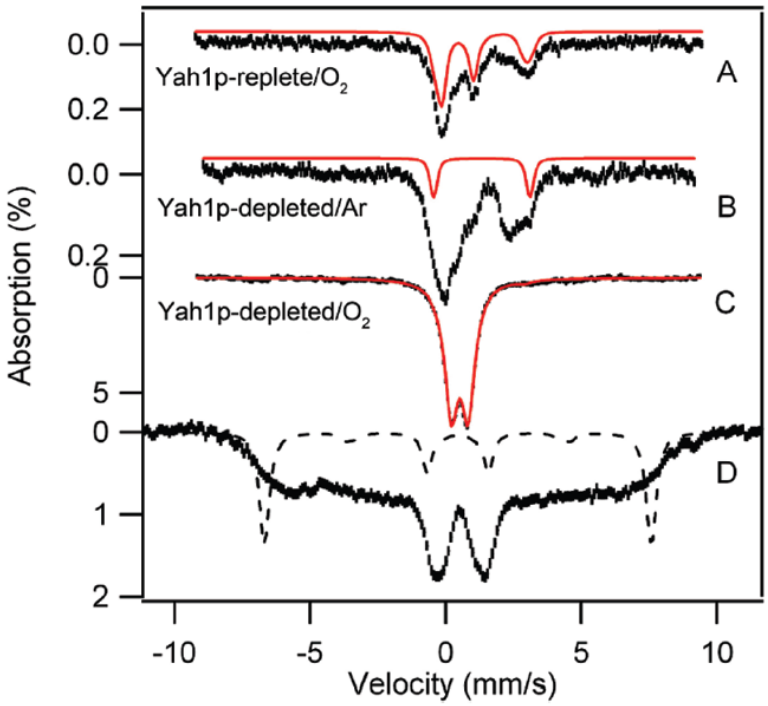

Figure 4-2: 4.2 K Mössbauer spectra of Gal-YAH1 mitochondria samples. (A) Yahp1-replete/O_2 mitochondria. The solid red line outlines the sum of two major doublets, representing 70% of the iron. (B) Yah1p-depleted/Ar mitochondria. The doublet drawn above the data outlines a high-spin ferrous species with ΔE_Q = 3.55 mm/s and δ = 1.33 mm/s. (C) Yah1p-depleted/O_2 mitochondria. The solid red line is a quadrupole doublet with ΔE_Q = 0.62 mm/s and δ = 0.52 mm/s. (D) Yah1p-replete/O_2 mitochondria of (C) studied in an 8.0 T parallel field. If the material of (C) would represent magnetically isolated Fe^{3+} ions, one would expect a spectrum as outlined by the dashed black line; for the simulation we used $A/g_n\beta_n$ = - 21 T for the ^{57}Fe magnetic hyperfine coupling constant (this A-value is appropriate for ferric phosphate).

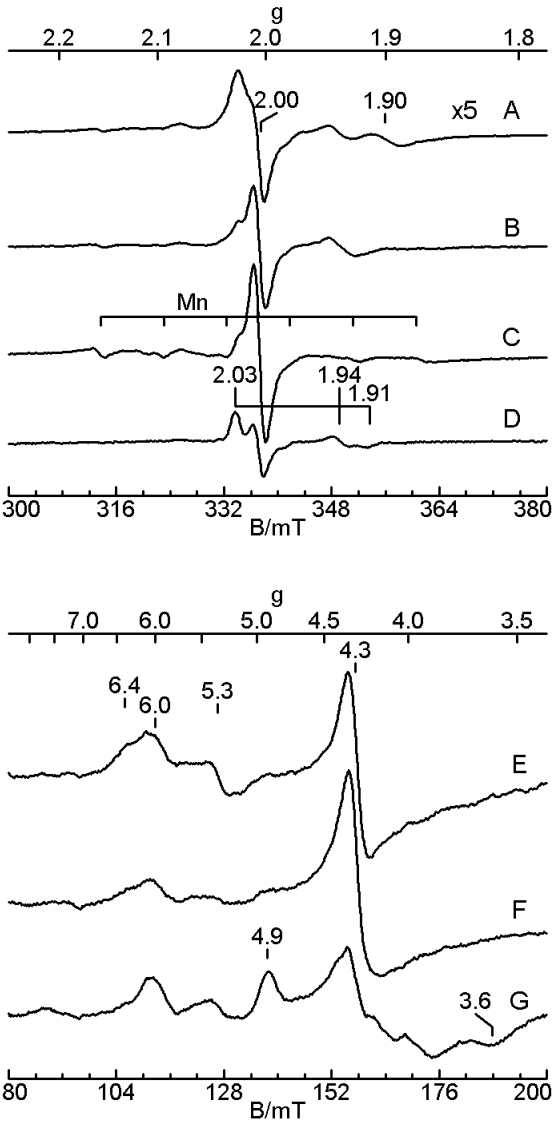

Figure 4-3: High-field (top) and low-field (bottom) EPR spectra of mitochondria isolated from Gal-YAH1 cells grown under various conditions and prepared in the as-isolated state. (A, B, E) Yahp1-replete/O_2; (C, F) Yah1p-depleted/O_2; (D, G) Yah1p-depleted/Ar. EPR parameters: temperature, 10 K; microwaves, 9.46 GHz, 20mW (A, E-G), 0.2 mW (B-D).

As-isolated mitochondria from Yah1p-replete/O_2 cells exhibited 4.2 K Mössbauer spectra (Figure 4-2A) similar to those of WT mitochondria grown under aerobic respiring conditions (*58*), in the sense that there are two major doublets, with $\Delta E_Q \approx 1.15$ mm/s; $\delta \approx 0.45$ mm/s (roughly 30% of Fe) and $\Delta E_Q \approx 3.3$ mm/s; $\delta \approx 1.35$ mm/s (roughly 40% of Fe). These doublets belong to (predominantly) $[Fe_4S_4]^{2+}$ clusters and high-spin Fe^{2+}, respectively. The superposition of these two doublets is outlined by the solid line drawn above the data.

Yah1p-replete/O_2 mitochondria prepared in the as-isolated state exhibited three EPR signals in the high-field region (Figure 4-3, A and B). One signal was isotropic with g = 2.005, the second was rhombic (g = 2.03, 1.94, and 1.91) with g_{ave} = 1.94, and the third was from aqua-Mn^{2+} with g = 2.00 and a magnetic hyperfine constant a = 9 mT. Quantitative analysis indicated spin concentrations of 1.2 μM (g_{ave} = 1.94) and 1 μM (Mn). The first signal may arise from a radical species, while the second probably originates from the $[Fe_2S_2]^{1+}$ cluster of succinate dehydrogenase (*58*). At higher power (Figure 4-3A), an additional resonance is observed at g = 1.90, which likely arises from the Rieske $[Fe_2S_2]^{1+}$ cluster from cytochrome bc_1 (g = 2.03, 1.90, 1.76), with the other resonances obscured by other species. The concentration of the $[Fe_2S_2]^{1+}$ cluster of succinate dehydrogenase from the Yah1p-replete/O_2 sample is reduced by an order of magnitude relative to mitochondria obtained from WT cells grown under respiring

conditions (*58*). This is consistent with the lower O_2 consumption observed for Yah1p-replete/O_2 mitochondria. As discussed above, such differences may be caused by differences in cell strain and/or growth conditions.

In the low-field region, as-isolated Yah1p-replete/O_2 mitochondria exhibited two EPR signals that arise from high-spin ferric hemes (Figure 4-3E). These signals contribute at $g_{x,y}$ = 6.4, 5.3 (E/D = 0.022) and $g_{\perp}$ = 6.0 (E/D = 0), with spin concentrations of 0.6 μM and 0.3 μM, respectively. Previously we have assigned both signals to a partially reduced state of the a:a_3 active site of cytochrome *c* oxidase in which heme a_3 is high-spin Fe^{3+} and Cu_b is in the 1+ state (*58*). The presence of these signals and the Fe/S signals in the g = 2 region indicates that Gal-*YAH1* cells synthesize Fe/S clusters and heme centers when grown under conditions in which Yah1p is induced. The signal at g = 4.3 is from a high-spin, non-heme Fe^{3+} species with rhombic symmetry (E/D ~ 1/3); it has a spin concentration of less than 1 μM. We cannot identify the coordination environment of such species from its EPR signal alone, but it is probably dominated by oxygen or nitrogen donor atoms.

Mössbauer and EPR Spectroscopy of Yah1p-Depleted/O_2 Mitochondria

The 4.2 K Mössbauer spectra of as-isolated mitochondria from Yah1p-depleted/O_2 cells (sample A, Figure 4-2C) were fundamentally different than those of Yah1p-

replete/O_2 cells. The spectrum of Figure 4-2C exhibits a single quadrupole doublet with $\delta \approx 0.52(2)$ mm/s, $\Delta E_Q \approx 0.62(3)$ mm/s (line-width $\Gamma \approx 0.55$ mm/s, full width at half maximum). Fe^{2+} species are below detection limit of Mössbauer spectroscopy. The observation of a broadened quadrupole doublet at 4.2 K, rather than a spectrum exhibiting paramagnetic hyperfine structure, indicates the presence of ***aggregated*** ferric ions. The doublet of Figure 4-2C was essentially identical to that observed for the *S. cerevisiae* (frataxin) deletion strain *yfh1*Δ. Based also on chemical analysis and (unpublished) EXAFS data, Lesuisse and coworkers have assigned the doublet of mitochondria from *yfh1D* cells to ferric phosphate nanoparticles (*18*).

Although sample A and the Yah1p-replete/O_2 sample described above were prepared and packed similarly into Mössbauer cuvettes, the spectral intensities of these samples differed significantly. On this basis, the ^{57}Fe concentration of the Yah1p-depleted/O_2 sample was roughly 10 times higher than that of the Yah1p-replete/O_2 sample, indicating that ferric ions accumulate in this mutant under aerobic growth conditions when Yah1p is depleted. This result is congruent with the analogous Fe concentrations determined by ICP-MS (see above). Using Mössbauer spectroscopy, we found no evidence for significant amount of ferric nanoparticles in the Yah1p-replete/O_2 sample of Figure 4-2A.

Figure 4-2D shows a Mössbauer spectrum of sample A recorded at 4.2 K in an applied magnetic field of 8.0 T. While the largest magnetic splitting observed is reminiscent of high-spin Fe^{3+}, the overall spectral shape reflects a distribution of magnetic hyperfine fields typically associated with a heterogeneous distribution of ferric nanoparticles. Although we do not fully understand the origin of these spectral features, some aspects are apparent. First, if the Fe yielding the doublet of Figure 4-2C were mononuclear non-aggregated Fe^{3+} (e.g. the type of iron yielding g = 4.3 or g = 6 EPR resonances), the 8.0 T spectrum would closely resemble the theoretical curve indicated by the dashed line. The spectrum of Figure 4-2D is readily synthesized by summing *ca*. 5 spectra of high-spin ferric species with different ^{57}Fe magnetic hyperfine coupling constants, corresponding to hyperfine fields from ≈ 10 - 52 T; however, in the absence of a physical model that considers very small, disordered nanoparticles that elaborate heterogeneous exchange interactions, such fits are not meaningful. Second, for ferromagnetically or antiferromagnetically ordered polycrystalline materials well-defined 6-line patterns can be observed below the Curie or Néel point (e.g. crystalline ferric phosphate is an antiferromagnet yielding a sharp 6-line spectrum at 4.2 K (*62*)). For nanoparticles an additional phenomenon is observed. As the temperature of the nanoparticles is raised, the thermal energy becomes comparable to the energy required to flip the bulk magnetic moment of the nanoparticle, giving rise to superparamagnetic

relaxation; e.g. see (*63*). For sufficiently fast flip rates (roughly > 10^8 s^{-1}) the ^{57}Fe magnetic hyperfine interactions average to zero and a quadrupole doublet is observed. In a population of nanoparticles with variable size, the smaller particles produce a quadrupole doublet at lower temperature. The temperature at which half of the iron in the sample exhibits a quadrupole doublet is called the blocking temperature T_B. The blocking temperature is specific to the time scale of measurement; e.g. T_B (Mössbauer) < T_B (EPR).

For the nanoparticles of Figure 4-2 C and D the blocking temperature must be well below 4.2 K, similar to an iron component observed in *Mycoplasma capricolum* cells (*64*). At 4.2 K, the latter exhibits a doublet identical to that observed in Figure 4-2C. The *M. capricolum* iron component has a blocking temperature near 2 K and yields a reasonably well defined 6-line pattern at T = 0.07 K. However, the *M. capricolum* magnetic hyperfine field, $B_{hf} \approx 43$ T, is distinctly smaller than the largest, and main, component, $B_{hf} = -52$ T, of the spectrum of Figure 4-2D, suggesting that the iron components observed for *M. capricolum* and Yah1p-depleted/O_2 cells differ in spite their identical E_Q and values.

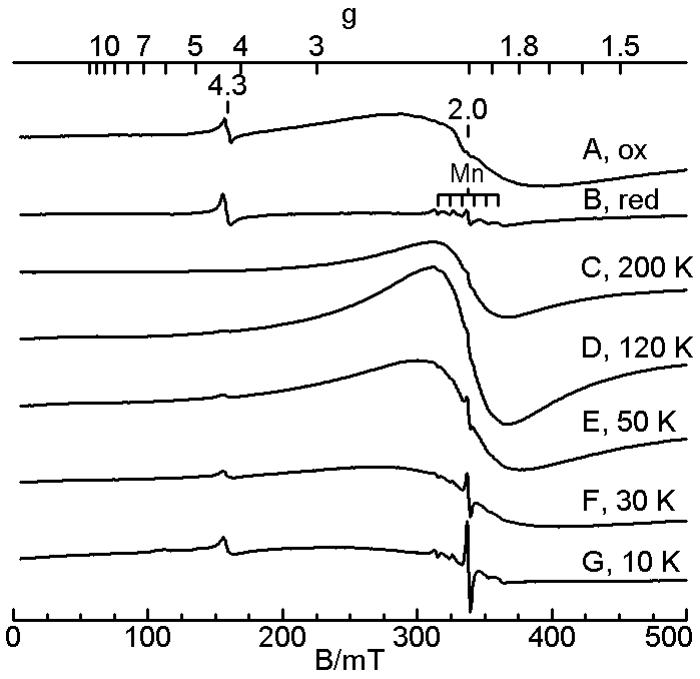

Figure 4-4: EPR spectra of Yah1p-depleted/O_2 mitochondria collected at different temperatures and in different redox states. (A) oxidized, 30 K; (B) reduced 30 K; (C-G) as-isolated, recorded at stated temperatures. EPR conditions: microwaves, 9.46 GHz, 20 mW.

Microcrystalline ferric nanoparticles often yield characteristic EPR spectra with features distinctly different from those observed for magnetically isolated Fe^{3+} ions (*65, 66*). Therefore, we have examined a Yah1p-depleted/O_2 sample with variable temperature EPR to search for such characteristics. A set of X-band spectra obtained at different temperatures is shown in Figure 4-4. Most prominent is a broad feature centered around g = 2. Such features have been shown to originate from fast thermal fluctuations of the magnetization of nanoparticles (referred to as superparamagnetic relaxation as it involved the magnetic moment of the entire particle) that average out anisotropic interactions. (For antiferromagnets the bulk magnetic moments results from uncompensated sublattice magnetizations.) Thus, this type of resonance is best observed at higher temperatures; at lower temperatures the thermal fluctuations are reduced and the amplitude of the $g \approx 2$ resonance declines, as observed here. The detailed shapes of the resonances depend strongly on shape and size distributions and on the magnetic properties of the particles. For the present study it is sufficient to note that the broad features around g = 2 are characteristic of superparamgnetic relaxation and present in the same state for which we observed the "nanoparticle" Mössbauer spectra of Figure 4-2C and D.

Other EPR Features of Mitochondria from Yah1p-Depleted/O_2 Cells

Although the focus of this study is on the superparamagnetic nanoparticles just described, mitochondria from Yah1p-depleted/O_2 cells exhibited other EPR features that contribute to their characterization. At 10 K, as-isolated Yah1p-depleted/O_2 mitochondria exhibited a 50% increase of the radical signal at g = 2.005 (Figure 4-3C). The concentration of the aqua-Mn^{2+} species (4 μM) increased 4-fold relative to that in the Yah1p-replete/O_2 sample. The broad nanoparticle signal is less evident in Figure 4-3C than in Figure 4-4 due to lower microwave power and reduced sweep width. The g_{av} = 1.94 signal was not detectable, indicating a significant decrease in the Fe/S clusters, and consistent with lower synthesis of these clusters in Yah1p-depleted/O_2 cells. This supports previous reports that Yah1p is required for Fe/S cluster assembly (*10*).

The low-field region of mitochondrial samples isolated from Yah1p-depleted/O_2 cells shows the same signal at g = 4.3 (Figure 4-3F) and at the same concentration as that observed in Yah1p-replete/O_2 samples. The g = 4.3 signal arises from magnetically isolated Fe^{3+} species and not from ferric nanoparticles. This EPR region also exhibited the signals from the two high-spin Fe^{3+} heme centers (with g = 6.4, 5.3, and g = 6.0). Compared to the corresponding signals observed from Yah1p-replete/O_2 mitochondria, the concentrations of these species are *ca*. 50% lower. This is consistent with previous

results showing that Yah1p is involved in heme *a* biosynthesis (*52, 53*), and with the known repression of heme synthesis under these conditions (*49*).

Electron Microscopy of Yah1p-Depleted/O_2 Mitochondria

The observation of nanoparticles observed by Mössbauer and EPR spectroscopy prompted us to collect STEM images as described in *Experimental Procedures*. In such images, brightness is directly related to the concentrations and atomic numbers of the contributing elements. High magnification STEM images of as-isolated Yah1p-depleted/O_2 mitochondria (Figure 4-5A) reveal bright punctate structures with diameters of 2-4 nm that associate into larger clumps. EDX spectra were collected within the boxed area, and transitions from C, Fe, O and P elements were observed. EDX mapping (Figure 4-5A) indicates that Fe, O and P concentrations maximize together (with roughly equimolar amounts of Fe and P) and co-localize with the punctate structures. Based on this analysis, as well as on the observed Mössbauer and EPR properties, we conclude that Fe in Yah1p-depleted mitochondria accumulates as 2-4 nm diameter ferric nanoparticles that weakly self-associate into larger clumps and are associated with phosphate ions in roughly a 1:1 molar ratio. Such ions are present in mM concentration in the mitochondrial matrix (*67*). Further studies are required to establish the exact composition of this material.

Figure 4-5: STEM-HAADF images of Yah1p-depleted/O_2 mitochondria in as-isolated (A) and dithionite-reduced (B) states. Image AIII is a magnified view of the region within the box shown in image AII. Image AII is a magnified view of the region within the box shown in AI. In these dark field images the contrast is reversed, so that a dark feature in a bright field transmission electron microscopy image may look bright. Those Z-contrast images collected from highly scattered electrons show distinct brightness in the high Z (atomic number) area with high spatial resolution. In addition, the combination of STEM and EDX also allows compositional analysis of a nanometer-scale area. In fact, when an EDX spectrum was obtained from the red-box area Fe, P, and O elements were the only clearly detected elements other than carbon. To see the spatial distribution of each element, elemental maps for Fe, P, and O are presented together after collection with a proper energy window assigned to the KR X-ray fluorescent transition of each element. They were acquired from a region similar but not identical to that within the box of image IA. In these pixelated elemental maps the brighter pixel indicates a higher concentration of the element. Therefore, comparison of the micrographs and the maps shows that the brightness in the STEM image is generally proportional to the concentration of the three elements.

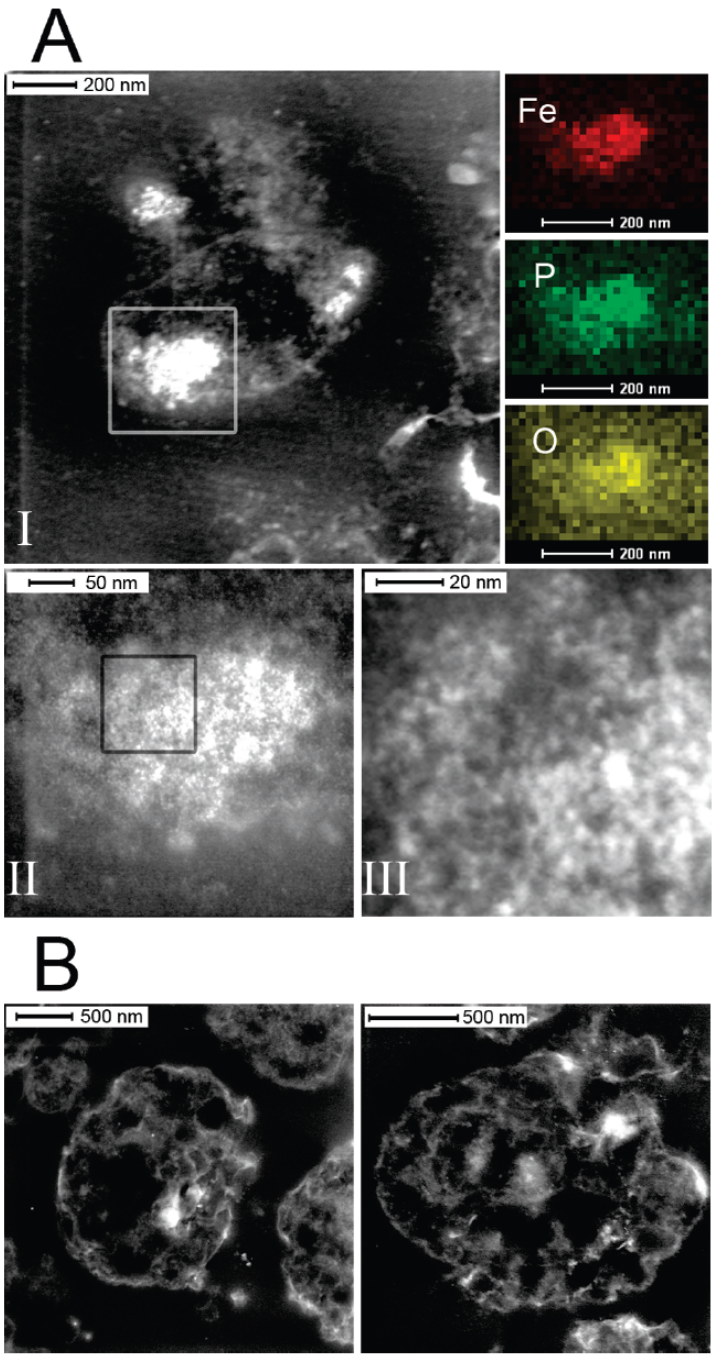
A
200 nm
Fe
200 nm
P
200 nm
O
200 nm
I
50 nm
20 nm
II
III
B
500 nm
500 nm

Oxyblot™ Assay

The iron that accumulates in mitochondria of the Yah1p-depleted/O_2 cells is very similar, in terms of Mössbauer properties, to that in *yfh1D* mitochondria. Organelles from the latter mutant also contain nanoparticles, attributed to ferric phosphate (*18*). The homologous mutation in human fibroblasts reportedly accumulates mitochondrial nanoparticles in the form of ferrihydrite (*68*). We wondered whether these similarities extended to the effects on reactive oxygen production. Bulteau *et al*. 2007 (*55*) reported greater oxidative damage in *yfh1D* mitochondria than in WT mitochondria. To evaluate the relative extent of oxidative damage in our system, mitochondria isolated from Yah1p-replete/O_2 and Yah1p-depleted /O_2 cells were subjected to the Oxyblot™ assay. As shown in Figure 4-6, the extent of oxidatively carbonylated proteins in extracts of mitochondria isolated from Yah1p-depleted/O_2 cells (Lane 2) is greater than that in equivalent extracts from Yah1p-replete/O_2 mitochondria (Lane 4). This indicates that mitochondria depleted in Yah1p (from cells grown under an O_2 atmosphere) generate more reactive oxygen species than do mitochondria replete with Yah1p.

Treatment of Yah1p-Depleted/O_2 Mitochondria with Dithionite

After recognizing that the as-isolated sample of Yah1p-depleted/O_2 mitochondria contained ferric nanoparticles, we wondered to what extent the iron of these particles

could be dissolved by treating intact mitochondria with a suitable reductant. To examine this, a sample of Yah1p-depleted/O_2 mitochondria was divided in two, and the control half was packed into a Mössbauer cup by centrifugation and then frozen. The other half was treated with dithionite as described in *Experimental Procedures*, and then packed by centrifugation (yielding also a supernatant fraction that was discarded in this experiment) and frozen. In both cases, the volume of the packed samples was ~ 250 μL.

The control half (Sample A) exhibited the spectra of Figure 4-2C and D, while the dithionite-treated sample (Sample B) exhibited the 4.2 K spectrum of Figure 4-7A. The spectrum of sample B exhibits a new component representing 90% of Fe with ΔE_Q = 3.55(4) mm/s and δ = 1.33(2) mm/s. The nature of the remainder of the absorption is not clear, but is not due to ferric nanoparticles. This doublet, with parameters characteristic of high-spin Fe^{2+}, was observed in four separate experiments. The observation of one ferrous doublet with well defined parameters suggests that the Fe^{2+} is bound in a specific complex, rather than to heterogeneous ligand environments as is often the case with adventitiously bound Fe^{2+}.

Interestingly, as judged by Mössbauer spectroscopy the amount of total iron in sample B was four-fold less than that observed in sample A. This suggests that ferrous ions are exported out of mitochondria during incubation with dithionite and then removed with the buffer in the centrifugation stage. Whether the Fe is exported through

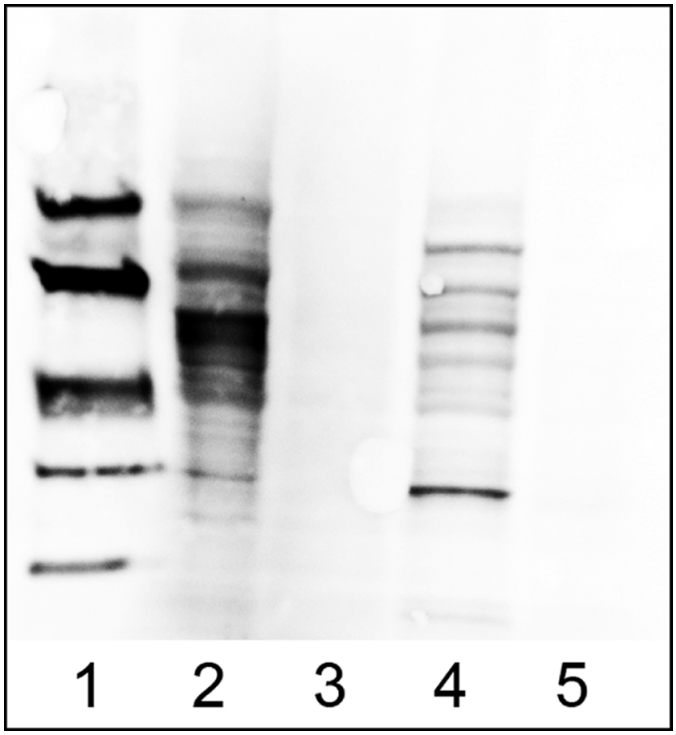

Figure 4-6: Oxyblot assay of Yah1p-depleted/O_2 and Yah1p-replete/O_2 SDS-solubilized mitochondrial extracts. From left to right: lane 1, Oxyblot molecular weight standards corresponding to (from top to bottom) 97.4, 68, 43, 29, and 21 kDa, respectively; lane 2, Yah1pdepleted/O_2; lane 3, Yah1p-depleted/O_2, negative control with no DNPH added; lane 4, Yah1p-replete/O_2; lane 5, Yah1p-replete/O_2, negative control with no DNPH added. Equivalent amounts (15 μg) of mitochondrial proteins were loaded onto lanes 2-5.

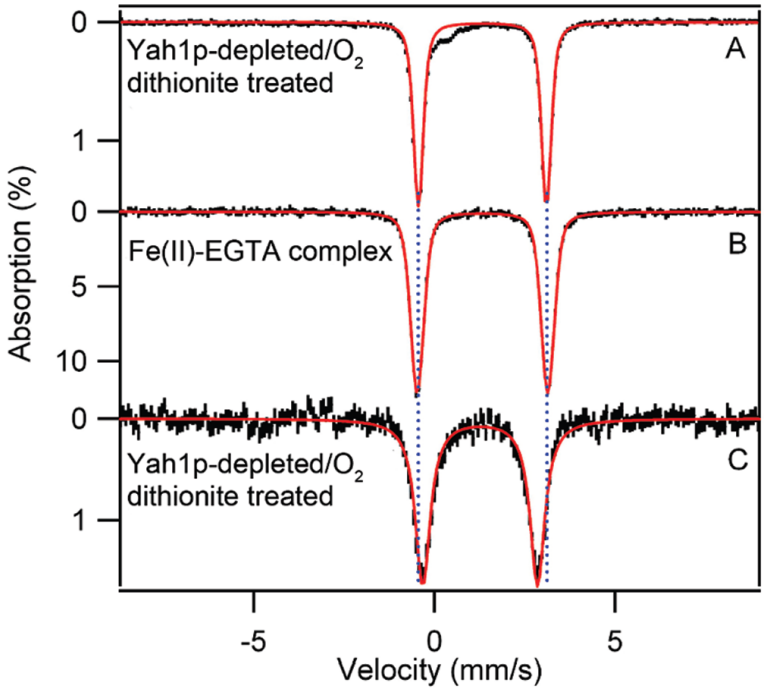

Figure 4-7: 4.2 Mössbauer spectra of dithionite-treated mitochondria (A, C) and Fe^{2+}-EGTA complex (B) recorded in 40 mT magnetic field. (A) Dithionite-treated Yah1p-depleted/O_2 mitochondria (sample B), prepared in buffer containing EGTA; line width Γ_V = 0.25 mm/s. (B) Fe^{2+}-EGTA complex in sorbital/tris buffer, as described in Experimental Procedures; Γ_V = 0.40 mm/s. (C) Dithionite-treated Yah1p-depleted/O_2 mitochondria in EGTA-free buffer; Γ_V = 0.60 mm/s. The solid lines are simulations assuming that the main feature is described by one quadrupole doublet. In all cases we have used Voigt profiles which assume distributions in ΔE_Q; Γ_V = 0.40 mm/s is a Voigt shape obtained by convoluting a Lorentzian of 0.15 mm/s full width into a Gaussian of full width σ_G = 0.40 mm/s. Vertical lines mark the positions of the doublet in the top panel.

a leaky IM, possibly arising from an Fe-induced membrane permeability transition (*69*), or through an IM transporter, is unknown.

We have attempted to identify the ΔE_Q = 3.55 mm/s species. The parameters ΔE_Q = 3.55 mm/s and δ = 1.33 mm/s are unlike those observed for $Fe^{2+}(H_2O)_6$ coordination environments; the latter typically yield $\Delta E_Q \approx 3.15 - 3.35$ mm/s and $\delta \approx 1.38$ mm/s (*70*). This prompted us to test various components contained in the mitochondria or in the buffer used (see APPENDIX I for this supplementary information). Fe^{2+}-phosphate and Fe^{2+}-ATP complexes did not yield similar Mössbauer parameters. However, as shown in Figure 4-7B, EGTA-containing buffer gave a $\Delta E_Q \approx 3.62$ mm/s, $\delta \approx 1.33$ mm/s component, suggesting that the doublet observed in Figure 4-7A may arise from the Fe^{2+}-EGTA complex. This interpretation is supported by the observation that dithionite-treated mitochondria lacked the ΔE_Q = 3.55 mm/s species when EGTA was omitted from the buffer; instead, a doublet with $\Delta E_Q = 3.17(3)$ mm/s and $\delta = 1.26(1)$ mm/s was observed (Figure 4-7C). We cannot identify the coordinating ligand(s) of these ions from Mössbauer parameters alone. EPR spectra of dithionite-treated Yah1p-depleted/O_2 mitochondria were also examined. Such samples essentially lacked the broad $g \approx 2$ resonance attributed to ferric nanoparticles (Figure 4-4B).

It has been reported that EGTA does not to penetrate the mitochondrial IM (*71*). This would suggest that some or all of the species of Figure 4-7A is *external* to the

mitochondria, perhaps contained in the buffer remaining after centrifugation following dithionite incubation. Indeed we have examined this supernatant fraction by Mössbauer and found that it contained high-spin Fe^{2+} ions. We have also studied the ΔE_Q= 3.55 mm/s species observed in dithionite-treated mitochondria, as well as the Fe^{2+}-EGTA buffer complex of Figure 4-7B, in strong applied magnetic fields (not shown). The high-field spectra of the Fe^{2+} components were quite similar and exhibited no indication that the Fe^{2+} species of Figure 4-7A and B are associated with nanoparticles.

STEM-HAADF images of dithionite-treated Yah1p-depleted/O_2 mitochondria also indicated substantially fewer nanoparticles (Figure 4-5B) and suggested that the resulting material is dominated by phosphorus atoms (Fe:P ratio of 1:9). It would not be surprising if some residual nanoparticles remained after dithionite treatment, as our Mössbauer results suggest that the extent of reaction with dithionite is somewhat variable (60% - 100% reduction). The extents of reduction evident from the spectra shown in Figure 4-7 A and C were the greatest achieved in our four attempts.

An EPR spectrum of dithionite-treated Yah1p-depleted/O_2 mitochondria is shown in Figure 4-4B. The spectrum lacks the broad EPR feature of Figure 4-4F, indicating that dithionite reduced the Fe^{3+} of the nanoparticles, but it exhibited an aqua-Mn^{2+} signal with the same intensity as exhibited by as-isolated Yah1p-depleted/O_2 mitochondria (Figure 4-4F). We suspect that the Mn^{2+} ions are located within the mitochondria,

because they were not removed during isolation in EGTA-containing buffer. The presence of the Mn^{2+} signal in dithionite-treated and untreated mitochondria suggests that in contrast to the behavior observed with Fe^{2+} ions, the Mn^{2+} ions are not displaced from the mitochondria upon treatment with dithionite. The chelator EGTA is also present in these samples, but it must not be interacting with the Mn^{2+} ions, since chelation of Mn^{2+} by EGTA would result in loss of the sharp 6-line hyperfine pattern at g = 2 (*72*). This suggests that Fe^{2+} ions were not removed from dithionite-treated Yah1p-depleted/O_2 mitochondria due to a leaky IM.

The intensity of the g_{ave} = 2.005 signal declined with dithionite-treatment (Figure 4-4B). Dithionite can penetrate phospholipid bilayer membranes and reduce species contained therein (*73*, *74*); perhaps it reduced the species with g_{ave} = 2.005. The corresponding region of an O_2-treated Yah1p-depleted/O_2 mitochondria sample lacked a strong g_{ave} = 2.005 signal (Figure 4-4A), suggesting that this signal arises from species that can be oxidized into EPR-silent states.

Mössbauer and EPR Spectroscopy of Yah1p-Depleted/Ar Mitochondria

Iron is presumably imported into the mitochondria in the ferrous state (see *Introduction*) suggesting that an oxidant is required to form ferric nanoparticles. To explore the possibility that the O_2 used in the cell growth was involved, we grew Gal-

YAH1 cells using glucose as a carbon source (to repress the synthesis of Yah1p) under a strict argon atmosphere. In this case, the iron concentration of the isolated mitochondria was comparable to that of isolated Yah1p-replete/O_2 mitochondria and ~ 6-fold less than that of Yah1p-depleted/O_2 mitochondria. Thus, Fe did not accumulate when Yah1p-depleted cells were grown anaerobically. The 4.2 K Mössbauer spectrum of Yah1p-depleted/Ar mitochondria (Figure 4-2B) also indicated an ^{57}Fe concentration 8-to-10-fold less than that observed for Yah1p-depleted/O_2 mitochondria, but similar to that of Yah1p-replete/O_2 mitochondria. The difference in these fold-reductions may reflect differences in the methods (ICP-MS or Mössbauer) used. As seen in Figure 4-2B, ~60% of the Mössbauer absorption belongs to a group of doublets with parameters typical of high-spin Fe^{2+}. One doublet, with $\Delta E_Q \approx 3.6$ mm/s (solid line in Figure 4-2B) might arise from the Fe^{2+}-EGTA complex residing in the buffer, though this requires further investigation. Most, if not all, of the remaining iron in the sample belongs to unidentified ferric species. The spectrum of Figure 4-2B provides no evidence for ferric nanoparticles or $[Fe_4S_4]^{2+}$ clusters; if present, they account for no more than 10% and 15% of the total Fe, respectively.

At 10 K, as-isolated Yah1p-depleted/Ar mitochondria exhibited an EPR spectrum in the high-field region (Figure 4-3D) that is similar to WT mitochondria (see Figure 4-6A of (*58*)), but with more than a 10-fold decrease in the intensity of all signals. The

spectrum is not dominated by the g = 2.005 radical signal. The g_{ave} = 1.94 signal ($[Fe_2S_2]^{1+}$ cluster of succinate dehydrogenase) is 2-fold less intense than in spectra of Yah1p-replete/O_2 mitochondria. This suggests that Fe/S cluster assembly is attenuated under anaerobic growth conditions in Yah1p-depleted mitochondria. The resonance at g = 2.03 appears to have a contribution from oxidized $[Fe_3S_4]^{1+}$ clusters (<0.5 μM).

In the low-field region (Figure 4-3G), the spectrum shows signals from heme centers in similar amounts to that of Yah1p-replete/O_2 mitochondria (Figure 4-3E), showing that hemes are present in mitochondria from Gal-*YAH1* cells grown under anaerobic conditions. This is unexpected, because heme biosynthesis is O_2-dependent and transcriptionally repressed under low O_2 pressures (*45*). Several studies (*75-77*) suggest that anaerobically grown yeast cells synthesize a considerable amount of heme and hemoproteins, comparable in some reports to that synthesized under aerobic conditions. Trace amounts of O_2 could have been present during the growth or harvesting of these nominally anaerobic cells, and such miniscule amounts might have been sufficient for heme synthesis (*75*). Interestingly, additional new signals are observed at g = 4.9 and 3.6. Signals in this region are not common and at present we are unable to assign them. Simulations suggest that the resonances originate from an S = 5/2 system with E/D = 0.23, and if so, the concentration of this species would be ~ 3 μM.

Conclusion

In this study we have characterized mitochondria from the Gal-*YAH1* strain of *S. cerevisiae* using EPR and Mössbauer spectroscopy, focusing on the Fe that accumulates when the strain is grown on glucose/O_2. When grown in this manner, cells are depleted in Yah1p, a ferredoxin required for Fe/S cluster assembly. Our results show that the mitochondria in these cells accumulate Fe in the form of aggregated ferric nanoparticles that contain iron and phosphate ions in approximately equimolar amounts. Nanoparticles with the same ΔE_Q and δ values were observed for *yfh1D and were previously assigned to ferric phosphate.* The exact composition of this material remains uncertain, but ferrihydrites tend to have somewhat larger ΔE_Q values, 0.67-0.85 mm/s, and smaller δ values, $\approx$ 0.48 mm/s, than was observed. When the same strain is grown on galactose, cells are replete with Yah1p and thus serve as a control in our study. We have no evidence for the presence of accumulated Fe^{3+} nanoparticles in the mitochondria isolated from these cells; if present they would account for < 8% of the total Fe.

Reducibility of Nanoparticles

Upon removal of O_2 and incubation of mitochondria in dithionite-containing buffer, the ferric nanoparticles were reductively dissolved. We are unaware of published reports indicating that the precipitated material in any other strain (e.g. *yfh1*Δ) could be reduced,

but we suspect that it can. The ability to reduce this material in Yah1p-depleted/O_2 mitochondria shows a potential efficacy of removing precipitated Fe^{3+} by reductive dissolution at the particle surface and then chelating the more soluble Fe^{2+} form from the cytosol. Kaplan and coworkers have reported that the aggregated material in mitochondria from Yfh1p-depleted cells can be eliminated by expressing *YFH1* (40), suggesting that Yfh1p directly or indirectly promotes the reduction of the aggregated material and its export from or utilization by the mitochondria.

Similarity to the yfh1D Phenotype

The Fe that accumulates as ferric nanoparticles in mitochondria of Yah1p-depleted/O_2 cells has the same Mössbauer spectrum, within the signal/noise, as that observed in mitochondria from *yfh1D* cells (*18*). Another aspect of what appears to be a shared phenotype is an increase in oxidative damage, relative to WT cells, as evidenced by the results of the Oxyblot™ assay reported here and elsewhere (*55*). These two mitochondrial proteins function at different stages in Fe/S cluster assembly, but both act upstream of reactions involving the later stages of assembly and/or release of Fe/S clusters by scaffold proteins Isu1/2p. It is unlikely that the accumulation and aggregation arise from a blockage of heme biosynthesis, since disrupting the heme biosynthesis pathway in yeast does not cause Fe to accumulate (*78*). Rather, these common

phenotypic effects probably arise from distinct malfunctions, one involving Yah1p and the other involving Yfh1p, that both block Fe/S cluster assembly.

Iron Accumulation is O_2 Dependent

Iron is imported into the mitochondria in the 2+ state (*79*), but the Fe which accumulates occurs in the form of Fe^{3+} nanoparticles, suggesting that the imported Fe^{2+} must become oxidized to the Fe^{3+} state before it aggregates. Fe^{3+} nanoparticles accumulate only in mitochondria from Gal-*YAH1* cells that are both depleted in Yah1p AND grown under aerobic conditions. The absence of Fe accumulation in mitochondria from Yah1p-depleted/Ar cells indicates that accumulation requires both a deficiency of Yah1p (or Yfh1p) and exposure to O_2 during cell growth. We conclude that the accumulation of Fe depends, either directly or indirectly, on the prior oxidation of Fe^{2+} to Fe^{3+}.

Has the Regulation of Fe Import Gone Awry in Yah1p-depleted Mitochondria?

Although many details of the homeostatic Fe regulatory mechanism in mitochondria remain to be clarified, we consider the general scheme shown in Figure 4-8. Accordingly, the concentration of Fe^{2+} ions in the matrix is presumed to be sensed by IM Fe transporters (dashed line). If the steady-state concentration of Fe^{2+} ($[Fe^{2+}]_{ss}$)

equals some optimal set-point concentration ($[Fe^{2+}]_{sp}$), the IM Fe transporter imports Fe^{2+} at a modest, regulated rate. When $[Fe^{2+}]_{ss} > [Fe^{2+}]_{sp}$, the rate of Fe^{2+} import decreases; when $[Fe^{2+}]_{ss} < [Fe^{2+}]_{sp}$, the rate increases. A similar regulatory mechanism could involve Fe exporters in the IM, which would respond oppositely to these comparative conditions.

Could the accumulation of Fe in yah1p-depeleted and *yfh1D* cells be caused by a malfunction in this regulatory mechanism, such that the rate of Fe^{2+} import was "locked" at an excessive rate? Fe^{2+} ions did not accumulate in Yah1p-depleted/Ar cells, suggesting that the homeostatic mechanism for regulating mitochondrial Fe *does* function appropriately under Yah1p-depleted conditions – *as long as O_2 is excluded*. We also observed a substantial (~75%) release of Fe^{2+} from the mitochondria following incubation in dithionite-containing buffer. Although we cannot exclude the possibility that the dithionite-induced increase in Fe^{2+} within the mitochondria caused the membrane to become leaky, it could also be that the condition $[Fe^{2+}]_{ss} > [Fe^{2+}]_{sp}$ increased the rate of Fe^{2+} export. Considered collectively, our results suggest (but do not establish) that the absence of Yah1p (and by extension Yfh1p) do not cause a malfunction in the homeostatic Fe regulatory mechanism in mitochondria.

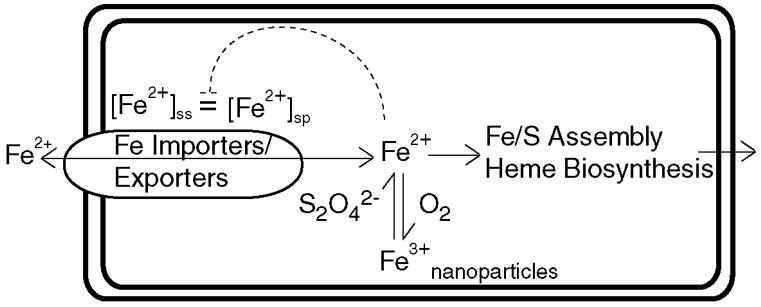

Figure 4-8: Scheme for explaining the accumulation of ferric nanoparticles in mitochondria from Yah1p-depleted/O_2 and *yfh1D* cells. See text for details.

Why do Ferric Nanoparticles Form in Yah1p-depleted/O_2 (and yfh1D) Cells but Not in WT Cells?

We suggest two explanatory models, one based on a difference in the coordination environment of the $Fe^{2+/3+}$ ions in the mitochondrial matrix, the other based on a difference in the redox status of the matrix region in the presence of O_2. Aqueous Fe^{3+} is highly insoluble (*80*) but the Fe^{3+} in oxidized mitochondria from respiring WT cells is not present in nanoparticles that exhibit a quadrupole doublet with ΔE_Q = 0.62 mm/s (*58*). We are uncertain whether the Fe^{3+} ions observed in WT mitochondria are located ***within*** the organelle, but if they are, it would appear that they have a coordination environment that prevents their precipitation. Fe^{3+} ions in Yah1p-depleted/O_2 (and *yfh1D*) mitochondria might lack such protection and thus precipitate, forming the Fe^{3+} nanoparticles observed here. The protective ligand may not be synthesized in these mutant strains, or the large amount of Fe^{3+} ions that develops might simply overwhelm the amount of protective ligand available. The former possibility would suggest that Yah1p (and Yfh1p) somehow promote the synthesis of the protecting ligand, which seems unlikely. The latter possibility could be realized by the inability of these cells to synthesize Fe/S clusters. In this case, aqueous Fe^{2+} ions would build up; thus under oxidizing conditions, they would become oxidized to aqueous Fe^{3+} ions which would precipitate immediately.

The second explanatory model assumes that the Fe^{3+} observed in WT mitochondria (*58*) is adventitiously bound to proteins or membranes on the exterior of the organelle. This model further assumes that in WT cells, the mitochondrial matrix region remains largely "reducing" in terms of electrochemical potential, ***even when cells are grown in an O_2 atmosphere*** (and when anaerobically isolated mitochondria are briefly exposed to O_2, as we have done (*58*)). This assumption is supported by the Oxyblot™ results reported here and elsewhere (*55*), which indicate higher oxidative stress in these mutant cells. According to this model, the reducing environment of the matrix in WT cells minimizes iron oxidation such the concentration of Fe^{3+} does not exceed its solubility limit. In mutant mitochondria, the more oxidizing matrix environment increases [Fe^{3+}] beyond its solubility limit, and the ions precipitate. The mechanisms by which WT cells establish such a reduced matrix and that by which the mutant cells disestablish it are beyond the scope of the model. However, it does not appear as simple as abolishing oxidative phosphorylation (e.g. by blocking the synthesis of Fe/S clusters and hemes) because there are examples in which such abolition in yeast does not cause Fe accumulation (*8, 81*). We view this as evidence against this model, but perhaps not sufficient to discard it. The concept of oxidative stress is sufficiently vague such that there may be other unidentified mechanisms for establishing whether the matrix is oxidizing or reducing.

Apart from these differences, the mechanism of ferric nanoparticle formation is the same for both models. In Yah1p-depleted/O_2 or *yfh1D* mitochondria, either the absence of a "protecting" ligand or the presence of a more oxidizing matrix environment leads to the formation of Fe^{3+} followed by precipitation. As these ions precipitate the equilibrium shifts towards Fe^{3+}. This, in turn, affords the condition $[Fe^{2+}]_{ss} < [Fe^{2+}]_{sp}$, which activates Fe importers (or deactivates Fe exporters), resulting in the observed accumulation of Fe. According to these models, the presence of ferric nanoparticles is *not* sensed by the IM Fe transporters, so the build-up of this material proceeds without perturbing the regulatory sensing condition. In the absence of O_2, the equilibrium is *not* shifted towards Fe^{3+} such that the condition $[Fe^{2+}]_{ss} \approx [Fe^{2+}]_{sp}$ holds and the Fe transporters import Fe^{2+} at a regulated rate. In the presence of dithionite (and absence of O_2), the precipitated material is reductively dissolved such that $[Fe^{2+}]_{ss} > [Fe^{2+}]_{sp}$, and the transporters export Fe^{2+} at an increased rate.

Both models, and the regulatory mechanism that was assumed to develop them, require extensive additional testing. For example, the concentration of other Fe species besides matrix-bound $[Fe^{2+}]$ may be sensed, and other species besides IM transporters may be regulated. Nevertheless, these models represent a testable molecular-level description for the formation of the ferric nanoparticles. Understanding the molecular basis for the formation of these nanoparticles in Yah1p-depleted/O_2 and *yfh1D* cells may

ultimately contribute to a more in-depth understanding of Friedreich's ataxia. One obvious test would be to identify the ligands coordinating Fe^{2+}/Fe^{3+} ions in WT mitochondria and in the Fe^{2+} ions obtained by treating ferric nanoparticles with dithionite. Such experiments are underway.

CHAPTER V

BIOPHYSICAL CHARACTERIZATION OF THE IRON IN MITOCHONDRIA FROM ATM1P-DEPLETED *SACCHAROMYCES CEREVISIAE**

Introduction

Mitochondria play a major role in cellular iron homeostasis, as they are sites where iron is inserted for heme biosynthesis (*82*) and where iron-sulfur clusters (ISCs) are assembled (*83*). The ferrous ions used in these processes are imported from the cytosol through the Mrs3p/4p high-affinity inner-membrane (IM) transporters. Some such centers are installed into mitochondrial apo-proteins, and some heme centers are exported to cytosolic targets. The *Cytosolic Iron-Sulfur Protein Assembly* (CIA) machinery is thought to depend on the mitochondrial ISC machinery, via an arrangement involving the IM protein Atm1p. Atm1p is an ATP Binding Cassette (ABC) "half-transporter" (*84*) that uses the free energy of ATP hydrolysis to transport an unknown molecular species, termed "*X"*, from the matrix to the intermembrane space (*83, 85*). The structure of *X* is unknown, but an Fe chelator (*11*), an Fe/S cluster "precursor" that

---

*****This chapter is reproduced from: "Biophysical Characterization of the Iron in Mitochondria from Atm1p-Depleted *Saccharomyces cerevisiae*" by Ren Miao, Hansoo Kim, Uma Mahendra Kumar Koppolu, E. Ann Ellis, Robert A. Scott and Paul A. Lindahl, *Biochemistry*, 2009, 48, 9556-9568, copyright 2009 American Chemical Society.

contains sulfur and perhaps iron (*19*), or a peptide with multiple reduced thiol residues (*85*) have all been suggested. Guarente and Mason (*86*) have suggested that mitochondrially-synthesized hemes are exported and sensed in the cytosol, but the possibility that *X* is a heme has been discounted (*84*). Once exported into the cytosol, *X* has been proposed to assist the CIA machinery in cytosolic ISC synthesis and regulate cellular Fe homeostasis.

S. cerevisiae cells lacking Atm1p have a respiratory defect as well as diminished levels of heme prosthetic groups (*84*) and cytosolic ISC-containing proteins (*19*). There is reportedly no defect in mitochondrial ISC maturation (*19*). Depletion and deletion of Atm1p also causes Fe to accumulate in mitochondria to concentrations that are 20- to 30-times higher than in WT controls (presuming no difference in overall mitochondrial protein concentration) (*11, 48*). However, the form of the accumulated Fe has not been investigated by biophysical methods. Fe also accumulates in mitochondria of strains in which ISC assembly components are abrogated or repressed by genetic manipulation (e.g., Yfh1p-deleted or Yah1p-depleted cells). In these cases the accumulated Fe is present as aggregated ferric nanoparticles that exhibit superparamagnetic relaxation (*18, 87*).

The accumulation of Fe results from a shift in cellular Fe homeostasis, a partially understood process involving the Fe-sensing transcription factors Aft1p and Aft2p (*88*).

Under Fe-deficient conditions, Aft1p (and presumably Aft2p) moves into the nucleus where they up-regulate a group of genes known as the *iron regulon*. The net effect of this is to increase the rate of cellular Fe import and probably mitochondrial Fe import. Abolishing ISC assembly in mitochondria has a similar effect, causing Aft1p/Aft2p to behave *as though* the cytosol is Fe-deficient. Rutherford *et al.* (*7*) hypothesized that *X* is generated as a product of mitochondrial ISC assembly, and that this signaling molecule is transferred to the cytosol via Atm1p where it is sensed by Aft1p/Aft2p. Thus, in the absence of ISC assembly, or under Atm1p-depleted conditions, the cytosol would be deficient in *X*, thereby causing Aft1p/Aft2p to up-regulate the iron regulon.

An Atm1p homolog in *Chlamydomonas reinhardtii*, Cds1p, is up-regulated when cells are exposed to Cd (*89*). This ABC half-transporter exports Cd(II) multi-thiol phytochelatin complexes from the mitochondrial matrix for metal detoxification. Although Fe does not accumulate in mitochondria of Cds1p-deficient cells, such cells are hypersensitive to Fe, indicating an indirect association with Fe homeostasis.

ABCB7 is the human functional orthologue of Atm1p (*90, 91*). Patients with *X-linked Sideroblastic Anemia with cerebellar Ataxia* (XLSA/A) have genetic mutations in ABCB7. In this disease, Fe accumulates in the form of ring-shaped sideroblasts, and mitochondria are loaded with iron (*92*). Heme biosynthesis and Fe regulation are also abrogated in a mouse model of this disease (*93*). Thus, understanding the function of

Atm1p has considerable implications for human health.

In this study, we have examined the type of Fe that accumulates in mitochondria of Atm1p-depleted yeast cells using Mössbauer spectroscopy, electron paramagnetic resonance (EPR), electronic absorption (UV-vis) spectroscopy, X-ray absorption spectroscopy (XAS), and electron microscopy (EM). We find that the accumulated Fe is similar to that found in Yah1p-depleted (*87*) and Yfh1p-deleted (*18*) mitochondria. In contrast to previous results (*19, 83*), we also observed a significant ISC defect in mitochondria from aerobic cells fully and partially depleted in Atm1p. There is no ISC defect in *anaerobic* Atm1p-depleted cells, confirming previous studies that Atm1p is not directly involved on ISC assembly (*19*). Collectively, these results suggest that Fe/S clusters may assemble in Atm1p-depleted mitochondria of aerobic cells, but then rapidly degrade upon exposure to O_2 or ROS.

Results

W303 and Gal-ATM1 Cells Grown under Different Carbon Sources

This study involved *S. cerevisiae* strains W303 and Gal-ATM1. W303 is a wild-type (WT) strain while Gal-ATM1 is a derivative of W303 in which the natural promoter for *ATM1* has been replaced by a truncated galactose-inducible promoter. The latter strain expresses Atm1p when grown on galactose but not when grown on glucose. Most

batches of cells were grown with O_2 bubbled through the media, but some were bubbled with argon. Atm1p should express in W303 cells grown aerobically or anaerobically on glucose (W303/Glu/O_2 and W303/Glu/Ar), and grown aerobically on galactose (W303/Gal/O_2). Atm1p should also express in Gal-ATM1 cells grown aerobically on galactose (Gal-ATM1/Gal/O_2), but it should not express in Gal-ATM1 cells grown on glucose, regardless of whether growing cells are bubbled with O_2 (Gal-ATM1/Glu/O_2) or argon (Gal-ATM1/Glu/Ar).

Consistent with this, Atm1p in our samples was virtually undetectable by Western blot analysis of mitochondrial extracts of Gal-ATM1/Glu/O_2 cells (Figure 5-1, lane 4), while it was readily detected in extracts of W303/Gal/O_2 (Lane 1), W303/Glu/O_2 (Lane 2) and Gal-ATM1/Gal/O_2 cells (Lane 3). When normalized to the density of the porin control (Figure 5-1, bottom panel), the Atm1p expression level in Gal-ATM1/Gal/O_2 cells was calculated to be 45 ± 5% of that in W303/Gal/O_2 cells. Thus, in cells grown on minimal medium containing galactose, the Atm1p expression level was lower when the truncated galactose-inducible promoter was used. A similar result has been observed previously (*19*). This had some biophysical consequences (see below).

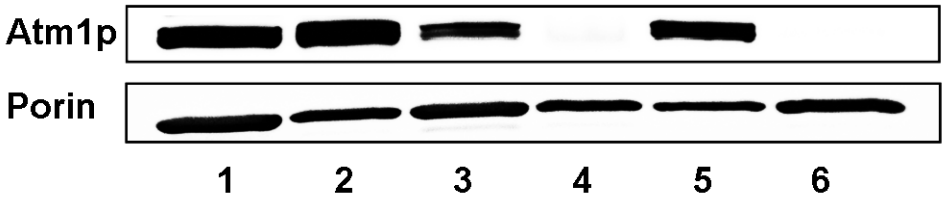

Figure 5-1: Western blots of Atm1p and porin in isolated mitochondria. Lane 1, W303/Gal/O_2; Lane 2, W303/Glu/O_2; Lane 3, Gal-ATM1/Gal/O_2; Lane 4, Gal-ATM1/Glu/O_2; Lane 5, W303/Glu/Ar; Lane 6, Gal-ATM1/Glu/Ar. Top panel, blot treated with anti-Atm1p antibody; Bottom panel, blot treated with an antibody for the mitochondrial outer membrane protein porin which served as a loading control.

Table 5-1. Fe and protein concentrations in packed mitochondria, and enzyme activities in isolated mitochondrial suspensions (the error for activity assays is estimated at 20%). [a] N.D., activity not detectable (lower than 20 units/mg protein).

	W303/Glu/O_2	Gal-ATM1/Glu/O_2	W303/Glu/Ar	Gal-ATM1/Glu/Ar
[Fe] (μM)	630 ± 40	8900 ± 400	170 ± 10	180 ± 10
[Protein] (mg/mL)	57 ± 5	26 ± 3	31 ± 4	34 ± 5
Aconitase activity (units/mg protein)	670	80	650	700
Succinate dehydrogenase activity (units/mg protein)	14	5	(not determined)	(not determined)
Leu1p activity (units/mg protein)	150	N.D.[a]	320	N.D.[a]

Purified mitochondria from Gal-ATM1/Glu/O_2 cells contained 14-times higher levels of iron than mitochondria from W303/Glu/O_2 cells (Table 5-1). The Fe concentration in Gal-ATM1/Gal/O_2 cells ([Fe] ~ 2 mM, estimated from Mössbauer intensity, as described in (*40*)) was intermediate. The accumulation of Fe in Atm1p-depleted and partially-depleted mitochondria suggests that under these conditions, the import flux of Fe into the organelle had increased.

The protein concentration of mitochondria (mg protein per mL of packed mitochondria) from Gal-ATM1/Glu/O_2 cells, determined by the Bradford method, was lower than that from W303/Glu/O_2 cells (Table 5-1). To assess whether this lower-than-expected value arose from interference from Fe(III) nanoparticles (see below), we quantified proteins by the BCA method (Pierce); however, no difference relative to the WT value was observed. The difference in protein concentration may be real – perhaps resulting from the repression of respiration/citric acid cycle proteins (*83*).

The Fe concentration of packed mitochondria isolated from Gal-ATM1 cells grown under anaerobic conditions was similar to that of anaerobically grown WT cells, and both were lower than in aerobic WT mitochondria (Table 5-1). The protein concentration of anaerobic mitochondria was also low – about 50% of that isolated from aerobically grown WT cells. There are significant differences between anaerobic *vs.* aerobic mitochondria. Although the morphology of both is similar (*94*), the

concentration of many proteins, including Fe-containing proteins such as the respiratory complexes and particular citric acid cycle enzymes, are significantly reduced in anaerobic mitochondria (*61*). This may result in the lower Fe and protein concentrations observed. Alternatively, anaerobic mitochondria may simply not pack as tightly as aerobic mitochondria, perhaps due to differences in lipid composition (*95*). These differences do not appear to have affected the density of the anaerobic organelles, as they were purified using the same Nycodenz gradients as mitochondria from aerobically grown cells. The lower Fe concentration indicated that Fe did not hyper-accumulate in mitochondria from Atm1p-depleted cells grown under anaerobic conditions.

Ferric Phosphate Nanoparticles in Atm1p-depleted Mitochondria

4.5 K low-field Mössbauer spectra of Atm1p-depleted mitochondria (Figure 5-2A) exhibited an intense single quadrupole doublet with isomer shift δ = 0.53 mm/s, quadrupole splitting ΔE_Q = 0.73 mm/s and linewidth G = 0.68 mm/s. These parameters are similar to the doublet exhibited by ferric nanoparticles in Yah1p-depleted cells (δ = 0.52 mm/s, ΔE_Q = 0.63 mm/s, and G = 0.55 mm/s) (*87*). A high-field spectrum of Atm1p-depleted mitochondria (Figure 5-2B) was also similar to that of Yah1p-depleted one.

Figure 5-2. 4.5 K Mössbauer spectra of mitochondria from Gal-ATM1 and W303 cells. A, Gal-ATM1/Glu/O_2, collected with 40 mT field applied parallel to gamma rays (low applied field). The solid red line is the sum of the Fe(III) nanoparticle doublet (δ = 0.53 mm/s, ΔE_Q = 0.73 mm/s) and a HS Fe(II) doublet; B, same as A, but with 8 T applied field; C, Gal-ATM1/Gal/O_2, low applied field. The solid red line is the sum of the Fe(III) nanoparticle double (δ = 0.52 mm/s, ΔE_Q = 0.73 mm/s) and a HS Fe(II) doublet; D, same as A but reduced with sodium dithionite; E, same as C but reduced with sodium dithionite. The solid line above the data outlines a $[Fe_4S_4]^{2+}$ doublet (δ = 0.45 mm/s, ΔE_Q = 1.15 mm/s); F, W303/Glu/Ar, low applied field, the solid line above the data outlines the sum of two major doublets ($[Fe_4S_4]^{2+}$ and HS Fe(II)), representing ~ 70% of Fe; G, Gal-ATM1/Glu/Ar, low applied field. The solid line above the data outlines the sum of two major doublets, representing ~ 80% of Fe.

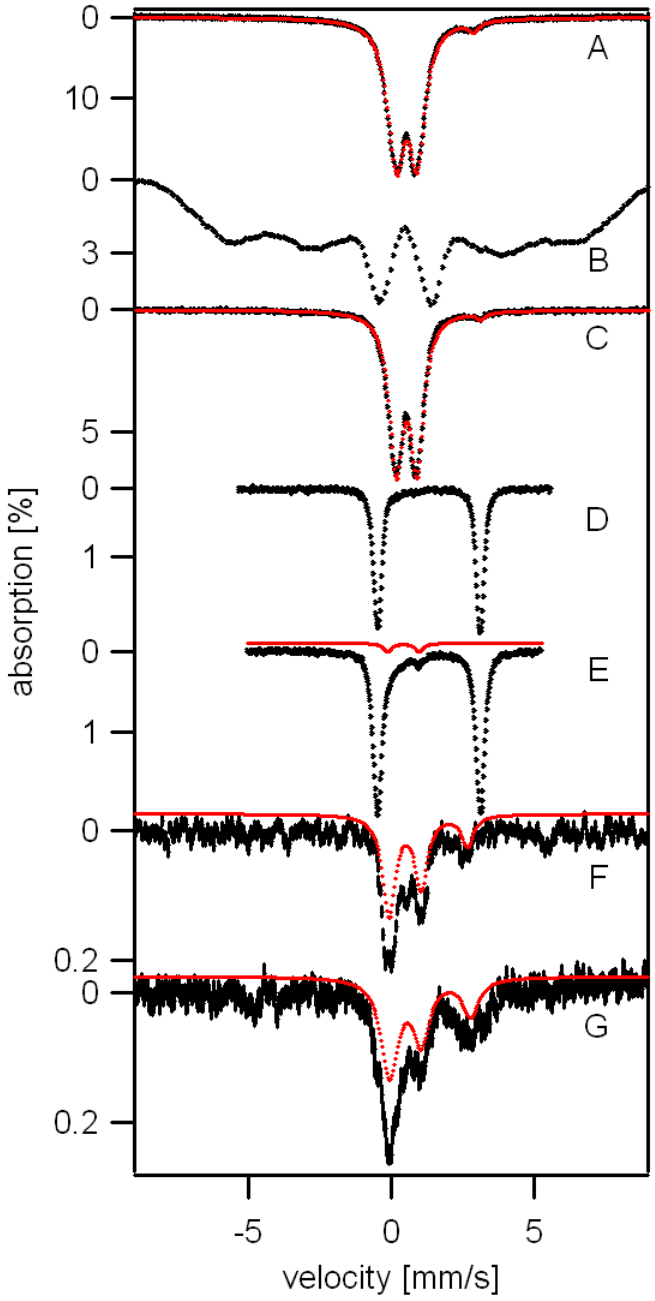
0
A
10
0
3
B
0
C
5
0
D
1
0
E
1
0
F
0.2
0
G
0.2
absorption [%]
-5
0
5
velocity [mm/s]

Figure 5-3: X-band EPR spectra of isolated mitochondria from Gal-ATM1 and W303 cells. Top panel, from Gal-ATM1/Glu/O_2 cells. A, 10 K; B, 30 K; C, 80 K; microwave frequency for all spectra, 9.46 GHz; microwave power for A, B and C, 20 mW. Middle panel, g = 2 region. A, W303/Gal/O_2; B, Gal-ATM1/Glu/O_2; C, same as B, but reduced with sodium dithionite; D, W303/Glu/Ar; E, Gal-ATM1/Glu/Ar; temperature. Temperature, 10 K, microwave power, 0.2 mW. Bottom panel, g = 4-6 region. A, as-isolated Gal-ATM1/Glu/O_2 mitochondria; B, same as A but treated with sodium dithionite. Temperature, 10 K; microwave power, 20 mW.

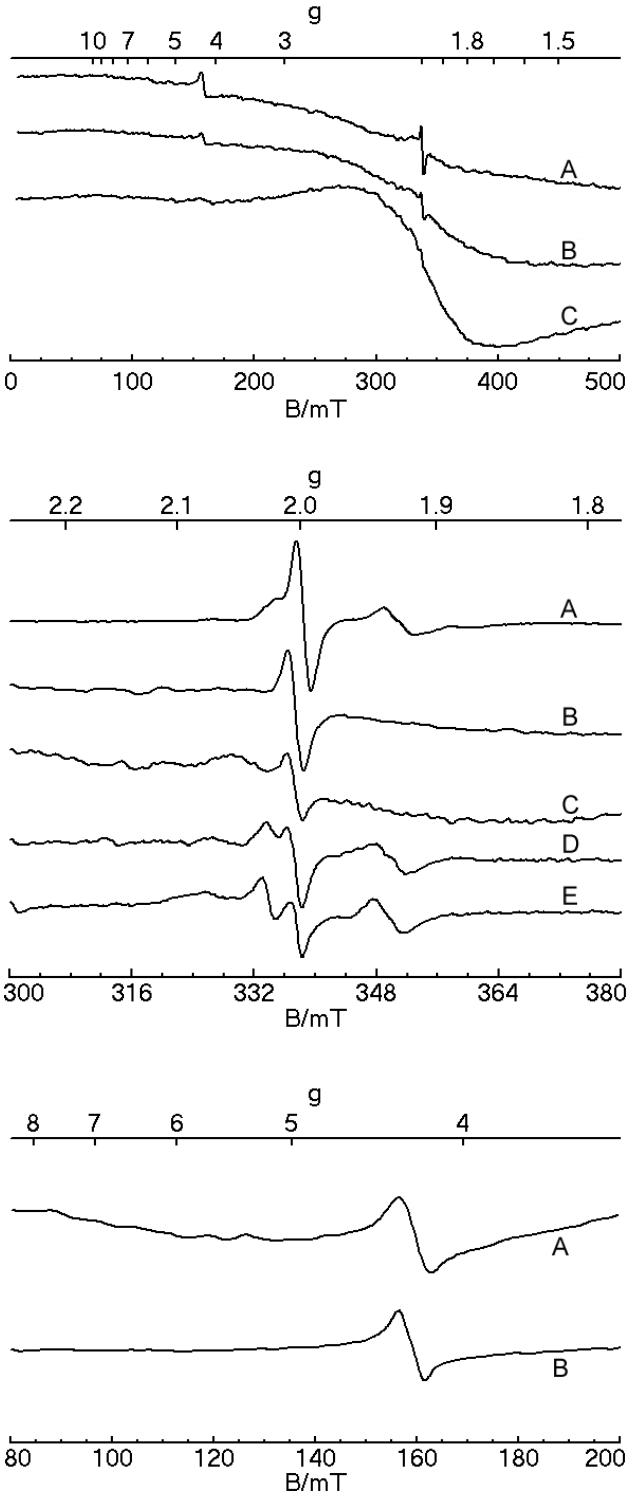
g
10 7 5 4 3 1.8 1.5
A
B
C
0 100 200 300 400 500
B/mT
g
2.2 2.1 2.0 1.9 1.8
A
B
C
D
E
300 316 332 348 364 380
B/mT
g
8 7 6 5 4
A
B
80 100 120 140 160 180 200
B/mT

Atm1p-depleted mitochondria exhibited a very broad EPR signal centered at g ~ 2.0 and with inverse Curie-Law behavior (Figure 5-3, top panel), similar to that exhibited by Yah1p-depleted mitochondria (*87*). Such signals indicate superparamagnetic relaxation, consistent with the aggregation of ferric nanoparticles. The superparamagnetic EPR signal from Atm1p-depleted mitochondria was ~ 1.7-fold broader than that from Yah1p-depleted mitochondria, which might indicate subtle differences in size, composition and/or microcrystallinity of the nanoparticles. The only other EPR signals evident in the spectra is a minor feature at g = 4.3 due to a small amount of rhombic high-spin Fe(III) and an isotropic signal at g ~ 2.00 probably due to organic-based radicals.

Atm1p-depleted mitochondria were investigated by analytical electron microscopy. In STEM-HAADF micrographs (Figure 5-4), Fe species within Gal-ATM1/Glu/O_2 mitochondria appear brighter than background. Brightness in these images depends on the relative concentration and atomic number (Z) of contributing atoms. High magnification STEM images (Figure 5-4, panels on left) revealed bright spheres indicating high Z elements such as iron. Elemental maps (panels on right) reveal that those areas are rich in both iron and phosphorus, with a molar {Fe:P} ratio of {0.7:1.0} (relative uncertainty ~ 10%). These particles are also associated with oxygen but not with carbon (Figure 5-4) or nitrogen (data not shown). Close-up images (Figure 5-4, bottom left panel) suggest 2-4 nm diameters for these ferric phosphate nanoparticles.

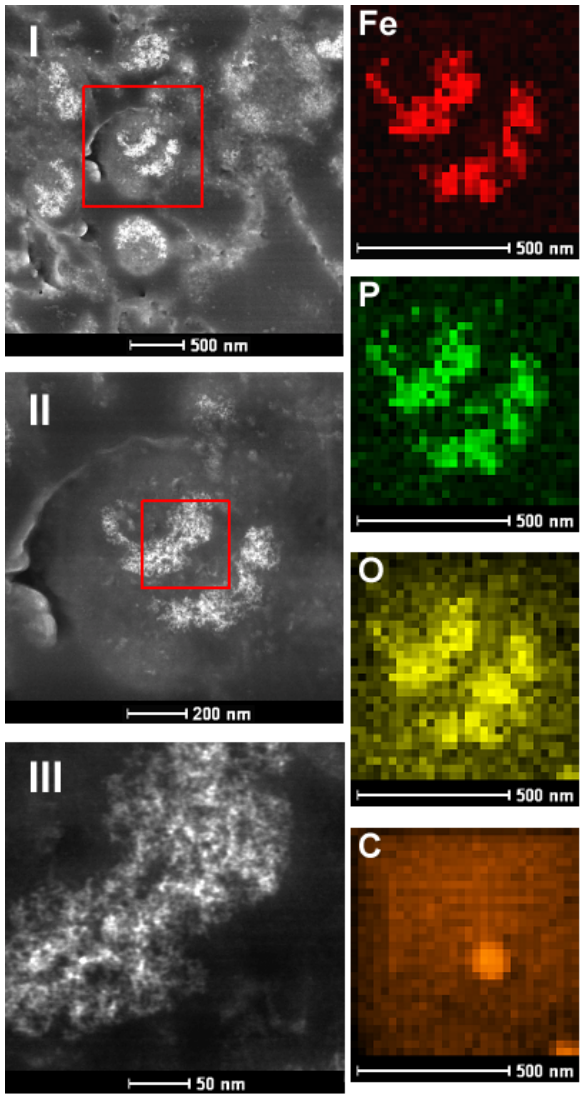

Figure 5-4: STEM-HAADF images and elemental maps of iron deposits in mitochondria isolated from Gal-ATM1/Glu/O_2 cells. Images I, II, and II were obtained at increasing magnification, with the red box in each panel corresponding approximately to the full image in the next lower panel. The red box in image I also corresponds to the region scanned for Fe, P, O, and C maps. The bright spots around the center and the corner of the carbon map are probably a beam-damaged mark.

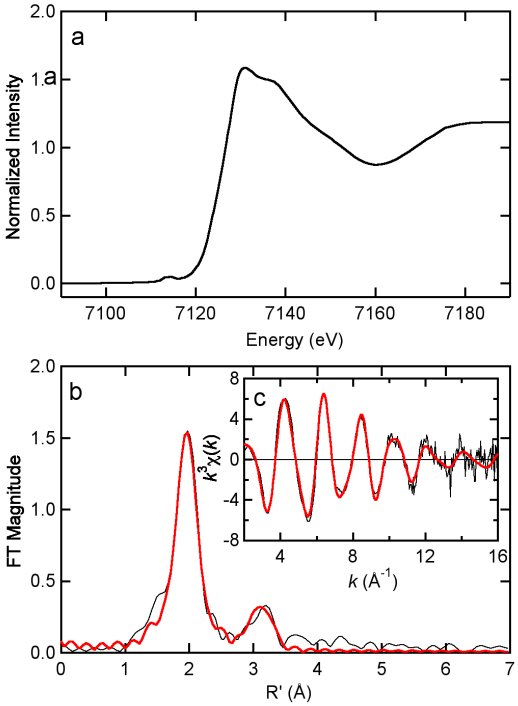

Figure 5-5: X-ray absorption spectra of mitochondria isolated from Gal-ATM1/Glu/O_2 cells. a, XANES; b, FT (k = 2.0 – 16.0 Å^{-1}, k^3 weighting); c, EXAFS. Solid red lines are simulations assuming the FeO_5P_2 model of Table 5-2.

Table 5-2. Curve fitting results for Fe K edge EXAFS[a,c] .

Sample, filename (k range) $\Delta k^3\chi$	Fit	Shell	R_{as} (Å)	σ_{as}^2 (Å^2)	ΔE_0 (eV)	f'[b]
FMG0B (k = 2 – 16 Å^{-1}) $\Delta k^3\chi$ = 12.6477	1	Fe-O_5	1.973	0.0055	-2.92	0.070
	2	Fe-O_5	1.973	0.0055	-2.92	0.058
		Fe-P_1	3.210	0.0025	[-2.92]	
	3	Fe-O_5	1.973	0.0055	-2.84	0.057
		Fe-P_2	3.210	0.0067	[-2.84]	
	4	Fe-O_5	1.973	0.0055	-2.80	0.063
		Fe-Fe_1	3.020	0.0105	[-2.80]	
	5	Fe-O_5	1.974	0.0055	-2.74	0.062
		Fe-Fe_2	3.003	0.0163	[-2.74]	

[a] Shell is the chemical unit defined for the multiple scattering calculation. Subscripts denote the number of scatterers per metal. R_{as} is the metal-scatterer distance. σ_{as}^2 is a mean square deviation in R_{as}. ΔE_0 is the shift in E_0 for the theoretical scattering functions.

[b] f' is a normalized error (chi-squared):

$$f' = \frac{\left\{\sum_i \left[k^3\left(c_i^{obs} - c_i^{calc}\right)\right]^2 / N\right\}^{1/2}}{\left[\left(k^3 c^{obs}\right)_{max} - \left(k^3 c^{obs}\right)_{min}\right]}$$

[c] BVS = $\Sigma\exp[(r_o\text{-}r)/B]$, B = 0.37, r_0(Fe(III)-O) = 1.759 (*96*). A chemically reasonable set of distances should yield a BVS value close to the expected valence (3.00 in this case). For all 5 fits shown in the table, BVS = 2.80.

[d] Numbers in square brackets were constrained to be either a multiple of the above value (σ_{as}^2) or to maintain a constant difference from the above value (R_{as}, ΔE_0).

X-ray absorption spectroscopy (XAS) was used to further characterize the ferric nanoparticles in mitochondria from Atm1p-depleted cells. The XANES region (Figure 5-5a) was typical of Fe(III) ions coordinated by O/N donor ligands, but was not typical of Fe-S centers. Neither tetrahedral nor square-planar geometries appear likely, but various 5-coordinate or distorted 6-coordinate geometries are possible. The 1s **à** 3d transition on the edge was more intense than expected for a perfect octahedron. The assumption of 5-coordinate Fe-O gave a slightly better BVS than when 6-coordination was assumed. The corresponding background-subtracted EXAFS data (Figure 5-5c) are of high quality, extending to $k \sim 16$ Å^{-1}. The Fourier transform of these data (Figure 5-5b) exhibited a single first-shell peak from oxygen and/or nitrogen backscatterers at an average distance of 1.97 Å as well as a clear outer shell FT peak at 3.21 Å. Results of fits to various models are shown in Table 5-2 (plots comparing EXAFS and FTs of all fits are provided in APPENDIX II as supporting information). The long-distance back scatterer fitted well to P but not to Fe. The fit assuming a single second-shell P from a phosphate ion bound to Fe yielded an Fe-P Debye-Waller factor that was too small to be physically meaningful, whereas the fit assuming two phosphate groups (Figure 5-5b and 5c, red solid lines) yielded a Debye-Waller factor that is larger and physically reasonable (Table 5-2). Thus, this latter fit was preferred, though we cannot exclude a mixture of Fe sites with one and two phosphate ligands, an environment expected for nanoparticles where

there are both interior and surface Fe sites.

Characterization of Iron in Gal-ATM1/Gal/O_2 Mitochondria

We initially expected that mitochondria from Gal-ATM1 cells grown on galactose/O_2 would serve as a control in which Atm1p would be expressed at WT levels. However, Western blot analysis revealed that Atm1p concentrations were reduced (Figure 5-1, compare lanes 1 and 3). Interestingly, this reduction appears to have been sufficient to alter the phenotype of the strain. Mössbauer spectra of as-isolated Gal-ATM1/Gal/O_2 mitochondria were typical of ferric nanoparticles (Figure 5-2C). Mössbauer parameters for the nanoparticle doublet was similar to that of Gal-ATM1/Glu/O_2 mitochondria (δ = 0.52 mm/s, ΔE_Q = 0.73 mm/s) except for a lower percentage effect which was consistent with a lower Fe concentration in these organelles.

These results illustrate the effect of reducing but not fully depleting Atm1p levels in cells. The qualitative (but less severe) development of the same phenotype as observed for mitochondria that were fully depleted in Atm1p suggests that there is *not* a large functional excess of Atm1p in WT mitochondria for the cells grown on minimal media. Had Atm1p been present in excess in WT cells, a 2.5-fold decline of concentration would probably not have caused the observed phenotype. In the following studies WT (W303) cells grown under the same condition served as a control.

Atm1p-depleted Mitochondria from Gal-ATM1/Glu/O_2 Cells Have Reduced Levels of Fe/S Clusters

Mössbauer spectra of Gal-ATM1/Glu/O_2 mitochondria (Figure 5-2, A and B) did not include features typical of S = 0 $[Fe_4S_4]^{2+}$ clusters; such features dominate spectra of WT mitochondria (*40*). To explore whether any such clusters were "hiding" underneath the broad doublet due to ferric nanoparticles, we treated Gal-ATM1/Glu/O_2 mitochondria with dithionite. The resulting Mössbauer spectrum (Figure 5-2D) was dominated by a quadrupole doublet due to high-spin Fe(II) ions. Our analysis suggests that no more than ~2% of spectral intensity could reflect S = 0 $[Fe_4S_4]^{2+}$ clusters. In WT samples, about half of the Fe in mitochondria arises from such clusters (*40*). The spectral intensity for the reduced sample was lower than for the as-isolated sample, suggesting that ~ 2/3 of the Fe had been exported from the mitochondria as a result of dithionite treatment. A similar phenomenon was observed upon reduction of Yah1p-depleted mitochondria (*87*). Assuming an [Fe] of ~ 3 mM, a 2% spectral intensity would correspond to 60 μM Fe. This would represent a ~ 7-fold reduction of $[Fe_4S_4]$ clusters relative to WT levels.

Analysis of the Gal-ATM1/Gal/O_2 sample allowed another estimate of $[Fe_4S_4]$ cluster levels. After treatment with dithionite, the Gal-ATM1/Gal/O_2 sample (that yielded the spectrum of Figure 5-2C) exhibited the spectrum of Figure 5-2E; it was again dominated (~ 90% of spectral intensity) by a HS Fe(II) doublet. A small feature,

representing *ca*. 5% of spectral intensity, was simulated as the high-energy line of a quadrupole doublet due to $[Fe_4S_4]^{2+}$ clusters. We regard this as an upper limit. Assuming an [Fe] of 2 mM for this sample, 5% would correspond to 100 μM Fe, suggesting a ~ 4-fold reduction of S = 0 $[Fe_4S_4]^{2+}$ clusters relative to WT mitochondria.

EPR spectroscopy is better suited to observe Fe/S clusters in their reduced state, and so Atm1p-depleted mitochondria were transferred from Mössbauer to EPR holders (while maintaining them at LN_2 temperature). The resulting EPR spectra (Figure 5-3, middle panel, trace B for the as-isolated sample and trace C for dithionite-reduced sample) were virtually devoid of g_{ave} = 1.94 or 1.90 signals. These signals were present in spectra of WT mitochondria (Figure 5-3, middle panel, trace A), and they probably arise from the S = ½ $[Fe_2S_2]^{1+}$ clusters of succinate dehydrogenase and the Rieske Fe/S protein (*40*). Low-field spectra of both as-isolated and dithionite-reduced Gal-ATM1/Glu/O_2 mitochondria samples did not exhibit features at g = 4-6 which typify S = 3/2 $[Fe_4S_4]^{1+}$ clusters (Figure 5-3, bottom panel).

Previous conclusions that Atm1p-depleted mitochondria contain WT concentrations of Fe/S clusters were based largely on the presence of substantial aconitase activities in Atm1p-depleted cell extracts and on ^{55}Fe incorporation into mitochondrial Fe/S proteins under low iron conditions which precluded mitochondrial iron overload (*11*, *19*). Using WT and *atm1*Δ strains grown on yeast extract:peptone

medium containing 2% galactose, Kispal *et al.* reported that the aconitase activity of *atm1*Δ mitochondria was ~ 40% of WT levels (*11*). When the Gal-ATM1 strain was grown on lactate to deplete Atm1p, the aconitase activity in mitochondria was ~ 70% of WT levels (*19*). The same assay performed on our samples revealed reduced (but still nonzero) activities. The aconitase activity of a Gal-ATM1 mitochondrial extract was ~12% of the WT level in mitochondrial extracts (for cells grown on glucose in minimal media) (Table 5-1). In extracts of mitochondria isolated from galactose-grown cells, aconitase levels (900 units/mg) were 64% of WT levels (1400 units/mg). Thus, there was an effect of growth media, carbon source, and/or the extent of Atm1p depletion on mitochondrial Fe/S levels and therefore on aconitase activities. Succinate dehydrogenase activities showed a similar pattern (Table 5-1).

These activities imply significantly reduced levels of Fe/S clusters in mitochondria that are *fully* depleted in Atm1p, and moderately reduced levels under conditions of *partial* depletion. They are consistent with our biophysical results, but are perhaps somewhat higher than indicated by them. One possible explanation is that Fe/S clusters are inserted preferentially into apo-aconitase (or apo-succinate dehydrogenase) molecules, such that this activity overestimate the total level of mitochondrial Fe/S clusters. Also apparent is that there is a relationship between aconitase activity and the extent of Atm1p depletion, which in turn depends sensitively on media and growth

conditions. Our results are generally consistent with those of Kispal *et al*. in that they also observed lower aconitase activities in Atm1p-depleted and *atm1*Δ strains (*11, 19*), relative to WT levels. However, based on the moderate decline in activity of mitochondrial Fe/S proteins observed for Atm1p-depleted cells relative to the loss of extra-mitochondrial Fe/S proteins, Kispal *et al.* (*11, 19*) concluded that neither depleting nor deleting cells of *ATM1* had any significant effect on the function of Fe/S proteins inside the organelle. The more significant decline observed here along with our biophysical data indicate that the level of ISC assembly in Atm1p-depleted mitochondria is ***reduced substantially*** relative to WT – by a factor of 4 - 8.

Atm1p-depleted Mitochondria from Gal-ATM1/Glu/O_2 Cells are Deficient in Hemes

Previous studies have reported that Atm1p-depleted cells have either WT levels or reduced levels of heme centers, depending on growth media (*83*). To evaluate this in our Atm1p-depleted mitochondria, samples were examined by electronic absorption spectroscopy. Difference spectra (Figure 5-6) revealed that heme $a+a_3$, b, and $c+c_1$ concentrations were each ~ 6-fold lower in Gal-ATM1/glucose/O_2 mitochondria relative to those in WT mitochondria grown on the same carbon source. This decrease in heme concentrations is roughly similar to that observed in overall ISC concentrations.

Atm1p-depleted Mitochondria Accumulate High-spin (HS) Fe(II) Ions

Besides the dominant Fe(III) nanoparticle doublet, the low-field 4.5 K Mössbauer spectrum of Atm1p-depleted mitochondria from Gal-ATM1/Glu/O_2 cells exhibited a quadrupole doublet typical of high-spin Fe(II) ions (Figure 5-2A and close up in Figure 5-7A). The Mössbauer parameters associated with this doublet could not be determined accurately since the low-energy line was buried in the nanoparticle doublet. The high-energy line was located at 2.75 ± 0.02 mm/s (average of three batches), which is different from the high-energy line of hexaqua high-spin Fe(II) ions in phosphate buffer at pH 7.4 (2.9 mm/s) (Supporting Information of (*87*)). The linewidth of the doublet was quite broad (Γ ~ 1 mm/s), suggesting multiple species. The doublet corresponded to 3% - 5% of spectral intensity, which may seem insignificant. However, assuming ~10 mM total [Fe] for this sample, the concentration of HS Fe(II) ions in these nanoparticle-packed mitochondria would correspond to 300 – 500 μM, roughly half of the total Fe concentration in WT mitochondria!

A similar HS Fe(II) doublet was present in spectra of mitochondria from Gal-ATM1/Gal/O_2 cells (Figure 5-2C and 7B). In this case, the high-energy line was at 3.08 mm/s ± 0.02 mm/s (average of 2 batches) which is slightly different from that for glucose-grown mitochondria and the HS Fe(II) high-energy line of hexaqua Fe(II) ions. Also, the linewidth (Γ~0.5mm/s) of the high-energy line in spectra of Gal- ATM1/Gal/O_2

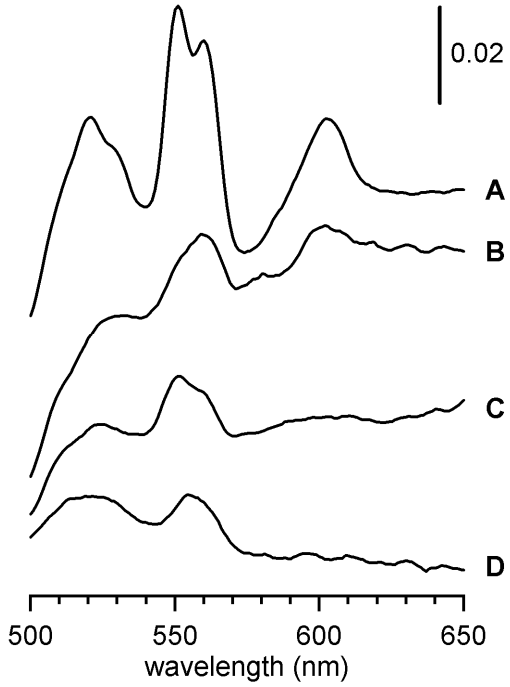

Figure 5-6: Electronic absorption reduced-minus-oxidized difference spectra of mitochondria isolated from W303 and Gal-ATM1 cells. Spectra were obtained at room temperature from samples treated with sodium dithionite. They were subtracted from those obtained from samples treated with ferricyanide. A, W303/Glu/O_2; B, Gal-ATM1/Glu/O_2; C, from W303/Glu/Ar; D, Gal-ATM1/Glu/Ar.

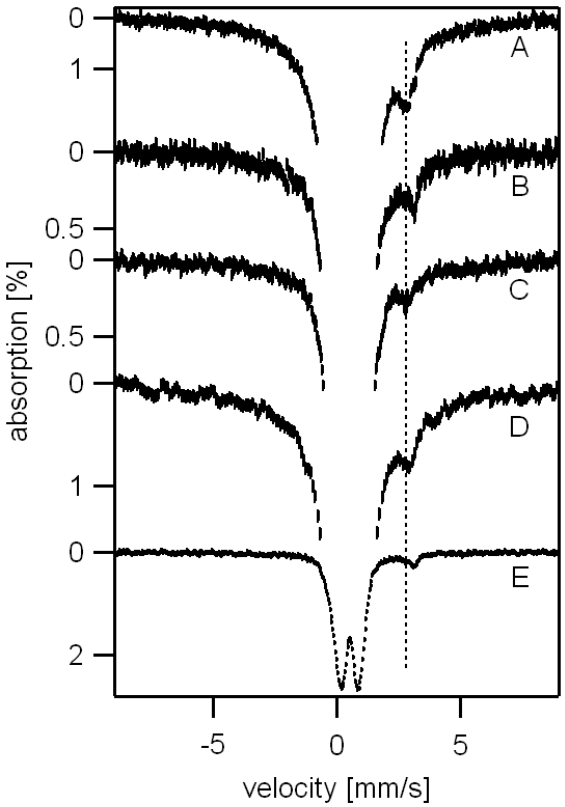

Figure 5-7: Mössbauer spectra showing high-spin Fe(II) species in Atm1p-depleted and Yah1p-depleted mitochondria and whole cells. All spectra were collected 4.5 K with 40 mT parallel applied field. A, Gal-ATM1/Glu/O_2 mitochondria; B, Gal-ATM1/Gal/O_2 mitochondria; C, Gal-ATM1/Glu/O_2 cells; D, mitochondria from Yah1p-depleted cells grown on glucose/O_2 (batch 1); E, Same as B, but a different batch harvested after 35 hr of growth. A vertical dashed line is drawn at 2.75 mm/s.

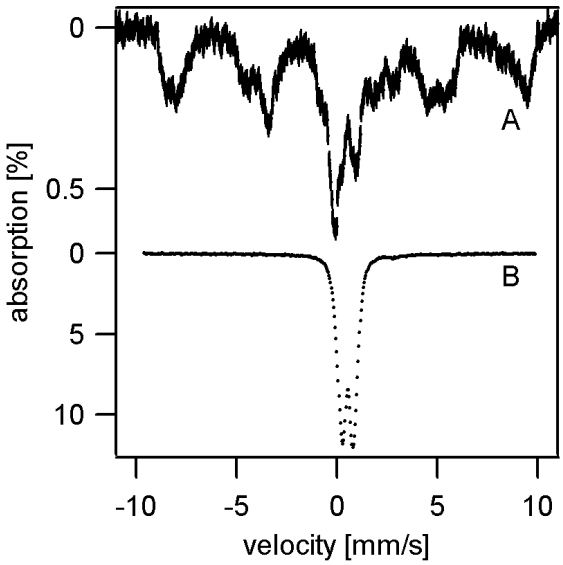

Figure 5-8: 4.5 K Mössbauer spectra of whole yeast cells. A, W303/Glu/O_2; B, Gal-ATM1/Glu/O_2. A 40 mT parallel field was applied.

mitochondria was substantially narrower than that for glucose-grown cells, suggesting that fewer species contribute.

The overall spectral intensity in a batch of mitochondria from Gal-ATM1/Gal/O_2 cells that were harvested after 35 hrs of growth on minimal galactose-containing medium was ~ 2.5% effect (Figure 5-7E) while that for a batch harvested 45 hrs after inoculation was ~ 6% effect (Figure 5-2C). The difference in percent effect suggests that the ***extent of nanoparticle accumulation increases with growth time***. The spectral intensity of the HS Fe(II) doublet ***decreased*** (4% for the 35 hr batch and 2% for the 45 hr batch), but the estimated concentration of HS Fe(II) in the mitochondria were essentially invariant (~ 50 μM in each case).

No HS Fe(II) doublet was reported in a Mössbauer spectrum of mitochondria isolated from Yah1p-depleted mitochondria (*87*) even though these organelles also contained ferric phosphate nanoparticles. However, careful re-inspection of the published spectrum revealed the possibility of such a species, and spectra from two other batches of Yah1p-depleted mitochondria (Figure 5-7D and another not shown) confirmed that these mitochondria also contain substantial amounts of HS Fe(II) ions. In these spectra, the intensity of the Fe(II) doublet represented ~ 5% of the intensity, similar to that for Atm1p-depleted mitochondria. Assuming 7.4 mM Fe (*87*), this corresponds to ~ 150 μM which is again a substantial concentration. Analogous inspection of the

published Mössbauer spectrum of Yfh1-depleted mitochondria (*18*) failed to reveal any evidence for this doublet.

Cellular Accumulation and Redistribution of Iron in Atm1p-depleted Mitochondria

By growing wild-type yeast cells on minimal media enriched in ^{57}Fe, we were able to obtain *whole cell* Mössbauer spectra (Figure 5-8A). High-spin Fe(III) species from an unknown but non-mitochondrial location in the cell dominated the spectrum, while a quadrupole doublet with parameters typical of $[Fe_4S_4]^{2+}$ clusters was also evident. Thus, our first glimpse of the iron-ome of a fermenting yeast cell reveals that the vast majority of its Fe is present as mononuclear Fe(III) complexes.

The corresponding 4.5 K Mössbauer spectrum of whole Gal-ATM1/Glu/O_2 cells (Figure 5-8B) is dramatically different in three major respects. First, the Fe concentration was higher by a factor of 10. Second, most of that Fe appeared to be in the form of ferric nanoparticles. Third, the high-spin mononuclear Fe(III) species observed in WT cells was absent (see Figure 5-7C for close-up). Also present at the level of ~ 2% of cellular Fe were high-spin Fe(II) ions, as evidenced in a close-up of the baseline (Figure 5-7C). The central doublet typical of Fe/S clusters was also not observed in spectra of Atm1p-depleted whole cells. A small contribution of such clusters could have been present but undetectable due to the dominance of the nanoparticle doublet.

Anaerobic Growth of Atm1p-depleted Cells

In a previous study, we found that mitochondria of Yah1p-depleted cells did not accumulate Fe when such cells were grown anaerobically (with Ar rather than O_2) on glucose (*87*). A similar experiment was carried out using Gal-ATM1/Glu/O_2 cells. The resulting 4.5 K low-field Mössbauer spectrum (Figure 5-2G) was dominated by two doublets. One accounted for ~ 30% of spectral intensity and was due to high-spin Fe(II) ions (δ ~ 1.3 mm/s, ΔE_Q = 2.8 mm/s). The other doublet, representing ~ 50% of spectral intensity, possessed parameters typical of $[Fe_4S_4]^{2+}$ clusters. The percent effect was quite low indicating no hyper-accumulation of Fe or evidence of ferric nanoparticles. The spectrum of WT cells grown under anaerobic conditions was similar (Figure 5-2F). UV-vis spectra of these mitochondria revealed low concentrations of heme centers (Figure 5-6C and 6D), reflecting O_2-dependent heme biosynthesis (*45*). Hemes a+a_3 were essentially absent, probably due to a direct requirement of O_2 for heme a synthesis (*52*).

Aconitase activities in mitochondria isolated from anaerobic W303/Glu/O_2 and Gal-ATM1/Glu/O_2 cells were also determined. The results (Table 5-1) show high activities in both strains, indicating the presence of mitochondrial Fe/S clusters. Leu1p is a cytosolic Fe/S-containing enzyme and its activity was measured to assess the functioning of the CIA machinery. The results (Table 5-1) show the absence of Leu1p activity in Gal-ATM1/Glu cells grown under either aerobic or anaerobic conditions.

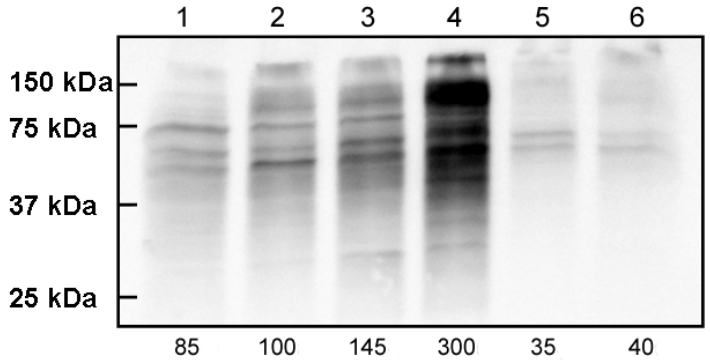

Figure 5-9: Oxyblot analysis of mitochondria isolated from W303 and Gal-ATM1 cells. Lane 1, W303/Gal/O_2; lane 2, W303/Glu/O_2; lane 3, Gal-ATM1/Gal/O_2; lane 4, Gal-ATM1/Glu/O_2; lane 5, W303/Glu/Ar; lane 6, Gal-ATM1/Glu/Ar. The total level of carbonylated proteins was calculated from each lane, normalized relative to the intensity in lane 2 and shown as a percentage of that at the bottom of the figure.

Oxidative Stress Levels in Atm1p-depleted Mitochondria

Using the Oxyblot™ assay, we examined the level of oxidative stress associated with mitochondria isolated from Gal-ATM1 cells. Relative to the degree of oxidative stress associated with mitochondria from W303/Gal/O_2 and W303/Glu/O_2 cells (Figure 5-9, lanes 1 and 2), mitochondria from Gal-ATM1 cells grown on galactose/O_2 (lane 3) and glucose/O_2 (lane 4) exhibited greater levels of oxidative stress, consistent with previous findings (*11*). The extent of oxidative damage was especially severe for Gal-ATM1/Glu/O_2 mitochondria in that the total carbonylated protein level was ~ 300% of the WT amount. The extent of damage was higher than reported for mitochondria isolated from *yfh1*Δ strain (~ 250% relative to WT) (*55*). The extent of oxidative damage appeared proportional to the amount of hyper-accumulated Fe, with mitochondria from galactose-grown cells exhibiting less ROS damage and less Fe accumulation than those from glucose-grown cells. As expected, the level of ROS damage was less in W303 and Gal-ATM1 cells grown under anaerobic conditions (Figure 5-9, lanes 5 and 6).

Discussion

No ISC Phenotype in Atm1p-depleted Mitochondria from Anaerobic Cells

In this study, we have used an integrative biophysical approach to characterize the Fe in Atm1p-depleted mitochondria. Our results indicate that under anaerobic growth

conditions, Atm1p-depleted mitochondria contain WT levels of Fe/S clusters and heme groups, and do not hyper-accumulate Fe. Since heme synthesis is O_2-dependent, the WT level of hemes in anaerobic cells is substantially reduced relative to that in aerobically grown cells. In terms of mitochondrial ISC and heme centers, such mitochondria cannot be distinguished from mitochondria of WT cells grown anaerobically. This indicates that *Atm1p is not required for mitochondrial Fe/S cluster assembly or heme biosynthesis*.

In anaerobic cells, lack of Atm1p in the mitochondria does not appear to perturb the mechanism that regulates the import flux of Fe into the mitochondria. In aerobic cells, this mechanism involves Aft1p, Aft2p, Fet3p, and other proteins of the iron regulon and other iron responsive genes (*83*). The Atm1p-exported species ***X*** has been proposed to regulate this system, with a deficiency of cytosolic ***X*** (e.g. caused by a deficiency of Atm1p) up-regulating the import of Fe into the cell and subsequently into mitochondria (see the model of Hausmann ***et al.*** (*83*)). Taken at face value, our results appear inconsistent with this proposal; however, the mechanism that regulates Fe in anaerobic cells is different. In anaerobic yeast cells, Hassett ***et al.*** (*97*) has shown that the high affinity Fe transporter system (Fet3p) is significantly repressed and not functioning; instead the low affinity transporter (Fet4p) is up-regulated and serves as the major cellular Fe uptake pathway (*6*). Fet4p is transcriptionally regulated by Aft1p and Rox1p and the cytosolic Fe status (via an unknown mechanism); however, it appears to have an

effective post-translational regulation so that its Fe uptake is actually independent of Aft1p (*98*); rather, the cytosolic Fe status seems to be the only decisive factor for Fe uptake rate for anaerobic cells. Thus, our results indicate that Atm1p and ***X*** are not involved in regulating iron uptake in ***anaerobic*** cells – i.e. ***X*** is not a sensor for Fe regulation under anaerobic conditions. Our results have no bearing on whether ***X*** is the sensor for the *AFT1*/*AFT2*-based iron regulon system.

Iron-sulfur Cluster and Heme Defects in Atm1p-depleted Mitochondria Isolated from Aerobic Cells

The spectra presented here reveal that the concentrations of ISCs and heme groups in Atm1p-depleted mitochondria from aerobically grown cells are significantly (4- to 8-fold) reduced relative to WT mitochondria grown under the same conditions. For ISCs, this was confirmed by aconitase activities which were significantly reduced in Atm1p-depleted mitochondria, relative to that of WT cells. We cannot exclude the presence of ***some*** ISC- and heme-containing proteins in Atm1p-depleted mitochondria, but there is no doubt that there is an ISC defect in the organelle and that the levels of these clusters are diminished relative to those in WT mitochondria.

This contrasts with previous studies (*11, 19*) which concluded that there is no defect in ISC assembly in Atm1p-depleted mitochondria (from aerobic yeast cells). These

studies were based solely on the activity of various Fe/S cluster-containing enzymes; they did not involve a biophysical investigation. Actually, these studies also found reduced ISC levels in yeast mitochondria depleted in Atm1p or homologs, but the degree of reduction was regarded as being insufficient to conclude that there was an ISC assembly defect. Using HeLa cells in which the homolog *ABCB7* had been knocked down to 20% - 30% of WT level, Cavadini *et al.* (*99*) found that mitochondrial and cytosolic aconitase activities were ~ 50% and ~ 20% of control values, respectively, and that the activity of succinate dehydrogenase, a mitochondrial enzyme, was ~ 80% of WT level. They implied that there is no significant ISC defect in the mitochondria by suggesting that ABCB7 exports Fe from the mitochondria to the cytosol.

Differences in mitochondrial Fe/S-containing enzyme activities and ISC level in yeast cells may arise from differences in the growth media and the extent of Atm1p depletion. Atm1p-deleted cells do not grow on minimal media but grow slowly on rich media (*84*). Atm1p-depleted cells grow on minimal media, but they contain reduced levels of hemes relative to rich-media levels (*83*). Growth on minimal medium may stress cells and result in a more complete depletion of Atm1p and perhaps some additional secondary phenotypes. Differences in growth times may have also influenced outcomes, as shutting down *ATM1* expression is a slow process that occurs over the course of tens-of-hours (*19*).

Role of O_2 in the Development of the ISC Defect in Atm1p-depleted Mitochondria

The presence of ISCs in mitochondria from anaerobic cells suggests that such clusters are ***assembled*** in mitochondria from aerobic cells, but that they are rapidly degraded such that steady-state levels of these clusters are low. Our results show that high levels of reactive oxygen species (ROS) are generated in Atm1p-depleted mitochondria from aerobic cells. We have also discovered that high-spin Fe(II) ions accumulate in Atm1p-depleted mitochondria (see below). Although nothing is known about the properties of these ions, mononuclear high-spin Fe(II) ions are known to engage in Fenton chemistry to generate ROS (*100*). ISCs in Atm1p-depleted mitochondria may be degraded by reaction with O_2 or ROS generated in this way, similar to that found in other systems (*101*). Inorganic synthesis of ISCs or reconstitution of such centers on proteins generally requires anaerobic conditions. Oxygen exposure in isolated yeast mitochondria inhibits one or several steps in ISC assembly (*102*). The reduction in heme centers could be similarly rationalized, as originally suggested by Kispal ***et al.*** (6).

Characterization of Ferric Nanoparticles in Atm1p-depleted Mitochondria

In this study, we found that the Fe which hyper-accumulates in Atm1p-depleted mitochondria is in the form of ferric phosphate nanoparticles. We have characterized

these nanoparticles in some detail. EPR and Mössbauer spectra indicate superparamagnetically relaxing, magnetically interacting ferric ions, similar to that observed in Yah1p-depleted (*87*) and Yfh1p-deleted (*18*) mitochondria. EM images reveal individual particles 2 – 4 nm in diameter, clumped into larger aggregates. Our EM results show nanoparticles composed of Fe and P in approximately equimolar amounts.

Phosphate ions are present at high concentration in the mitochondrial matrix (estimated between 10 and 20 mM) (*67*), and this is almost certainly the form of phosphorus detected in the nanoparticles. For Fe-O-P(phosphate) units, Fe-O and O-P bond distances of 2.01 Å and 1.53 Å are commonly observed (*103*). By assuming a triangle with sides of length 2.01, 1.53 and 3.21 Å (the latter corresponding to the Fe-P length determined by EXAFS), the *Law of Cosines* indicates 130º for the Fe-O-P angle. This excludes a linear arrangement for these atoms. Bidentate coordination of Fe to two oxygen atoms from the same phosphate ion is also excluded, as this would require a shorter Fe-P distance ($\leq$ 2.46 Å) than is observed.

The other ligands coordinating the ferric ions in the nanoparticles are unknown but our EM results indicate that they involve oxygen atoms but probably not nitrogen or carbon atoms. These results, along with the observed average Fe-O bond distance of 1.97 Å, suggest a combination of water/hydroxide ligands. The Fe-O bond distances in Fe(III)-OH and Fe(III)-OH_2 arrangements are 1.91 Å and 2.05 Å, respectively (*104*). A

charge-neutral 5-coordinate ferric site with 2 Fe-O bonds (from phosphate) at 2.01 Å, 1 Fe-OH bond at 1.91 Å and 2 Fe-OH_2 bonds at 2.05 Å would have an average Fe-O bond length of 2.01 Å, slightly longer than the observed value of 1.97 Å, but near to the uncertainty of the EXAFS measurement. The Debye-Waller factor estimated from this disordered set of ligands of 0.003 $Å^2$ is somewhat smaller that the observed value of 0.0055 $Å^2$. Nevertheless, the difference is perhaps within the uncertainty of the measurement. A candidate ferric nanoparticle structure satisfying all of these relationships is shown in Figure 5-10.

The ferric ions in these nanoparticles were likely imported by passage through an IM transporter such as Mrs3p or Mrs4p (or by another unidentified low- or high-affinity Fe transporter) in the form of Fe(II) ions (*79*). Regardless of the transporter, the mechanism of import likely involves the transporter recognizing the structure of the low-molecular Fe(II) trafficking complex. Consider that the imported Fe(II) ions are coordinated by an unknown endogenous ligand L whose structure is recognized by the IM transporter. It seems unlikely that Fe(II):L would be "free" (i.e. hexaqua) ferrous ions as this would not provide the necessary discrimination required for trafficking. Moreover, hexaqua ferrous complexes are highly susceptible to oxidation and precipitation, and they could engage in Fenton chemistry that would damage the cell. Thus, we propose that L consists of species other than waters or hydroxide ions. This suggests that once

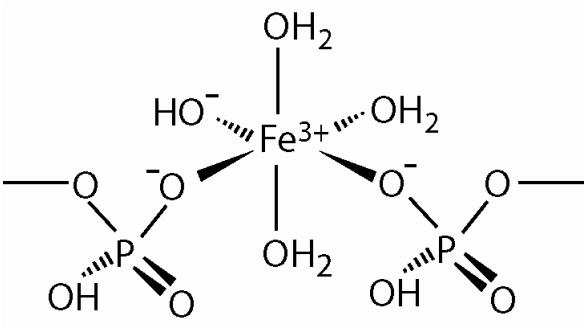

Figure 5-10: Candidate structure for the ferric nanoparticles in Atm1p-depleted mitochondria. Other geometries are possible. Other protonation states for water and hydroxide ligands are also possible, as long as overall charge neutrality is maintained.

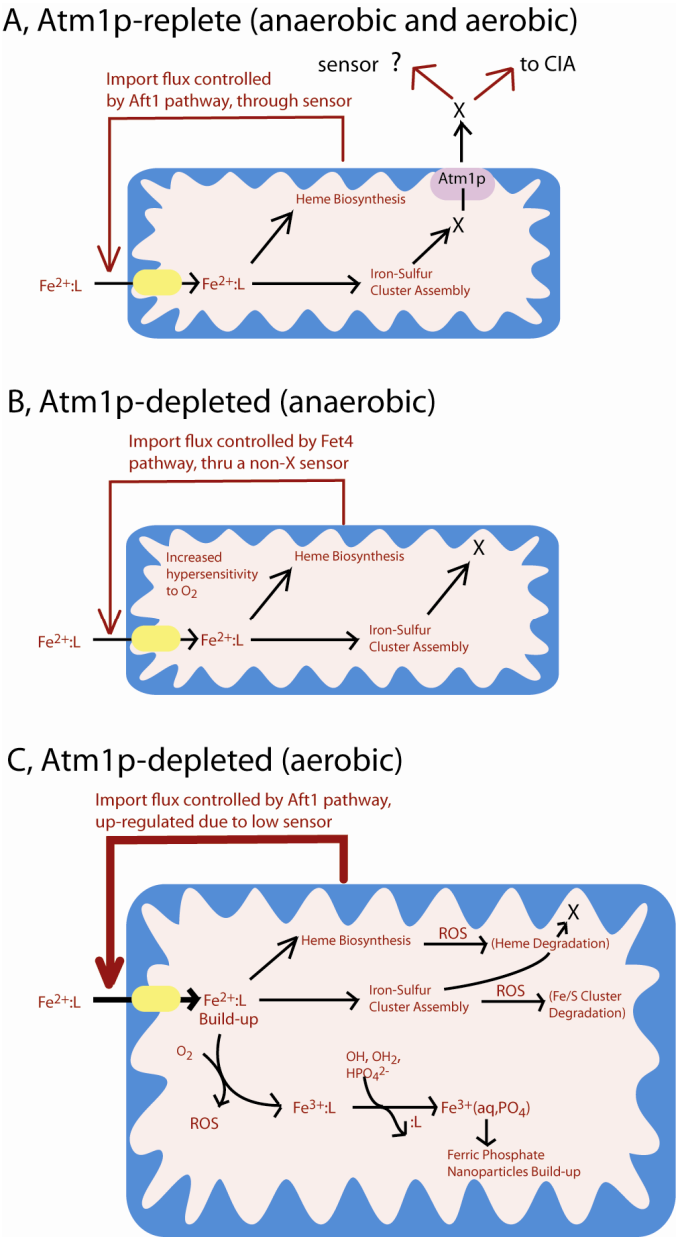

Figure 5-11. Working model for the effects of Atm1p depletion. The red line indicates a regulatory feedback mechanism in which the Fe status within the mitochondria is somehow sensed by the *AFT1*/*AFT2* system in aerobic cells and by the *FET4* system in anaerobic cells. See text for other details.

these Fe(II):L complexes are imported into the matrix, *the process of nanoparticle formation is initiated by oxidation to Fe(III) and the exchange of L for waters/hydroxide/phosphate ions.* The resulting Fe(III) species would precipitate into nanoparticles. This model is illustrated in Figure 5-11C.

High-spin Ferrous Ions in Mitochondria from Atm1p-depleted and Yah1p-depleted Cells

We have discovered that mitochondria from aerobically grown cells that are depleted in either Atm1p or Yah1p also accumulate nonheme high-spin Fe(II) ions. The concentration of such ions within these organelles is substantial; we estimate 300 - 500 μM for Atm1p-fully-depleted, 50 μM for Atm1p-partially-depleted and ~ 150 μM for Yah1p-depleted mitochondria. Such ions are also present in whole Atm1p-depleted cells. Nonheme HS Fe(II) ions are present in mitochondria from WT cells (data not shown) but at lower levels. Interestingly, no such ions appear to be present in Yfh1p-depleted mitochondria (*18*), suggesting that this may be a distinguishing property of the ISC phenotype. Further studies are required to explore this possibility.

We have characterized these accumulated Fe(II) complexes preliminarily. The linewidth of the HS Fe(II)-associated doublet from mitochondria of Gal-ATM1/Glu/O_2 cells was about twice that of the same doublet associated with Gal-ATM1/Gal/O_2 cells. The linewidth of the HS Fe(II) doublet of mitochondria of glucose-grown cells was so

large as to suggest that more than one species contributes. Mitochondria from Atm1p-partially-depleted cells grown on galactose could contain a single HS Fe(II) complex. None of these species appears to be hexaqua Fe(II) ions.

Function of Atm1 and X

Given the complexity of cells, determining the exact cellular functions of Atm1p and *X* is exceedingly difficult, with limited number of experimental results to guide us. Two functions for Atm1p and *X* have been suggested (*83*). One links mitochondrial ISC assembly to cytosolic ISC assembly (CIA). *X* would be produced in proportion to the rate of mitochondrial ISC assembly and exported into the cytosol where it would serve either as a substrate or co-catalyst for CIA-dependent ISC assembly. When mitochondria would be depleted in Atm1p, *X* would not be exported, halting cytosolic ISC assembly but not mitochondrial ISC assembly. Our results show a defect in mitochondrial Fe/S clusters under aerobic conditions but not under anaerobic conditions. We interpret this to mean that ISC's *are* assembled in Atm1p-depleted mitochondria but that they are rapidly degraded by ROS under aerobic conditions. These results are consistent with the previously proposed function of Atm1p/*X*, which imply that Atm1p is not involved in mitochondrial Fe/S cluster assembly.

We also considered whether the ROS generated in this process, rather than the

lack of *X* in the cytosol, might be responsible for the lack of CIA-dependent Fe/S cluster assembly in Atmp1-depleted cells. However, the absence of Leu1p activity in Atm1p-depleted cells grown under anaerobic conditions eliminates this possibility. Rather, this result provides independent evidence supporting the hypothesis that CIA-dependent ISC assembly requires *X* as a substrate or catalyst.

Kispal *et al*. (*19*) cautiously suggested that *X* might contain both sulfur and iron, and that the accumulated Fe in Atm1p-deleted mitochondria might be *X* itself (*19*, *46*). Other researchers have suggested this possibility as well (*105*-*107*). Our results demonstrate that the accumulated Fe is ferric phosphate nanoparticles, inconsistent with this suggestion.

The second proposed function of *X* is to communicate the status of mitochondrial ISC assembly to the Aft1p-controlled iron regulon and other iron-responsive genes (*83*). Here, the presence of cytosolic *X* would signal to the Aft1p-controlled system that mitochondrial ISC assembly is functioning properly. Accordingly, a deficiency of cytosolic *X* would alert the system of depressed rates of mitochondrial ISC assembly, prompting an increased import flux of Fe into cells and probably into mitochondria. Our results show that this flux is not increased in Atm1p-depleted anaerobic cells, but this has no bearing on this proposed function for Atm1p/*X*, in that the *AFT1/AFT2*-based iron regulon is not the primary regulator of cellular Fe under anaerobic conditions.

Model for the Development of the ISC Phenotype in Atm1p-depleted Cells

Our study has shown that the phenotypes for mitochondria obtained from Atm1p-depleted and Yah1p-depleted cells are largely indistinguishable, at least when grown under aerobic conditions on minimal medium. The recent study of Hausmann *et al.* (*83*) supports this conclusion. In that study, a microarray analysis of the transcriptome of Yah1p-depeleted and Atm1p-depleted yeast cells revealed significant differences in expression levels of ~ 200 genes relative to WT cells, but the changes in expression levels of these genes were rather similar (not identical) for both strains. This makes it difficult to correlate the ISC phenotype to the functions of proteins the lack of which cause the phenotype. Also, since there are many aspects to that phenotype, primary and secondary effects cannot be easily distinguished. Thus, proteins affording the ISC phenotype may primarily alter other aspects of metabolism (e.g. involving sulfur, oxygen, cellular redox homeostasis and/or regulation) and the observed effects on Fe metabolism may be secondary effects.

Despite these difficulties, it is interesting to consider the sequence of events that might lead to the ISC phenotype. We found here that the contents and distribution of Fe in WT and Atm1p-depleted cells are essentially indistinguishable under anaerobic conditions (Figure 5-11B), but dramatically different under aerobic conditions. WT aerobic cells show little response to O_2 exposure (Figure 5-11A) while the mutant strains

show several strong phenotypes including the ISC defect. Thus, we suggest that Atm1p-depletion (and Yah1p-depletion) increases the cell's *sensitivity* to O_2 exposure. According to the model of Figure 5-11C, Fe(II):L in Atm1p-depleted mitochondria is easily oxidized to Fe(III):L in the presence of O_2 (somehow this doesn't happen in WT cells). This generates ROS (directly or indirectly) and prompts L, assumed to prefer Fe(II) coordination, to dissociate. Under these conditions, ISCs and perhaps heme groups are synthesized, but are degraded quickly as they react with the newly generated ROS.

Hyper-accumulation of Iron

"Free" Fe(III) ions are essentially insoluble at neutral and alkaline pHs and, according to our model, would rapidly precipitate in the mitochondrial matrix to form nanoparticles. These nanoparticles accumulate beyond the level of Fe that is typically found in WT mitochondria, suggesting that the formation of nanoparticles is likely associated with an increased flux of Fe(II):L ions into the matrix, probably as a homeostatic regulatory response. We previously suggested that Fe regulation operated at the level of mitochondria (e.g. where the concentration of HS Fe(II) ions in the mitochondrial matrix served as a sensor to regulate import flux) (*87*). However, the high levels of HS Fe(II) ions present in the mitochondria that are experiencing this increased

import flux could be used to argue against this. One possibility is that the particular HS Fe(II) complex (or complexes) formed under these circumstances is(are) not the particular HS Fe(II) complex(es) that is(are) sensed. Another possibility, which we regard as more likely, is that mitochondrial Fe(II):L import flux is regulated at the cellular level via *AFT1*/*AFT2* and the iron regulon, and that the sensor is something other than Fe(II):L. In this model, regulation would still involve a species whose concentration reflects the Fe status within the mitochondria (e.g. *X*, see above). Changes in the concentration of this sensor would be monitored (directly or indirectly) by the *AFT1*/*AFT2* system, ultimately affecting the import flux of Fe(II):L. The sensor's concentration might change as a response to either Fe(II) oxidation, ligand exchange, or nanoparticle formation. Besides *X*, a molecule oxidized by ROS or the ligand L that is released during exchange should be viewed as candidates for this sensor. The nanoparticles themselves are probably chemically inert and thus unlikely to be the sensor. Moreover, the sensor would need to be exported from the mitochondria and to interact with the *AFT1*/*AFT2* system – roles that nanoparticles could not play.

Further evidence for a cellular (rather than organellar) level response to the Atm1p-dependent changes occurring within the organelle is provided by the massive alteration of the Fe content of whole WT cells *vs.* whole Gal-ATM1/Glu/O_2 cells. Although much work remains to understand these changes, it is clear that a deficiency of Atm1p in the

IM of the mitochondria has global consequences, ultimately influencing Fe metabolism throughout the cell.

CHAPTER VI

COMPARATIVE STUDY OF CELLULAR IRON DISTRIBUTION IN AFT1-1UP AND YAH1P-DEPLETED YEAST

Introduction

Iron plays numerous critical roles in cellular metabolism, including mitochondrial respiration and myriad catalytic events (*1*). It can also promote reactions (e.g. Fenton chemistry) that induce formation of highly deleterious reactive oxygen species (ROS). Therefore cellular trafficking and regulation are especially important for iron.

Traffic flow starts with the influx of Fe from the growth media into the cytosol via transporters in the plasma membrane (*108*). A portion of these ions enters mitochondria and vacuoles, which are considered as major Fe traffic "hubs". Mitochondria house respiratory complexes while vacuoles store Fe. The nucleus regulates traffic by controlling expression of genes that encode membrane-bound Fe transporters as well as other proteins involved in Fe regulation and trafficking.

In budding yeast *Sacchromyces cerevisiae* there are three major cellular iron uptake pathways. The dominant Fe import pathway under regular growth condition consists of the plasma membrane proteins Fet3p and Ftr1p. These proteins form ferroxidase-permease complexes and function together to import Fe with high affinity. The other minor Fe import pathway under regular aerobic condition involves low-

affinity ferrous iron transporter Fet4p Although *S. cerevisiae* does not produce siderophores itself, it has siderophore transporters Arn1-4p that can uptake siderophores that are produced by other organisms (*5*). Once in the cytosol, Fe status is sensed by Aft1p and Aft2p, transcription factors that control expression of FET3, FTR1 and ~ 20 other genes collectively known as the *iron regulon* (*109*). Aft1p (and possibly Aft2p) moves between the cytosol and the nucleus in an iron-dependent manner. It has been proposed that when the cytosolic Fe level is low, Aft1p remains in the nucleus where it binds the promoter region of iron regulon genes and activates their expression. In contrary, when cytosolic Fe levels are high, Aft1p evacuates the nucleus, and the expression level of the iron regulon declines. *Daft1* cells grow slowly on Fe-deficient media (achieved by adding BPS) due to the inability to uptake iron, whereas WT cells grow normally. Both cell types grow normally when the media Fe concentration is high (*110*). The molecular mechanism by which a need for cellular Fe is transduced to Aft1p is uncertain but it appears to include Fra1/2p and Grx3/4p which may bind an [Fe_2S_2] cluster (*111*).

Mitochondria are the primary cellular sites of Fe/S cluster assembly and heme biosynthesis. Ferrous ions enter the mitochondria through the high-affinity transporters Mrs3/4p, located on the inner membrane (IM) and probably some other low-affinity transporters. Once imported, the iron may form a pool used for Fe/S cluster assembly

and heme biosynthesis. It has been recently discovered that mitochondria from fermenting yeast cells contain a large pool of nonheme high-spin Fe^{2+} ions (*9*). This pool shrinks under respiring conditions, when production rates of respiratory complexes are higher (*112*), suggesting that this pool is filled by Mrs3/4-mediated influx of Fe, and drained for Fe/S cluster and heme biosynthesis.

Downstream events in the synthesis of Fe/S clusters include the transfer of Fe by the chaperon protein Yfh1p to the Fe-S scaffold protein Isu1/2p. Cysteine desulfurase (Nfs1) extracts sulfur from cysteine while the Yah1p-Arh1p electron transferring chain donates electrons required for Fe/S cluster biosynthesis. Chaperone proteins Ssq1p, Jac1p, Mge1p and Grx5p help transfer Fe-S clusters from scaffold proteins to various acceptor apo-proteins including respiratory complexes. The IM protein Atm1p exports an unknown species *X*, hypothesized to be produced during Fe/S cluster biosynthesis, from the matrix to the cytosol where is used in cytosolic Fe/S cluster assembly. Deletion of any of these ISC-related proteins results in several common phenotypes including: a respiration defect, the constitutive activation of iron-regulon genes, the accumulation of ferric phosphate nanoparticles in mitochondria and increased levels of ROS.

Vacuoles are the other major organelle involved in cellular Fe metabolism and homeostasis. It is considered as the major site of cellular Fe storage. CCC1 is the only known vacuolar iron importer. *Dccc1* cells contain less than normal amounts of Fe in

vacuoles while the CCC1 overexpression strain contains elevated amounts (*13*). Fet5p and Smf3p are vacuolar membrane proteins that export Fe into the cytosol (*5*). Kosman *et. al* has proposed that vacuolar Fe is in the Fe^{III} state (*113*) and this is consistent with our previous observations (*9*).

The cytosol also plays important roles in Fe trafficking and homeostasis, as inferred from genetic studies. *DDMrs3/4* cells show a growth defect in BPS-treated media, but they grow well on Fe-replete media. Assuming that the concentration of Fe in the cytosol is proportional to that in the media, this experiment suggests that cytosolic Fe can be imported into mitos in the absence of Mrs3/4, but only when the concentration of cytosolic Fe is high. Conversely, *Dccc1* cells grow normally in Fe-deficient media but show a growth defect in high-iron (100 μM Fe) media (*13*). Vacuoles lacking CCC1 may have a diminished ability to store Fe due to impaired Fe import from the cytosol; the "overflow" Fe in the cytosol probably inhibits cell growth (maybe via ROS damage) when cells are grown in media containing high Fe concentrations (*114*). This same toxicity can be suppressed by overproducing Mrs3/4p (*114*). This suggests that the overflow cytosolic Fe (caused by CCC1 deletion) can be imported into the mitochondria via Mrs3/4p, and that this Fe is no longer toxic when contained in mitochondria. The simplest explanation may be that mitochondria and vacuoles draw from a common pool of cytosolic Fe.

This pool of cytosolic Fe also appears connected to the nanoparticles that can accumulate in mitochondria isolated from ISC mutants. Like other ISC-related proteins, deletion of Yfh1 causes nanoparticle accumulation in mitochondria. However, no accumulation occurs (and there is no respiratory defect) in *Dmrs3Dmrs4Dyfh1* cells (*115*). This implies that the cytosolic Fe that enters the mitochondria and accumulates as nanoparticles in these ISC-related strains is imported by Mrs3/4p. Overexpressing CCC1 also prevents Fe accumulation in *Dyfh1* mitochondria (*14*), further evidence that vacuoles and mitochondria draw from the same cytosolic pool of Fe.

The two organelles, mitochondria and vacuole have recently been shown to interact functionally. In *DMrs3/4 cells*, mitochondria are deficient in Fe and have reduced Fe/S and heme levels (probably due to inability to import sufficient Fe into the organelle), whereas the vacuolar Fe level in these cells is increased because CCC1 is activated (to store the additional Fe located in the cytosol). The activation of CCC1 is thought to reduces cytosolic Fe levels thus activates Aft1p (*14*).

Cells deficient in Mrs3/4 grow poorly on low-media Fe because insufficient Fe enters the mitochondria (*47*). Mrs3/4-deficient cells have lower aconitase activity, but this activity can be recovered when CCC1 is deleted. This again suggests that vacuoles and mitochondria may draw from a common pool of Fe in the cytosol.

The Aft1-1up strain has a single mutation in which one residue has been changed

from cysteine to phenylalanine. This mutation causes Aft1p to stay in the nucleus, and constitutively activate AFT1-controlled iron regulon genes independent of the iron status in the cells. This increases the rate of cellular iron uptake regardless of the media iron concentration. Aft1-up cells cultivated in rich medium (that contains high Fe) also contain high Fe levels (*54*). Mutant cells with Fe/S cluster defects also have elevated iron levels. In this chapter, we apply our integrative biophysical methods to examine the cellular iron distribution in Aft1-1up strains and compare this distribution to that in wild type and Yah1p-depleted cells. Our results show that Aft1-dependent activation of the iron regulon increases the iron content of the cell but does not significantly alter the partitioning of cellular iron between the mitochondria and vacuoles. In contrast, disruption of the Fe/S biosynthesis pathway by Yah1p-depletion causes loss of vacuolar iron and massive import and precipitation of iron in the mitochondria.

Results

Location of Nonheme High-Spin Fe(III) Species in WT Cells

We previously reported (*9*) that the Fe in WT fermenting cells could be roughly divided into two categories: a quarter was present in mitochondria and could be subdivided into $[Fe_4S_4]^{2+}$ clusters, $[Fe_2S_2]^{1+}$ clusters, LS and HS Fe(II) hemes, mononuclear HS nonheme complexes and ferric phosphate nanoparticles. Most of the remaining three quarters was in the form of nonheme mononuclear (magnetically

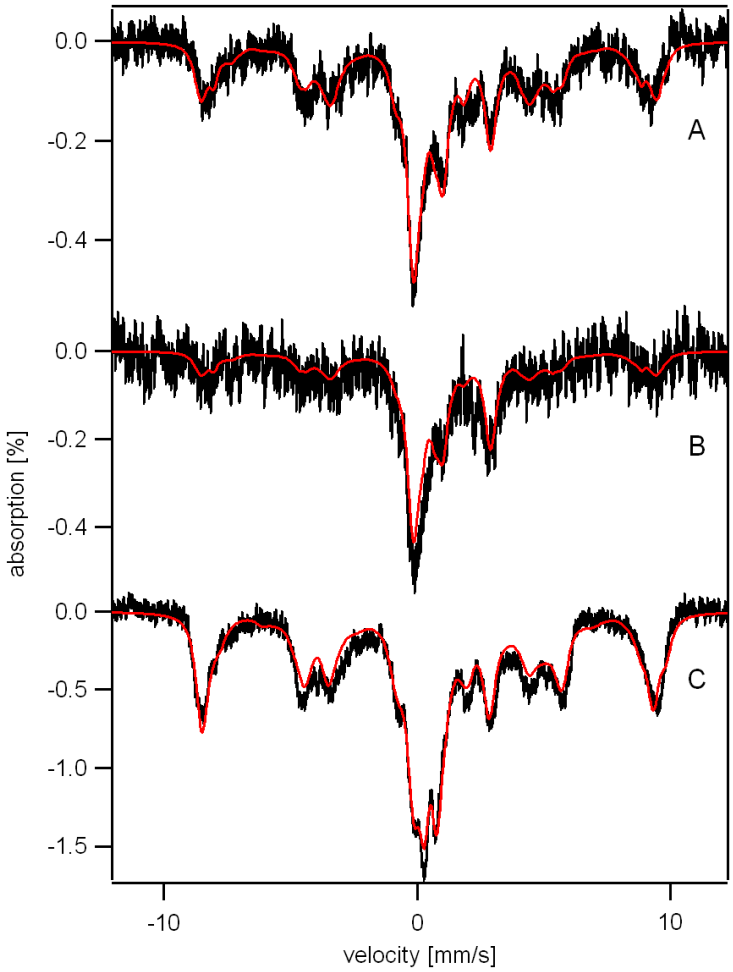

Figure 6-1: Mössbauer spectra of WT and CCC1 mutant whole cells. Cells were grown on complete minimal medium supplemented with 40μM ^{57}Fe. A, WT (W303) strain; B, *Δccc1* cells; C, CCC1-overexpressing cells. The red lines overlaying the spectra are simulations that include HS Fe(III), the central doublet, nonheme HS Fe(II) and Fe(III) nanoparticles using parameters given in Table 6-3.

isolated) HS Fe(III). This Fe does not appear to be associated with mitochondria because Mössbauer spectra of isolated mitochondria exhibit only minor intensity due to this form of Fe.

A control batch of WT fermenting cells grown in media containing 40 μM Fe (Figure 6-1 A) revealed a similar distribution; this sample had ~ 60% non-mitochondrial HS Fe(III). Mitochondrial Fe give rise to the central doublet, which has δ = 0.45 mm/s and ΔE_Q = 1.10 mm/s. This doublet originates from S = 0 $[Fe_4S_4]^{2+}$ clusters and S = 0 LS Fe(II) hemes and it accounted for 15% of the total iron in the sample. The spectrum also exhibited a nonheme HS Fe(II) doublet with δ ~ 1.3 mm/s and ΔE_Q ~ 3 mm/s (accounting for 16% of total iron), and poorly resolved absorption at ~ 0 mm/s (representing ~ 10% of total iron). Up to 8% of the spectral absorption, contained within the unresolved absorption, is probably due to Fe(III) nanoparticles, some or all of which are probably in the mitochondria (*9*).

We previously proposed that the non-mitochondrial HS Fe(III) species are located in vacuoles since this organelle is known to store Fe (*9*). Kosman et. al proposed that vacuolar Fe should be in the Fe(III) state, consistent with the observed oxidation state (*113*).

To test this proposal, we collected Mössbauer spectra of cells in which Ccc1p, the only known vacuolar Fe importer, was deleted. The solid line in the 5 K low-field

spectrum (Figure 6-1B) of *Dccc1* cells is a simulation that assumes that ~ 25% of spectral absorption is due to HS Fe(III), ~ 2.5 fold less, in terms of percentages, than that observed in WT spectra. This decline of HS Fe(III) species in *Dccc1* cells relative to in WT cells suggests that the majority of HS Fe(III) species in WT cells are located in vacuoles. However, our results cannot distinguish between a decline in the concentration of Fe in vacuoles and a decline in the volume of vacuoles. Thus, *Dccc1* cells may contain vacuoles with a lower-than-WT concentration of HS Fe(III) ions or they may contain fewer or smaller vacuoles (or some combination of these). The percentage decline of HS Fe(III) absorption in *Dccc1* cells could also, in principle, be due to an increased concentration of Fe in these cells. However, based on estimation of the intensity of the Mössbauer spectra, there is less iron in *Dccc1* cells than in WT. Given the role of Ccc1p, the simplest conclusion is that the concentration of Fe in the vacuole decreases in the absence of this vacuolar Fe importer.

Although the amount of HS Fe(III) species in *Dccc1* cells was reduced relative to that in WT cells, ~ 25% of the Fe in *Dccc1* cells is still due to HS Fe(III) species. These ions could be partially located in vacuoles, in which case we would conclude that these organelles possess a second CCC1-independent Fe import pathway. These ions could also be located in the cytosol or in another organelle. In any event, the data can exclude the possibility that the HS Fe(III) ions that are blocked from entry into vacuoles have

collected in the cytosol. The spectra indicate a *decline* in HS Fe(III), not a *shift* of such ions from one location to another. This suggests that when cytosolic Fe is prevented from entering the vacuole, cells respond by reducing the import flux of Fe from the environment into the cytosol. This is evidence of a homeostatic regulatory mechanism in which the concentration of cytosolic Fe is maintained at some level (there is little, if any, build-up of cytosolic Fe when the import flux into vacuoles is reduced or abolished).

Apart from the absorption due to HS Fe(III) species, the Mössbauer spectrum of *Dccc1* cells exhibit a high-energy line that arises from a quadrupole doublet of nonheme HS Fe(II); this component represents ~ 22% of spectral intensity. Also evident is a feature at ~ 1 mm/s, consistent with the presence of a central doublet (mitochondrial $[Fe_4S_4]^{2+}$ and LS Fe(II) hemes). Simulations suggest that this component represents ~ 15% of spectral intensity. The remaining 35% of the spectral absorption is unresolved (the feature is centered at ~ 0 mm/s in Figure 6-1B) and cannot be assigned. We suspect that at least 10% of the unassigned absorption arises from Fe(III) nanoparticles, but this is not established.

We have also examined a yeast strain in which CCC1 is overexpressed. Approximately 60% of the intensity of the 5 K Mössbauer spectrum of these cells (Figure 6-1C) is due to HS Fe(III) species, slightly lower than in WT cells. Given the role of Ccc1p as a vacuolar Fe importer, we had expected that the proportion of HS

Fe(III) would have *increased*. The percentage declined because a substantial portion of the absorption in the CCC1-overexpression cells (but not in WT cells) arises from Fe(III) nanoparticles (representing ~ 18% of total iron). Another ~ 14% of the intensity arises from a HS Fe(II) doublet. We suspect that a small central doublet is present but partially obscured by the nanoparticle absorption (estimated to be less than 6% of total iron).

Perhaps the most revealing difference between the CCC1-overexpression and WT spectra is a ~ 3-fold higher Percent Effect in the spectrum of the CCC1 overexpression strain. This indicates a higher-than-WT cellular Fe concentration, which means, in turn, that the absolute concentration of HS Fe(III) species in the CCC1 overexpression strain is indeed > 2 fold higher than that in WT cells.

The cellular location of these Fe(III) nanoparticles requires further investigations. If these nanoparticles are indeed located in mitochondria (as we have found under other genetic strains where nanoparticles form), this would raise the issue of why the overexpression of a *vacuolar* Fe importer would *increase* the flow of Fe into mitochondria. Indeed, if vacuoles and mitochondria imported cytosolic Fe from the same pool, a *decline* in mitochondrial Fe would be expected from an increased rate of vacuolar Fe import. The observed increase of flow into mitochondria would result if the

Table 6-1. Quantification of mRNA level of different genes under iron-rich[a] and iron-depleted[b] conditions using RT-PCR.

Mean Ct[c] / Gene	WT+BPS	WT–BPS	Aft1-1up +BPS	Aft1-1up –BPS
Act1	17.9	17.0	17.6	17.1
Fet3	17.4	22.6	16.9	16.5
Fre1	19.4	25.0	19.8	21.5

[a] Iron-rich condition: iron-free minimal medium supplemented with 40 μM Fe(III)-citrate.

[b] Iron-depleted condition: iron-free minimal medium supplemented with 100 μM BPS.

[c] Ct: threshold cycle; reported numbers are average of two measurements.

Table 6-2. Characterization of Aft1-1up whole cells and isolated mitochondria.

Growth Medium [Fe], μM	1	5	40	500
Whole Cell [Fe], μM	480 ± 20	1600 ± 200	2000 ± 300	2400 ± 300
Isolated Mitochondria [Fe], μM	1100 ± 50	N.D.	6200 ± 100	N.D.
Isolated Mitochondria [protein], mg/mL	55 ± 5	N.D.	65 ± 6	N.D.
Aconitase Activity[a]	480	N.D.	150	N.D.

[a] Aconitase activity in units/mg was measured using purified mitochondria; estimated relative error for the activity assay is 20% ($n \geq 2$).

Table 6-3. Parameters used for Mössbauer spectral simulation and the percentage of the component species. See Figure 6-1 and 6-2 for the spectra and the simulations.

Spectrum	HS Fe(III)[a]	Central Doublet[b]	HS Fe(II)[c]	Fe(III) nanoparticles[d]
Fig. 6-1A	60%	15%	16%	8%
Fig. 6-1B	25%	15%	22%	10%
Fig. 6-1C	60%	6%	14%	18%
Fig. 6-2A	75%	8%	10%	5%
Fig. 6-2B	70%	7%	5%	12%
Fig. 6-2C	60%	8%	6%	25%
Fig. 6-2D	58%	8%	8%	22%
Fig. 6-2E	80%	5%	5%	8%
Fig. 6-2F	70%	5%	7%	14%

[a] Parameters used for HS Fe(III) simulation: D= 1.5 cm^{-1}, E/D= 0.28; three HS Fe(III) species were used: (reported value corresponds to the sum of these three species)

1) ΔEq= 0.5mm/s, Eta= -3, A_{iso}= -240 kG, δ= 0.55mm/s, Γ= 0.3mm/s
2) ΔEq= 0.2mm/s, Eta= -3, A_{iso}= -218 kG, δ= 0.46mm/s, Γ= 0.4mm/s
3) ΔEq= 0.5mm/s, Eta= 0, A_{iso}= -235 kG, δ= 0.52mm/s, Γ= 0.5mm/s

[b] Parameters used for central doublet simulation:

ΔEq= 1.08mm/s, δ= 0.45mm/s, Γ= 0.6mm/s

[c] Parameters used for HS Fe(II) simulation:

ΔEq= 3.0mm/s, δ= 1.35mm/s, Γ= 0.6mm/s

[d] Parameters used for Fe(III) nanoparticles simulation:

ΔEq= 0.5mm/s, δ= 0.52mm/s, Γ= 0.5mm/s

mitochondria imported Fe directly from the vacuole and if the rate of import was proportional to the concentration of Fe in the vacuole. Another explanation of the observed results is that the observed nanoparticles are located in vacuoles.

In summary, the major conclusion of this section (which will be assumed for the remainder of the chapter) is that most or all of the HS Fe(III) species observed in WT cells is located in vacuoles. More studies are required to explore the other issues raised by these experiments.

Characterization of the Aft1-1up Strain

The iron regulon genes, including FET3 and FRE1, should be strongly induced in WT cells grown under Fe-deficient conditions (e.g. in the presence of BPS). Under Fe replete conditions (e.g. with 40 μM medium Fe), the induction of these genes should decline. This behavior was verified using quantitative PCR. Under Fe-deficient conditions, the level of FET3 and FRE1 mRNA levels in WT cells were 30-50 fold higher than under Fe replete condition (see Table 6-1). In contrast, Aft1-up cells under Fe-replete and Fe-deficient conditions afforded similar FET3 and FRE1 mRNA levels, indicating that these genes are constitutively activated regardless of medium Fe availability. This is consistent with published behavior of the Aft1-1up strain (*110*) and it verifies the genotype of the strain used in this study.

Aft1-1up cells were grown in minimal medium containing various Fe concentrations (1, 5, 40, 500 μM added ^{57}Fe). The cellular iron concentration increased with the concentration of Fe in the medium (Table 6-2). The values reported represent the iron concentration in packed cells. Actual cellular Fe concentrations should be slightly higher, as the tabulated values were not corrected for the interstitial volume between packed cells. This correction factor will not affect the observed trend of higher cellular iron concentrations for cells grown with higher concentrations of Fe in the media.

At the lowest media [Fe] tested, the Fe concentration of Aft1-up cells was similar to that of WT cells (*9*). This is probably because the expression levels of the iron regulon in Aft1-up and WT cells under low media-iron concentrations are similar. In growth media containing 40 μM Fe, the Fe concentration in Aft1-1up cells was ~ 4 fold higher than that in WT cells. This build-up is undoubtedly caused by the expression of the iron regulon in Aft1-up cells under high media-iron conditions; in WT cells, where Aft1 is functioning properly, the iron regulon is not expressed under these growth media conditions. This was the same concentration used in the growth media of the cells used in the quantitative PCR experiment (Table 6-1). When the Fe concentration of the growth media was ≥ 40μM, the iron concentration in Aft1-up cells only increased marginally, perhaps reflecting the saturation of cellular iron uptake systems.

We used Mössbauer spectroscopy to examine the iron content of Aft1-up cells

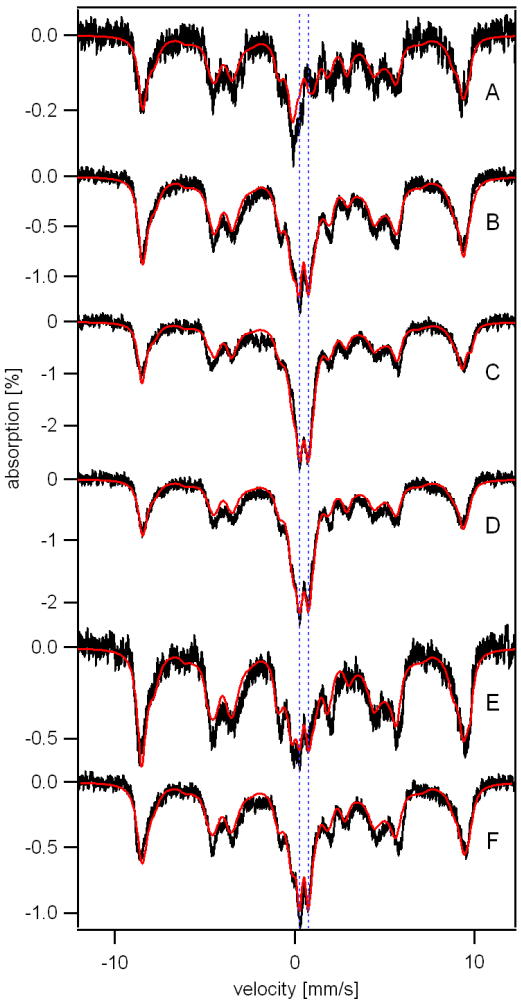

Figure 6-2: Mössbauer spectra of Aft1-up whole cells grown minimal or rich medium with various ^{57}Fe added. A-D, cells grown on complete minimal medium supplemented with 1μM, 5μM, 40μM and 500μM ^{57}Fe, respectively. E-F, cells grown on YPD medium supplemented with 20 and 400μM ^{57}Fe. The red line in each spectrum represents a simulation for HS Fe(III), central doublet, HS Fe(II) and Fe(III) nanoparticles (See Table 6-3 for the percentage and parameters). The blue dash line indicates the doublet due to Fe(III) nano-particles. Mössbauer spectra were collected at ~ 5K.

grown in media containing different concentrations of Fe. Cells grown in minimal media supplemented with ~ 1 μM ^{57}Fe exhibited a 5 K low-field Mössbauer spectrum (Figure 6-2A) similar to that of WT cells (Figure 6-1A). The major difference was a higher-than-WT percentage of HS Fe(III) (~ 75% in Aft1-1up vs. ~60% in WT. This suggests that the rate of Fe import into vacuoles relative to the rate of Fe import into mitochondria is greater for Aft1-up cells than for WT cells. Consistent with this idea, the shoulder due to the central doublet in spectra of WT cells is less obvious in spectra of Aft1-up. The same situation holds for the HS Fe(II) doublet; this feature is present in spectra of WT cells but not in spectra of Aft1-up cells grown with 1 μM Fe. Note that only insignificant amounts of Fe(III) nanoparticles exist (≤5% of total iron) in the spectrum of Aft1-up cells grown with 1 μM Fe.

The 5 K low-field Mössbauer spectrum of Aft1-up cells grown on media containing 5 μM ^{57}Fe also exhibited significant amounts of HS Fe(III) species (Figure 6-2B). The percentage of the cellular Fe in this form was diminished slightly relative to the cells grown on 1 μM ^{57}Fe (above); namely ~ 70% for cells grown on 5 μM ^{57}Fe and 75% for cells grown on 1 μM ^{57}Fe. However, the Percent Effect has increased substantially which reflects the ~ 3-fold increased concentration of Fe in the cells grown on 5 μM vs. 1 μM ^{57}Fe (note that the media contains 1-2 μM ^{56}Fe background). Thus, in terms of absolute amounts, the number of moles of Fe present as HS Fe(III) has increased ~ 3-fold. This is

constant with an increased flow of Fe into the cell (and into the vacuole) due to an increased concentration of Fe in the media. Approximately 12% of the intensity in the Mössbauer spectrum of Aft1-up cells grown with 5 μM Fe in the media was due to Fe(III) nanoparticles. The formation of these particles may reflect a greater import flow of Fe from the environment.

These same trends continue for Aft1-up cells grown on media containing 40 μM ^{57}Fe (Figure 6-2C), but a plateau of sorts is reached. In these cells, the percentage of Fe due to HS Fe(III) decreases slightly (to ~60% for cells grown on 40 μM Fe). Relative to the sample grown on 5 μM Fe, the Fe content of the 40 μM-Fe-grown cells was increased slightly (2.0 vs 1.6 mM) (see Table 6-2). The absolute amount of Fe present as HS Fe(III) has increased, again indicating an increased flow of Fe into the cell (and into the vacuole), as the concentration of Fe in the media increases. The relative absorption of nanoparticles has also increased in the 40 μM-Fe-grown cells (representing ~ 25% total iron), again suggesting an increased flow into mitochondria (see below).

The 5 K low-field Mossbauer spectrum of Aft1-up cells grown on 500 μM Fe is very similar to that from the 40 μM-Fe-grown cells. Also, the concentration of Fe in these cells was only slightly higher than in the 40 μM-grown cells. We conclude that the rate of Fe flow into the cells and then into the vacuoles and mitochondria does NOT increase much between cells grown on 40 μM Fe and those grown on 500 uM Fe; a

saturation level for the Fe import rate is reached in this region.

Fe(III) Nanoparticles are Associated with Mitochondria

To test whether the nanoparticles observed in Mössbauer spectra of Aft1-up cells grown in media containing high Fe concentrations were located in mitochondria, we isolated mitochondria from Aft1-up cells grown on media with 1 μM and 40 μM ^{57}Fe. The Fe concentration in mitochondria isolated from cells grown on 1 μM medium Fe was similar to what reported for mitochondria isolated from WT cells (Table 6-2). In contrast, the Fe concentration in mitochondria isolated from cells grown on 40 μM medium Fe was ~ 6 fold higher than in WT mitochondria.

The 5 K low-field Mössbauer spectrum of mitochondria isolated from Aft1-up cells grown on 40 μM ^{57}Fe (Figure 6-3A) showed that the vast majority of Fe in these organelles was present as ferric nanoparticles. Also evident is the high-energy line of a HS Fe(II) doublet corresponding to ~ 2% spectral absorption. Although this is a small percentage of the total intensity, the absolute concentration of the species represented by this feature is ~ 100 μM. Similar species have been reported for Yah1- and Atm1-depleted mitochondria (*87, 116*).

Mitochondria were also isolated from Aft1-up cells grown on 1 μM ^{57}Fe. The 5 K low-field Mössbauer spectrum of these organelles was dominated by unresolved

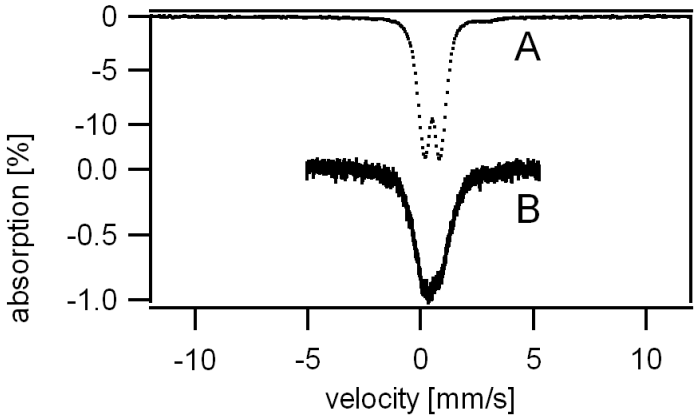

Figure 6-3: Mössbauer spectra of mitochondria isolated from Aft1-1up grown on complete minimal medium containing 40 μM (trace A) and 1 μM Fe (trace B).

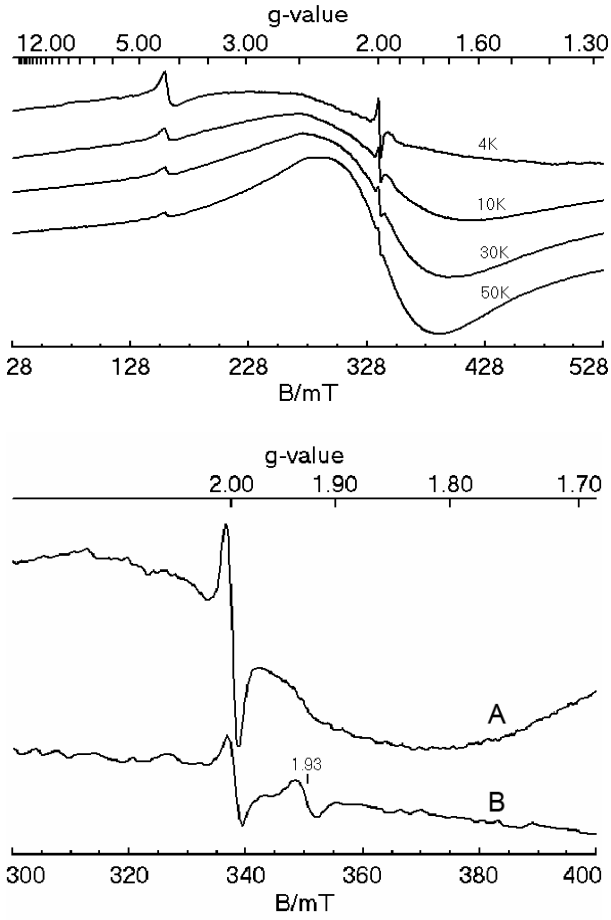

Figure 6-4: EPR spectra of the mitochondria isolated from Aft1-1up strain. Top: mitochondria isolated from Aft1-1up grown on 40 μM Fe recorded at temperature 4, 10, 30 and 50 K respectively. Bottom: mitochondria isolated from Aft1-1up grown on 40 μM (A) and 1 μM (B) medium Fe, recorded at temperature of 10 K.

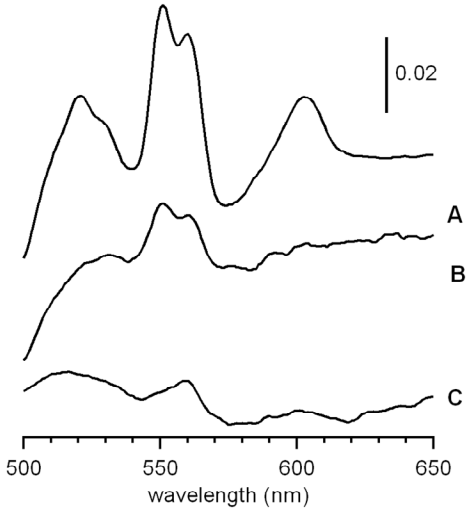

Figure 6-5: UV-vis of purified mitochondria isolated from WT and Aft1-1up cells. A, W303 grown on minimal medium (20 μM Fe); B, Aft1-1up grown on minimal medium (1 μM Fe); C. Aft1-1up grown on minimal medium (40 μM Fe).

absorption at ~ 0 mm/s. The Percent Effect was substantially reduced relative to the spectra of mitochondria from cells grown on media with 40 μM Fe. This is consistent with the corresponding whole-cell spectra (Figures 6-2A and 6-2C).

EPR spectroscopy provided further evidence for nanoparticles in mitochondria from Aft1-up cells grown on 40 μM media Fe. EPR spectra show a broad peak around g ~ 2 that exhibits anti-Curie Law behavior; it increases intensity as the sample temperature is raised from 10 K (Figure 6-4). We have observed the similar behavior in Yah1p- and Atm1p- depleted mitochondria where excess amount of Fe(III) nanoparticles exist.

We also examined the level of Fe/S clusters and hemes in Aft1-up cells. Aconitase is a mitochondrial protein that requires an [Fe_4S_4] cluster for activity. Aconitase activity was essentially unchanged in WT cells grown on media containing 1μM and 40μM Fe (Table 6-2). In contrast, Aft1-1up cells grown on media with 40 μM Fe showed lower aconitase activity than the same cells grown on 1μM medium Fe. This indicates that Fe-S cluster levels decline when nanoparticles accumulate in mitochondria. Further evidence for this comes from EPR spectroscopy. The g ~ 1.94 signal, which arises from reduced Fe/S clusters, was weaker in spectra of mitochondria isolated from cells grown on 40 μM medium Fe than in mitochondria from cells grown with 1 μM Fe (Figure 6-4).

Heme levels were also decreased in Aft1-1up cells relative to WT cells, even at 1 μM medium Fe concentration (Figure 6-5). The decline in Fe/S cluster and heme level is

possibly due to degradation caused by ROS damage accompanying Fe accumulation.

Fe(III) Nanoparticles Formation is Media-dependent

It has been reported that the mitochondria of Aft1-1up cells grown in YPGal medium do not accumulate Fe (*54*). Rich medium normally contains ~ 20 μM Fe (data not shown). In minimal media a similar Fe concentration caused substantial Fe nanoparticles buildup in mitochondria. We wondered whether this difference arose from differences in the media used to grow cells.

When 20 μM ^{57}Fe was added to the standard YPD medium (giving a total medium Fe of ~ 40 μM) the resulting spectrum (Figure 6-2E) did not contain significant amount of the Fe(III) nanoparticle doublet. In YDP media, nanoparticles formation required high medium Fe concentration (e.g. 400 μM medium Fe, as shown in Figure 6-2F). The extent of nanoparticle buildup with 40 μM Fe in YPD media was similar to the nanoparticle build-up with 1 μM Fe on minimal medium (Figure 6-2A). Supplementing YPD media with 400 μM Fe (Figure 6-2F) resulted in about the same level of nanoparticle as was obtained by supplementing minimal media with 5 μM Fe (Figure 6-2B).

YPD has additional nutrients relative to minimal media, which might allow cells to adjust more flexibly to an Aft1-up-induced perturbation. Alternatively, the perturbation

may be milder in YPD-grown cells. These results are consistent with the previous report (*54*) which shows that standard rich medium does not cause iron accumulation in Aft1-1up cells.

Fe Depletion in Vacuole in Yah1p-depleted Cells

We have reported in our previous study that disruption of Fe-S assembly causes a dramatic shift in cellular iron distribution (*87, 116*). Yeast cells depleted in proteins associated with mitochondrial iron-sulfur cluster assembly (e.g. Yah1p, Atm1p, Yfh1p) up-regulate expression of Aft1 target genes (maybe as a response to a sensed deficiency of Fe in the cytosol), similar to the situation in Aft1-1up cells. Besides activation of iron regulon genes, disruption of Fe/S cluster assembly or export machinery (ATM1) also alters other aspects of gene expression, such as repression of respiratory chain genes (*83*).

We wondered how disruption of Fe/S assembly (e.g. by Yah1p-depletion) affected the Fe distribution of whole Yah1p-defient cells. Gal-YAH1 cells were cultured in complete minimal medium containing galactose. In the presence of galactose, these cells express Yah1p. The resulting Mössbauer spectrum (Figure 6-6A) was typical of WT cells. Aliquots of this culture were diluted into fresh minimal medium containing glucose as carbon source for additional growth of 12 and 18 hrs, respectively; under these conditions YAH1 is repressed (see Figure 6-6, upper panel). After 12 hrs of growth, cells

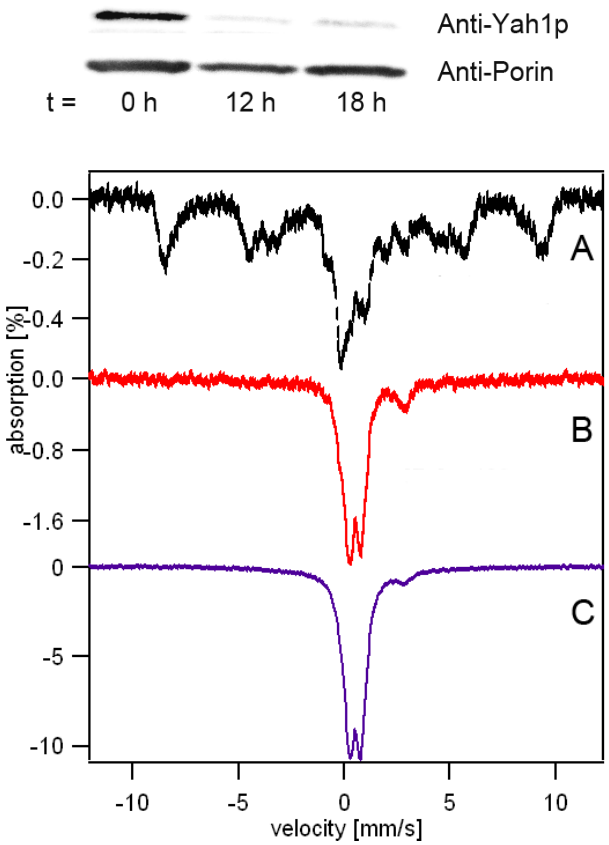

Figure 6-6: Western blot and whole cell Mössbauer spectra of Gal-YAH1 strain. Gal-YAH1 cells were cultured overnight in complete minimal medium containing galactose, then and diluted into fresh minimal medium containing glucose as carbon source for indicated time. Cells were harvested and washed. Crude mitochondria were prepared and used for western blot assay. Top panel: western blot analysis of Yah1p expression level; porin was also assayed as a loading control. Bottom panel: whole cell Mössbauer spectra of Gal-YAH1; A, Gal-YAH1 grown on galactose; B, culture from A was diluted into glucose containing medium and grown for 12 hours; C, same as B but grown on glucose-containing medium for 18 hours.

were harvested and examined by Mössbauer spectroscopy. The 5 K low-field spectrum (Figure 6-6B) was dominated by a nanoparticles doublet. The remaining ~ 5% of spectral intensity was present as a high-spin Fe(II) doublet. The low-field spectrum exhibited no evidence of mononuclear HS Fe(III). Thus, virtually all cellular Fe in these Yah1p-depleted cells was present as nanoparticles. In another similar experiment, Yah1p-depleted cells were harvested after 6 additional hours of growth. The 5 K low-field Mössbauer spectrum of these cells (Figure 6-6C) was similar to Figure 6-6B, except that the Percent Effect due to the nanoparticles had increased. Also, the percentage of the HS Fe^{II} form had decreased to 2% but the absolute concentration of the HS Fe(II) species may have remained about the same.

The major difference between the Mössbauer spectra of Aft1-up cells and Yah1-depleted (and Atm1-depleted) cells is that the former includes intense features arising from vacuolar HS Fe^{III} species (~ 60% of total iron) in addition to nanoparticles, while the latter spectrum exclusively exhibited a doublet due to nanoparticles. Previous studies have shown that the mitochondria of Yah1p-depleted cells contain ferric phosphate nanoparticles (*87*), and our current studies indicate the same for the mitochondria of Aft1-1up cells when medium Fe concentration is high.

The simplest explanation of these results is that all of the nanoparticles in Aft1-up, Yah1-depleted, and Atm1-depleted cells are located in mitochondria. We cannot exclude

the possibility that ***some*** of the nanoparticles are found in other cellular compartments (e.g. cytosol) but neither do we have evidence for this.

Discussion

The primary objective of this study was to better understand the regulation of cellular iron by Aft1p, a transcription factor involved in regulating the expression of the iron regulon genes. The activity of Aft1p is indirectly sensitive to the concentration of Fe in the growth media, such that low media Fe concentrations up-regulate these genes, which in turn causes an increased flow of Fe into the cell due to the increased production of Fe importers on the plasma membrane. It is likely that the concentration of ***cytosolic*** Fe is affected by the concentration of ***media*** Fe, and that Aft1p is directly sensitive to cytosolic Fe levels, but the evidence for this remains circumstantial. We wondered how the increased level of cellular Fe due to Aft1p activity was distributed in the cell, and so we studied the "Aft1-up" strain by our Mössbauer-centered biophysical approach to determine this distribution. In this strain, Aft1p has been genetically modified such that it constitutively up-regulates the iron regulon genes regardless of the media (i.e. cytosolic) Fe concentration.

The Fe in WT cells grown in 40 μM media Fe is roughly distributed into two groups. About 25% of this Fe is present in mitochondria while the remaining ~75% is

present elsewhere. The non-mitochondrial Fe is in the form of mononuclear (magnetically isolated) high-spin Fe(III).

Interpreting the effect of Aft1 activation on cellular Fe required that we first determine the location of the non-mitochondrial HS Fe(III) species. We had previously proposed that this form of Fe was located in vacuoles; our only evidence was that these organelles store Fe (*13*) and that Kosman had proposed that the stored Fe was in the oxidized Fe(III) state (*113*). Thus, a subsidiary objective of this study was to provide evidence for or against this proposal. We did this by determining the Fe distributions in cells lacking and overexpressing Ccc1p, the only known vacuolar iron importer. Cells lacking Ccc1p were largely (but not completely) devoid of HS Fe(III) species, while cell overexpressing Ccc1 contained a slightly greater percentage of HS Fe(III) relative to WT cells. The first experiment provides obvious evidence that that the vacuoles contain the majority of HS Fe(III) species observed in WT cells. About 25% of the Fe in *Dccc1* cells was present as HS Fe(III). This Fe could also be contained in vacuoles, in which case there might be a second (minor) vacuolar Fe importer that operates independently of Ccc1p. Alternatively, the HS Fe(III) species observed in *Dccc1* cells may be in another compartment (e.g. mitochondria or the cytosol). Distinguishing these possibilities will require further study.

We had expected that the CCC1-overexpression strain would contain a greater percentage of HS Fe(III) species than is found in WT cells. However, this strain also contained a substantial amount of ferric nanoparticles. If the nanoparticle contribution to the Mössbauer spectrum of the CCC1-overexpression strain is removed, it becomes clear that the amount of Fe present as HS Fe(III) in this strain has increased sharply relative to in WT cells. Thus, this experiment provides additional evidence that the majority of HS Fe(III) species in WT cells are in vacuoles and that these species dominate the iron content of the cell.

Parenthetically, we were intrigued by the increased level of nanoparticles observed in the spectrum of the CCC1-overexpression strain. As we have shown here and in our previous studies of Yah1p-depleted and Atm1p-depleted cells, nanoparticles tend to accumulate in the mitochondria. If the nanoparticles in the CCC1-overexpresison strain are also in mitochondria, we wonder why overexpressing a *vacuolar* Fe importer would cause nanoparticles to form in the *mitochondria*? This seems counterintuitive since vacuoles and mitochondria appear to compete for the same pool of cytosolic Fe. One possibility is that there is a ***direct pathway*** from vacuoles to mitochondria in which the flux of Fe is proportional to the concentration of Fe in the vacuole. Thus, in the ccc1 overexpression strain, the concentration of Fe in the vacuole would be greater than in WT vacuoles, and this would cause an increased flux of vacuolar Fe into mitochondria

(which would then aggregate). Alternatively, the nanoparticles might be located in the vacuoles. In this case, the HS FeIII in vacuoles might accumulate as nanoparticles when the concentration of these ions exceeds a particular value.

Knowing that the majority of HS Fe(III) ions in WT cells are located in vacuoles allowed us to better interpret the effects of Aft1p activation. We found that constitutive Aft1p activity increased the rate that media Fe was imported into fermenting yeast cells relative to WT cells. We also found that the imported Fe accumulated in ***both*** mitochondria and vacuoles. The form of Fe that accumulated in Aft1-up mitochondria was similar to that which accumulates in mitochondria from Yah1-depleted and Atm1-depleted cells – namely ferric nanoparticles. To this extent, our results agree with previous studies in which it was concluded that the Aft1-dependent iron regulon was up-regulated in Atm1-depleted and Yah1p-depleted cells; such cells "feel" as though they are Fe-deficient, and as a response, they up-regulate Aft1.

The main difference between the Fe regulation in Yah1-deficient and Atm1p-deficient cells, relative to Aft1-up cells, is that Aft1-1up cells contained significant amount of vacuolar Fe (accounting for ~ 60% of total iron). Yah1p-depleted or Atm1-depleted cells (and Yfh1p-depleted cells, data not shown) are essentially devoid of vacuolar Fe. The ***relative*** amount of vacuolar Fe in Aft1-up cells is similar to that found in WT cells. However, the ***absolute*** amount of vacuolar Fe in Aft1-up cells grown in Fe-

rich media is substantially larger than in WT cells, in that the overall concentration of Fe in Aft1-up cells grown under these circumstances is substantially higher.

The lack of vacuolar Fe in Yah1p-depleted, Atm1-depeleted (and Yfh1p-depleted) cells and the presence of vacuolar Fe in Aft1-up cells indicates a fundamental difference in Fe trafficking. Aft1p activity is undoubtedly responsible for the increased flow of Fe into the cell but we conclude from these differences that Aft1p activation is NOT responsible for the lack of vacuolar Fe in these ISC mutant strains. There must be another regulatory system that is responsible for this. Under conditions common to these other mutants, the Aft1-Independent Vacuolar Iron Regulatory system (abbreviated as AIVIR) increases the export flow of Fe from the vacuoles and/or decreases the import flow. It has been shown that in Yah1p- and Atm1p-depleted cells the vacuolar importer CCC1 is transcriptionally repressed and the vacuolar exporter complex Fet5/Fth1 is up-regulated (see supplementary information of (*83*)). This result nicely explains our findings: upon ISC defect, AIVIR decreases vacuolar iron import and increase vacuolar iron export.

We hypothesize that the Fe is imported from the media into the cytosol, and that the rate of this import depends on the concentration of Fe in the media, the density of Fe import proteins (e.g. Fet3) on the plasma membrane, and the activity of those importers. In Aft1-up cells, the density and activity of the plasma membrane Fe importers is high –

similar to the levels in WT cells under Fe deficient conditions. In Aft1-up cells under high media Fe conditions, the increased concentration of cyosolic Fe causes the increased flow of Fe into the vacuole and mitochondria (by mass action). The model for explaining the function of Aft1 in Aft1-up, Yah1p-depleted and WT cells is shown in Figure 6-7.

In Aft1-1up, the iron that builds up in the vacuole stays as HS Fe(III) (no nanoparticles). However, the Fe(II) that flows into the mitochondria becomes nanoparticles by oxidizing and exchanging its ligand(s) for phosphates and waters. This oxidation may generate ROS that subsequently damages Fe/S clusters and heme groups. At the high pH of the matrix, the resulting Fe(III) species precipitate to form nanoparticles. Why the mitochondria in these cells form nanoparticles is unclear; the matrix could be more oxidizing, the pH might be higher, or the chemical composition of the matrix may differ from that of WT mitochondria.

Fe/S clusters and heme levels are low in Aft1-up mitochondria especially when cells are grown on high medium iron concentration. Under these conditions, more nanoparticles form and more ROS is produced. In contrast to Yah1p-depleted and Yfh1p-deleted mitochondria, where Fe/S cluster assembly is disrupted by the absence of these proteins, there is no disruption of the Fe/S biosynthesis pathway in Aft1-up cells.

The fact that Fe/S cluster and heme levels are diminished indicates that these losses

could result from secondary effects in the Yah1p, Atm1p, and Yfh1p phenotypes. Assigning the function of proteins from in vivo genetic experiments is exceedingly difficult (because there are a number of responses to a single genetic change). In past experiments, depletion/deletion of various proteins resulted in the loss of Fe/S cluster and heme groups, and some of these results were interpreted as meaning that these proteins must function directly in these biosynthetic processes. The fact that Fe/S cluster and heme levels are diminished by activating Aft1 – a transcription factor that never enters the mitochondria and is not directly involved in these processes, highlights the possibility that certain "ISU-related" proteins might not be directly involved in these processes (even though their deletion/depletion causes Fe/S cluster and/or heme levels to diminish). The view has been that the disruption of the pathway caused elevated mitochondrial Fe uptake and the buildup of Fe in the mitos (since they cannot be used for Fe/S cluster assembly). One might argue that in the case of Aft1-1up cells, the ISC proteins and heme biosynthetic proteins are down-regulated (causing the decline of these centers). However, previous microarray studies show no evidence for down-regulation of ISC and heme biosynthesis proteins (*117*). Furthermore, BPS-treated cells show substantial levels of Fe/S clusters and hemes (unpublished results); here Aft1p-controlled iron regulon should also be activated (and there would be a similar "down regulation" of Fe/S assembly proteins). We suspect that the primary function of some of these proteins

remains to be uncovered, and that the ISC phenotype is a secondary effect of deletion of these genes.

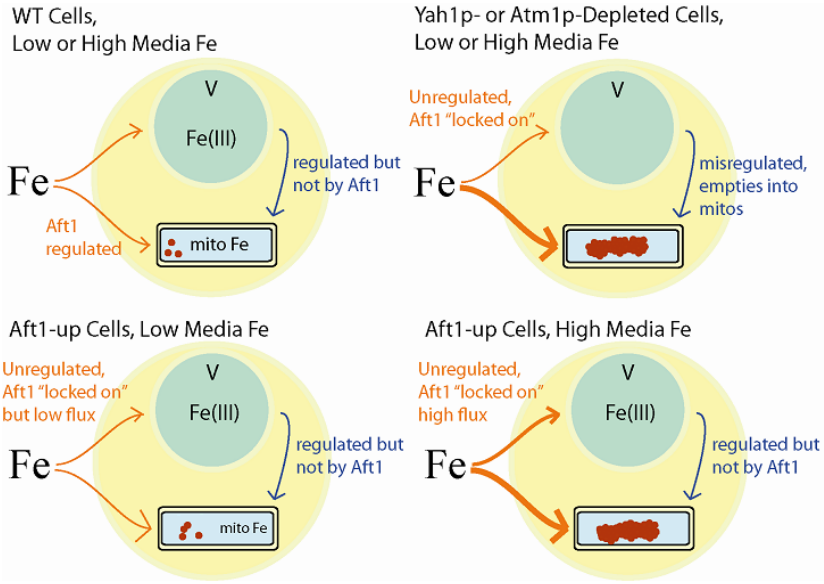

Figure 6-7: Model for explaining different cellular iron distribution in WT, Yah1p-depleted and Aft1-1up cells.

CHAPTER VII

SUMMARY AND FUTURE STUDIES

Summary

The major objective of this dissertation has been to address issues of iron metabolism and trafficking in budding yeast *Saccharomyces cerevisiae* using an integrative biophysical and biochemical approach that is centered on Mössbauer spectroscopy. The initial emphasis was to characterize the iron distribution in mitochondria isolated from wild-type (WT) cells grown under fermentative vs. respiratory conditions. This was a group effort in which my contribution was to study mitochondria isolated from galactose-grown cells. Under these conditions, cells respireferment (respire and ferment simultaneously). This study, described in Chapter 3, reveals that the Fe distribution in mitochondria from respirofermenting cells was similar to that in respiring cells, and substantially different from that in fermenting cells. In respiring and respirofermenting cells, most of the Fe in mitochondria is present as $[Fe_4S_4]^{2+}$ and heme prosthetic groups in the respiratory complexes. Mitochondria isolated from fermenting cells contained fewer Fe/S clusters and heme groups, but contained three pools of Fe, including mononuclear high-spin (HS) Fe(II) species, mononuclear HS Fe(III) species, and FeIII nanoparticles. The three pools may be in equilibrium with each other but this is uncertain. The sizes of these pools were much

larger than previous estimates; the HS Fe(II) pool concentration is ~ 150 μM. We propose that thee HS Fe(II) pool is used as feedstock for Fe/S cluster assembly and heme biosynthesis. Under fermenting conditions, the demand for these centers is reduced, allowing the size of these pools to increase.

Whole-cell Mössbauer spectra indicated that the iron in WT fermenting cells can be roughly divided into two major groups, including mitochondrial Fe, which accounts for about ¼ of the Fe in the sample, and non-mitochondrial Fe, which accounts for about ¾ of the Fe in the sample.

Our next study involved Yah1p, a mitochondrial [Fe_2S_2]-containing ferredoxin that may donate electrons during Fe/S cluster assembly and heme biosynthesis. Depletion of Yah1p causes Fe to accumulate in mitochondria; using Mössbauer, EPR, X-ray absorption spectroscopy and energy dispersive x-ray scanning electron microscopy, we found that the Fe accumulated as Fe(III) phosphate nanoparticles. Fe(III) nanoparticles were found to be chemically reducible; the resulting Fe(II) species are largely exported from the mitochondria. The formation of nanoparticles involves the oxidation of Fe^{II} to Fe^{III} along with the exchange of one or more endogenous ligand for phosphate and water groups. Reactive Oxygen Species (ROS) may be produced during this process. Elevated ROS damages Fe/S clusters and heme groups in mitochondria. The O_2 that is bubbled through cells during growth is required for nanoparticle formation,

and is probably the oxidant used to oxidize Fe(II) to Fe(III) prior to precipitation.

A similar study was performed on Atm1-depleted cells and mitochondria. Atm1p is a mitochondrial inner membrane protein that exports an unknown species "X" that is required by the cytosolic Fe/S cluster machinery to make cytosolic Fe/S clusters. When Atm1p is depleted, Fe accumulates in the mitochondria. Earlier studies suggested that X is an Fe/S cluster and that the Fe that builds up is in the form of X. These studies also concluded that there is NO Fe/S cluster defect in the mitochondria of Atm1-depleted cells. We investigated this by Mössbauer and other biophysical methods. Again Fe(III) phosphate nanoparticles had built-up in the mitochondria isolated from At1m-depleted cells. The phenotype was similar to that of Yah1, including a buildup of Fe(III) phosphate nanoparticles in the mitochondria of these cells. A small relative percentage of Fe in the mitochondria were present as HS Fe(II) ions, but the significance of this is uncertain. In absolute concentration, these ions represented a nontrivial concentration (100-200 μM). Atm1p-depleted cells also had a defect in heme and Fe/S cluster formation within the mitochondria and in the cytosol. This contrasts with previous studies in which no Fe/S cluster defect was observed in Atm1-depleted mitochondria. Whole cell Mössbauer spectra revealed that nearly all of the Fe in the cell was present as Fe(III) phosphate nanoparticles.

The iron in WT yeast cells can be roughly divided into two groups: mitochondrial Fe

species (the central doublet and HS Fe(II)) and non-mitochondrial HS Fe(III) species. Studies of a *Dccc1* deletion strain and a CCC1-overexpression strain were performed to evaluate the location of the non-mitochondria Fe(III). Most of the HS Fe(III) species were found to be located in vacuoles. Fe can be stored in this organelle and used as needed for cellular processes. Activation of the iron regulon genes alone (in Aft1-1up cells) increases the flow of Fe into the cell, but it does not alter the cellular iron distribution significantly (i.e the ratio between vacuolar iron and mitochondrial iron remains similar to that in WT cells). In contrast, virtually no Fe is present in vacuoles in Atm1p-depleted and Yah1p-depleted cells.

The iron distributions in Yah1p-depleted, Atm1p-depleted and probably Yfh1p-depleted cells reflects the activation of the Aft1/iron regulon system, but they also reflect changes in one or more previously unknown Fe regulatory systems that are independent of activation of Aft1 and the iron regulon. We hypothesize that there is an Aft1-independent vacuolar Iron regulatory (AIVIR) system controls the vacuolar Fe import and export rates. There may also be a direct pathway leading from the vacuole to mitochondria, and it may be controlled by AIVIR. In the CCC1-overexpression strain, there is a buildup of nanoparticles (probably in the mitochondria) associated with increased concentrations of HS Fe(III) in the vacuole. In this case, the V à M pathway must be activated. When Fe/S cluster assembly malfunctions in the mitochondria, AIVIR

appears to increase the export of Fe from the vacuole to the mitochondria, perhaps via a dedicated pathway, and at the same time decreasing the import of Fe from the cytosol into the vacuole.

Future Directions

There are several directions in this project that could be worth future investigations.

Human Fe/S cluster assembly is vital for cellular iron homeostasis and health. The major components of ISC assembly machinery are highly conserved from yeast to human (e.g. YFH1, ISU1, ATM1) (*2*). However, Fe/S cluster assembly in human cells still differs significantly from yeast cells, most notably in that ISCs are synthesized in both mitochondria and cytosol in mammalian cells whereas yeast mitochondria are the sole ISC biosynthesis location. A number of diseases have been reported to be linked to the defect in ISC assembly machinery (*2*). For example, mutations in frataxin (homolog of yeast gene YFH1) cause Friedreich's ataxia (FRDA); defect in ISCU (the major scaffold protein) leads to hereditary myopathy; mutations of ABCB7 (homolog of yeast gene ATM1) results in hereditary X-linked sideroblastic anemia and ataxia (XLSA/A). As a common symptom of the diseases caused by ISC defects, iron accumulation occurs in mitochondria of affected tissue cells (and possibly other cellular organelles). From our studies on yeast model of ISC mutants we showed that Fe accumulates as inorganic

Fe(III) phosphate nano-particles. The chemical characterization for iron in human mutant mitochondria is lacking and this future direction could be very important and informative due to its direct relationship to human diseases. Also human (and other mammalian) mitochondria have mitochondrial ferritin which yeast lacks and how this iron storage protein could affect the iron accumulation is of interest. Furthermore, deficiency in mitochondrial ISC biogenesis disturbs the cellular iron homeostasis and distribution (as shown by our yeast studies). It is interesting to examine the iron distribution in the whole cell of the mutant human cells and compare it to the normal cells. This will provide insights into the global cellular iron changes that Fe/S biosynthesis defects may cause in human cells.

We have observed excess iron accumulation along with elevated ROS damages in ISC mutant mitochondria. These two phenotypes are generally observed together in all ISC mutations. Disruption of ISC assembly will render cells respiration incompetent, but loss of respiration ability (by loss of mitochondrial DNA) does not lead to iron accumulation in mitochondria nor does it cause elevated ROS damage (*11*). Due to the fact that free Fe ions can induce generation of ROS species previous studies often suggest that excess iron is responsible for most of elevated ROS damages. However, as shown in our studies, most of accumulated Fe in ISC mutants does not exist as free Fe ions, instead it precipitates as inorganic Fe(III) nanoparticles. Compared to free Fe ions,

these nanoparticles should have diminished ability to generate ROS species. Thus most ROS species may not be produced by accumulated Fe *per se*; instead they may be produced in the process of oxidation of Fe(II) to Fe(III) prior to precipitation. A systematic study is required to establish the correlation between the amount of mitochondrial Fe accumulation and the level of ROS species/damages. These future efforts are important since the results might provide insights into the toxicological effect of such iron accumulation in ISC mutants. Level of iron buildup may be controlled in two ways: control iron availability in medium by adding BPS or adjusting medium iron addition; control iron availability to mitochondria by using a genetic strain where MRS3/4 are deleted. And the level of ROS damages could be determined using Oxyblot; the level of ROS species can be directly monitored using the chemical 2', 7'-Dichlorodihydrofluorescein Diacetate (DCFDA, available from Invitrogen).

We have shown that molecular oxygen is required for Fe buildup and ROS formation. It has been reported that O_2 availability significantly alters yeast cellular uptake system (*6*). We have studied yeast cellular iron contents in aerobic WT cells and several mutants. It is worthwhile to comparatively study the effect of oxygen on cellular iron distribution in yeast. In anaerobic cells Fet3/Ftr1 complexes are non-functioning and Fet4 (a divalent metal ion importer) is responsible for most of cellular iron uptake. It would be interesting to investigate the effect of oxygen on the cellular iron contents in

WT, ISC mutants (e.g. Yah1p-depleted strain) and Aft1-1up cells. We have determined that O_2 is required for iron accumulation in ISC mutant mitochondria; mitochondria isolated from anaerobic mutant cells exhibit WT level Fe concentration. How the availability of oxygen alters cellular iron contents in ISC mutants will be one of the objectives of these future studies. We have observed that Aft1-1up cells, when grown on aerobic condition, have iron accumulation both in vacuoles and mitochondria. Under anaerobic condition, however, Fet3/Ftr1 system is repressed and non-functioning; so the question is: will Aft1-1up cells still have iron accumulation? Taking all these information together we may be able to draw general conclusions on the effect of oxygen on yeast cellular iron distribution.

There are several other critical problems that need to be addressed in order to advance our understanding of iron regulation. For example, identification of the ligand (unlikely to be water or phosphate) that coordinates the Fe pool in mitochondrial matrix will help us understand the pathway of iron transport and probably the mechanism of nanoparticle formation. The substrate ("X") for Atm1p is a crucial player linking mitochondrial Fe/S cluster assembly to cellular iron homeostasis. It would be of great importance to identify this substrate.

Despite the impressive progress in research of iron regulation and homeostasis during past decades, extensive further explorations are still ahead of us. Numerous basic

science and biomedical research will be required to gain a more complete understanding of cellular iron metabolism and the diseases caused by iron misregulation.

REFERENCES

1. Lill, R. (2009) Function and biogenesis of iron-sulphur proteins, *Nature 460*, 831-838.

2. Ye, H., and Rouault, T. A. (2010) Human iron-sulfur cluster assembly, cellular iron homeostasis, and disease, *Biochemistry 49*, 4945-4956.

3. Imlay, J. A. (2008) Cellular defenses against superoxide and hydrogen peroxide, *Annu Rev Biochem 77*, 755-776.

4. Rotig, A., deLonlay, P., Chretien, D., Foury, F., Koenig, M., Sidi, D., Munnich, A., and Rustin, P. (1997) Aconitase and mitochondrial iron-sulphur protein deficiency in Friedreich ataxia, *Nat Genet 17*, 215-217.

5. Kosman, D. J. (2003) Molecular mechanisms of iron uptake in fungi, *Mol Microbiol 47*, 1185-1197.

6. Jensen, L. T., and Culotta, V. C. (2002) Regulation of *Saccharomyces cerevisiae* FET4 by oxygen and iron, *J Mol Biol 318*, 251-260.

7. Rutherford, J. C., Ojeda, L., Balk, J., Mühlenhoff, U., Lill, R., and Winge, D. R. (2005) Activation of the iron regulon by the yeast Aft1/Aft2 transcription factors depends on mitochondrial but not cytosolic iron-sulfur protein biogenesis, *J Biol Chem 280*, 10135-10140.

8. Chen, O. S., Hemenway, S., and Kaplan, J. (2002) Inhibition of Fe-S cluster biosynthesis decreases mitochondrial iron export: Evidence that Yfh1p affects Fe-S cluster synthesis, *P Natl Acad Sci USA 99*, 12321-12326.

9. Holmes-Hampton, G. P., Miao, R., Morales, J. G., Guo, Y. S., Munck, E., and Lindahl, P. A. (2010) A nonheme high-spin ferrous pool in mitochondria isolated from fermenting *Saccharomyces cerevisiae*, *Biochemistry 49*, 4227-4234.

10. Lange, H., Kaut, A., Kispal, G., and Lill, R. (2000) A mitochondrial ferredoxin is essential for biogenesis of cellular iron-sulfur proteins, *P Natl Acad Sci USA 97*, 1050-1055.

11. Kispal, G., Csere, P., Guiard, B., and Lill, R. (1997) The ABC transporter Atm1p

is required for mitochondrial iron homeostasis, *FEBS Lett 418*, 346-350.

12. Muhlenhoff, U., Richhardt, N., Ristow, M., Kispal, G., and Lill, R. (2002) The yeast frataxin homolog Yfh1p plays a specific role in the maturation of cellular Fe/S proteins, *Hum Mol Genet 11*, 2025-2036.

13. Li, L. T., Chen, O. S., Ward, D. M., and Kaplan, J. (2001) CCC1 is a transporter that mediates vacuolar iron storage in yeast, *J Biol Chem 276*, 29515-29519.

14. Chen, O. S., and Kaplan, J. (2000) CCC1 suppresses mitochondrial damage in the yeast model of Friedreich's ataxia by limiting mitochondrial iron accumulation, *J Biol Chem 275*, 7626-7632.

15. Li, L. T., Murdock, G., Bagley, D., Jia, X. A., Ward, D. M., and Kaplan, J. (2010) Genetic dissection of a mitochondria-vacuole signaling pathway in yeast reveals a link between chronic oxidative stress and vacuolar iron transport, *J Biol Chem 285*, 10232-10242.

16. Matusch, A., Depboylu, C., Palm, C., Wu, B., Hoglinger, G. U., Schafer, M. K., and Becker, J. S. (2010) Cerebral bioimaging of Cu, Fe, Zn, and Mn in the MPTP mouse model of Parkinson's disease using laser ablation inductively coupled plasma mass spectrometry (LA-ICP-MS), *J Am Soc Mass Spectrom 21*, 161-171.

17. Jensen, L. T., Sanchez, R. J., Srinivasan, C., Valentine, J. S., and Culotta, V. C. (2004) Mutations in *Saccharomyces cerevisiae* iron-sulfur cluster assembly genes and oxidative stress relevant to Cu,Zn superoxide dismutase, *J Biol Chem 279*, 29938-29943.

18. Lesuisse, E., Santos, R., Matzanke, B. F., Knight, S. A. B., Camadro, J. M., and Dancis, A. (2003) Iron use for haeme synthesis is under control of the yeast frataxin homologue (Yfh1), *Hum Mol Genet 12*, 879-889.

19. Kispal, G., Csere, P., Prohl, C., and Lill, R. (1999) The mitochondrial proteins Atm1p and Nfs1p are essential for biogenesis of cytosolic Fe/S proteins, *EMBO J 18*, 3981-3989.

20. Lindahl, P., Morales J.G., Miao R. and Holmes-Hampton G. (2009) Isolation of *Saccharomyces cerevisiae* mitochondria for Mössbauer, EPR, and electronic absorption spectroscopic analyses, *Methods Enzymol 456*, 267-285.

21. Kushnirov, V. V. (2000) Rapid and reliable protein extraction from yeast, *Yeast*

16, 857-860.

22. Parvin, R., Pande, S. V., and Venkitas.Ta. (1965) On colorimetric biuret method of protein determination, *Anal Biochem 12*, 219-229.

23. Bradford, M. M. (1976) Rapid and sensitive method for quantitation of microgram quantities of protein utilizing principle of protein-dye binding, *Anal Biochem 72*, 248-254.

24. Tamarit, J., Irazusta, V., Moreno-Cermeno, A., and Ros, J. (2006) Colorimetric assay for the quantitation of iron in yeast, *Anal Biochem 351*, 149-151.

25. Schilke, B., Voisine, C., Beinert, H., and Craig, E. (1999) Evidence for a conserved system for iron metabolism in the mitochondria of *Saccharomyces cerevisiae*, *P Natl Acad Sci USA 96*, 10206-10211.

26. Kohlhaw, G. B. (1988) Isopropylmalate dehydratase from Yeast, *Methods Enzymol 166*, 423-429.

27. Munujos, P., Collcanti, J., Gonzalezsastre, F., and Gella, F. J. (1993) Assay of succinate-dehydrogenase activity by a colorimetric continuous method using iodonitrotetrazolium chloride as electron-acceptor, *Anal Biochem 212*, 506-509.

28. Poiarkova, A. V., and Rehr, J. J. (1999) Multiple-scattering x-ray-absorption fine-structure Debye-Waller factor calculations, *Phys Rev B 59*, 948-957.

29. Schmitt, M. E., Brown, T. A., and Trumpower, B. L. (1990) A rapid and simple method for preparation of RNA from *Saccharomyces cerevisiae*, *Nucleic Acids Res 18*, 3091-3092.

30. Lill, R., and Mühlenhoff, U. (2008) Maturation of iron-sulfur proteins in eukaryotes: Mechanisms, connected processes, and diseases, *Annu Rev Biochem 77*, 669-700.

31. Barrientos, A., and Tzagoloff, A. (2003) Cytochrome *c* oxidase assembly in health and disease: The yeast model., *Am J Hum Genet 73*, 461-461.

32. Rouault, T. A., and Tong, W. H. (2008) Iron-sulfur cluster biogenesis and human disease, *Trends Genet 24*, 398-407.

33. Veatch, J. R., McMurray, M. A., Nelson, Z. W., and Gottschling, D. E. (2009) Mitochondrial dysfunction leads to nuclear genome instability via an iron-sulfur

cluster defect, *Cell 137*, 1247-1258.

34. Raha, S., McEachern, G. E., Myint, A. T., and Robinson, B. H. (2000) Superoxides from mitochondrial complex III: The role of manganese superoxide dismutase, *Free Radic Biol Med 29*, 170-180.

35. Reinders, J., Zahedi, R. P., Pfanner, N., Meisinger, C., and Sickmann, A. (2006) The complete yeast mitochondrial proteome: Multidimensional separation techniques for mitochondrial proteomics, *J Proteome Res 5*, 1543-1554.

36. Stevens, B. J. (1977) Variation in number and volume of mitochondria in yeast according to growth-conditions - study based on serial sectioning and computer graphics reconstitution, *Biol Cellulaire 28*, 37-56.

37. Egner, A., Jakobs, S., and Hell, S. W. (2002) Fast 100-nm resolution three-dimensional microscope reveals structural plasticity of mitochondria in live yeast, *P Natl Acad Sci USA 99*, 3370-3375.

38. Wang, H., Sauke, T., Debrunner, P. G., and Chan, S. I. (1988) The CO adduct of yeast cytochrome-C oxidase - Mössbauer and photolysis studies, *J Biol Chem 263*, 15260-15263.

39. Beinert, H., and Shaw, R. W. (1977) On identity of high-spin heme components of cytochrome-C oxidase, *Biochim Biophys Acta 462*, 121-130.

40. Hudder, B. N., Morales, J. G., Stubna, A., Münck, E., Hendrich, M. P., and Lindahl, P. A. (2007) Electron paramagnetic resonance and Mössbauer spectroscopy of intact mitochondria from respiring *Saccharomyces cerevisiae*, *J Biol Inorg Chem 12*, 1029-1053.

41. Swanson, M. A., Usselman, R. J., Frerman, F. E., Eaton, G. R., and Eaton, S. S. (2008) The iron-sulfur cluster of electron transfer flavoprotein-ubiquinone oxidoreductase is the electron acceptor for electron transfer flavoprotein, *Biochemistry 47*, 8894-8901.

42. Paradkar, P. N., Zumbrennen, K. B., Paw, B. H., Ward, D. M., and Kaplan, J. (2009) Regulation of mitochondrial iron import through differential turnover of Mitoferrin 1 and Mitoferrin 2, *Mol Cell Biol 29*, 1007-1016.

43. Lill, R., Dutkiewicz, R., Elsasser, H. P., Hausmann, A., Netz, D. J. A., Pierik, A. J., Stehling, O., Urzica, E., and Muhlenhoff, U. (2006) Mechanisms of iron-

sulfur protein maturation in mitochondria, cytosol and nucleus of eukaryotes, *Biochim Biophys Acta - Mol Cell Res 1763*, 652-667.

44. Kwok, E., and Kosman, D. (2006) Iron in yeast: Mechanisms involved in homeostasis, In *Molecular Biology of Metal Homeostasis and Detoxification: From Microbes to Man* (Tamás, M. J., and Martinoia, E., Eds.), pp 59 - 99, Springer.

45. Rosenfeld, E., and Beauvoit, B. (2003) Role of the non-respiratory pathways in the utilization of molecular oxygen by *Saccharomyces cerevisiae*, *Yeast 20*, 1115-1144.

46. Lill, R., and Mühlenhoff, U. (2006) Iron-sulfur protein biogenesis in eukaryotes: Components and mechanisms, *Annu Rev Cell Dev Biol 22*, 457-486.

47. Muhlenhoff, U., Stadler, J. A., Richhardt, N., Seubert, A., Eickhorst, T., Schweyen, R. J., Lill, R., and Wiesenberger, G. (2003) A specific role of the yeast mitochondrial carriers Mrs3/4p in mitochondrial iron acquisition under iron-limiting conditions, *J Biol Chem 278*, 40612-40620.

48. Lange, H., Mühlenhoff, U., Denzel, M., Kispal, G., and Lill, R. (2004) The heme synthesis defect of mutants impaired in mitochondrial iron-sulfur protein biogenesis is caused by reversible inhibition of ferrochelatase, *J Biol Chem 279*, 29101-29108.

49. Hausmann, A., Samans, B., Lill, R., and Muehlenhoff, U. (2008) Cellular and mitochondrial remodeling upon defects in iron-sulfur protein biogenesis, *J Biol Chem 283*, 8318-8330.

50. Muhlenhoff, U., Gerber, J., Richhardt, N., and Lill, R. (2003) Components involved in assembly and dislocation of iron-sulfur clusters on the scaffold protein Isu1p, *EMBO J 22*, 4815-4825.

51. Barros, M. H., and Nobrega, F. G. (1999) YAH1 of *Saccharomyces cerevisiae*: a new essential gene that codes for a protein homologous to human adrenodoxin, *Gene 233*, 197-203.

52. Barros, M. H., Nobrega, F. G., and Tzagoloff, A. (2002) Mitochondrial ferredoxin is required for heme A synthesis in *Saccharomyces cerevisiae*, *J Biol Chem 277*, 9997-10002.

53. Barros, M. H., Carlson, C. G., Glerum, D. M., and Tzagoloff, A. (2001) Involvement of mitochondrial ferredoxin and Cox15p in hydroxylation of heme O, *FEBS Lett 492*, 133-138.

54. Babcock, M., deSilva, D., Oaks, R., DavisKaplan, S., Jiralerspong, S., Montermini, L., Pandolfo, M., and Kaplan, J. (1997) Regulation of mitochondrial iron accumulation by Yfh1p, a putative homolog of frataxin, *Science 276*, 1709-1712.

55. Bulteau, A. L., Dancis, A., Gareil, M., Montagne, J. J., Camadro, J. M., and Lesuisse, E. (2007) Oxidative stress and protease dysfunction in the yeast model of Friedreich ataxia, *Free Radic Biol Med 42*, 1561-1570.

56. Aisen, P., Enns, C., and Wessling-Resnick, M. (2001) Chemistry and biology of eukaryotic iron metabolism, *Int J of Biochem Cell Biol 33*, 940-959.

57. Chaston, T. B., and Richardson, D. R. (2003) Iron chelators for the treatment of iron overload disease: Relationship between structure, redox activity, and toxicity, *Am J Hematol 73*, 200-210.

58. Hudder, B. N., Garber, J. M., Stubna, A., Münck, E., Hendrich, M. P., and Lindahl, P. A. (2007) Electron paramagnetic resonance and Mössbauer spectroscopy of intant mitochondria from respiring *Saccharomyces cerevisiae, J Biol Inorg Chem 12*, 1029-1053

59. Yeastgenome. Yeastgenome database: http://www.yeastgenome.org/straintable.shtml

60. Dedeken, R. H. (1966) Crabtree effect - a regulatory system in yeast, *J Gen Microbiol 44*, 149-156.

61. Kwast, K. E., Lai, L. C., Menda, N., James, D. T., Aref, S., and Burke, P. V. (2002) Genomic analyses of anaerobically induced genes in *Saccharomyces cerevisiae*: Functional roles of Rox1 and other factors in mediating the anoxic response, *J Bacteriol 184*, 250-265.

62. Battle, P. D., Cheetham, A. K., Gleitzer, C., Harrison, W. T. A., Long, G. J., and Longworth, G. (1982) A novel magnetic phase - transition in anhydrous iron(III) phosphate, $FePO_4$, *J Physics C: Solid State Physics 15*, 919-924.

63. StPierre, T. G., Chan, P., Bauchspiess, K. R., Webb, J., Betteridge, S., Walton, S., and Dickson, D. P. E. (1996) Synthesis, structure and magnetic properties of

ferritin cores with varying composition and degrees of structural order: Models for iron oxide deposits in iron-overload diseases, *Coord Chem Rev 151*, 125-143.

64. Bauminger, E. R., Cohen, S. G., Dekanter, F. L., Levy, A., Ofer, S., Kessel, M., and Rottem, S. (1980) Iron storage in Mycoplasma-capricolum, *J Bacteriol 141*, 378-381.

65. Weir, M. P., Peters, T. J., and Gibson, J. F. (1985) Electron-spin resonance studies of splenic ferritin and hemosiderin, *Biochim Biophys Acta 828*, 298-305.

66. Wajnberg, E., El-Jaick, L. J., Linhares, M. P., and Esquivel, D. M. S. (2001) Ferromagnetic resonance of horse spleen ferritin: Core blocking and surface ordering temperatures, *J Mag Reson 153*, 69-74.

67. Rauen, U., Springer, A., Weisheit, D., Petrat, F., Korth, H. G., de Groot, H., and Sustmann, R. (2007) Assessment of chelatable mitochondrial iron by using mitochondrion-selective fluorescent iron indicators with different iron-binding affinities, *ChemBioChem 8*, 341-352.

68. Popescu, B. F. G., Pickering, I. J., George, G. N., and Nichol, H. (2007) The chemical form of mitochondrial iron in Friedreich's ataxia, *J Inorg Biochem 101*, 957-966.

69. Rauen, U., Petrat, F., Sustmann, R., and de Groot, H. (2004) Iron-induced mitochondrial permeability transition in cultured hepatocytes, *J Hepatol 40*, 607-615.

70. Kalman, E., Radnai, T., Palinkas, G., Hajdu, F., and Vertes, A. (1988) Hydration of iron(II) ion in aqueous-solutions, *Electrochim Acta 33*, 1223-1228.

71. Virag, L., Scott, G. S., Antal-Szalmas, P., O'Connor, M., Ohshima, H., and Szabo, C. (1999) Requirement of intracellular calcium mobilization for peroxynitrite-induced poly(ADP-ribose) synthetase activation and cytotoxicity, *Mol Pharmacol 56*, 824-833.

72. Reed, G. H., Leigh, J. S., and Pearson, J. E. (1971) Electron paramagnetic relaxation and EPR Line shapes of Manganous ion complexes in aqueous solutions - frequency and ligand dependence, *J Chem Phys 55*, 3311-.

73. Langner, M., and Hui, S. W. (1993) Dithionite penetration through phospholipid - bilayers as a measure of defects in lipid molecular packing, *Chem Phys Lipids 65*,

23-30.

74. McIntyre, J. C., and Sleight, R. G. (1991) Fluorescence assay for phospholipid membrane asymmetry, *Biochemistry 30*, 11819-11827.

75. Zagorec, M., Buhler, J. M., Treich, I., Keng, T., Guarente, L., and Labbebois, R. (1988) Isolation, sequence, and regulation by oxygen of the yeast Hem-13 gene coding for coproporphyrinogen oxidase, *J Biol Chem 263*, 9718-9724.

76. Camadro, J. M., Thome, F., Brouillet, N., and Labbe, P. (1994) Purification and properties of protoprophyrinogen oxidase from the yeast *Saccharomyces-cerevisiae* - mitochondrial location and evidence for a precursor form of the protein, *J Biol Chem 269*, 32085-32091.

77. Buisson, N., and Labbe-Bois, R. (1998) Flavohemoglobin expression and function in *Saccharomyces cerevisiae* - No relationship with respiration and complex response to oxidative stress, *J Biol Chem 273*, 9527-9533.

78. Crisp, R. J., Pollington, A., Galea, C., Jaron, S., Yamaguchi-Iwai, Y., and Kaplan, J. (2003) Inhibition of heme biosynthesis prevents transcription of iron uptake genes in yeast, *J Biol Chem 278*, 45499-45506.

79. Lange, H., Kispal, G., and Lill, R. (1999) Mechanism of iron transport to the site of heme synthesis inside yeast mitochondria, *J Biol Chem 274*, 18989-18996.

80. Boukhalfa, H., and Crumbliss, A. L. (2002) Chemical aspects of siderophore mediated iron transport, *BioMetals 15*, 325-339.

81. Chen, O. S., and Kaplan, J. (2001) YFH1-mediated iron homeostasis is independent of mitochondrial respiration, *FEBS Lett 509*, 131-134.

82. Labbebois, R. (1990) The ferrochelatase from *Saccharomyces cerevisiae* - sequence, disruption, and expression of its structural gene Hem15, *J Biol Chem 265*, 7278-7283.

83. Hausmann, A., Samans, B., Lill, R., and Mühlenhoff, U. (2008) Cellular and mitochondrial remodeling upon defects in iron-sulfur protein biogenesis, *J Biol Chem 283*, 8318-8330.

84. Leighton, J., and Schatz, G. (1995) An ABC Transporter in the Mitochondrial Inner Membrane Is Required for Normal Growth of Yeast, *EMBO J 14*, 188-195.

85. Kuhnke, G., Neumann, K., Mühlenhoff, U., and Lill, R. (2006) Stimulation of the ATPase activity of the yeast mitochondrial ABC transporter Atm1p by thiol compounds, *Mol Membr Biol 23*, 173-184.

86. Guarente, L., and Mason, T. (1983) Heme regulates transcription of the Cyc1 gene of *S. Cerevisiae* via an upstream activation site, *Cell 32*, 1279-1286.

87. Miao, R., Martinho, M., Morales, J. G., Kim, H., Ellis, E. A., Lill, R., Hendrich, M. P., Münck, E., and Lindahl, P. A. (2008) EPR and Mössbauer spectroscopy of intact mitochondria isolated from Yah1p-depleted *Saccharomyces cerevisiae*, *Biochemistry 47*, 9888-9899.

88. Kaplan, J., Ward, D. M., Crisp, R. J., and Philpott, C. C. (2006) Iron-dependent metabolic remodeling in *S. cerevisiae*, *Biochim Biophys Acta - Mol Cell Res 1763*, 646-651.

89. Hanikenne, M., Motte, P., Wu, M. C. S., Wang, T., Loppes, R., and Matagne, R. F. (2005) A mitochondrial half-size ABC transporter is involved in cadmium tolerance in *Chlamydomonas reinhardtii*, *Plant Cell Environ 28*, 863-873.

90. Csere, P., Lill, R., and Kispal, G. (1998) Identification of a human mitochondrial ABC transporter, the functional orthologue of yeast Atm1p, *FEBS Lett 441*, 266-270.

91. Bekri, S., Kispal, G., Lange, H., Fitzsimons, E., Tolmie, J., Lill, R., and Bishop, D. F. (2000) Human ABC7 transporter: gene structure and mutation causing X-linked sideroblastic anemia with ataxia with disruption of cytosolic iron-sulfur protein maturation, *Blood 96*, 3256-3264.

92. Camaschella, C. (2008) Recent advances in the understanding of inherited sideroblastic anaemia, *Br J Haematol 143*, 27-38.

93. Pondarre, C., Campagna, D. R., Antiochos, B., Sikorski, L., Mulhern, H., and Fleming, M. D. (2007) Abcb7, the gene responsible for X-linked sideroblastic anemia with ataxia, is essential for hematopoiesis, *Blood 109*, 3567-3569.

94. Plattner, H., and Schatz, G. (1969) Promitochondria of anaerobically grown yeast. 3. morphology, *Biochemistry 8*, 339-343.

95. Paltauf, F., and Schatz, G. (1969) Promitochondria of anaerobically grown yeast. 2. lipid composition, *Biochemistry 8*, 335-339.

96. Liu, W. T., and Thorp, H. H. (1993) Bond valence sum analysis of metal-ligand bond lengths in metalloenzymes and model complexes .2. refined distances and other enzymes, *Inorg Chem 32*, 4102-4105.

97. Hassett, R. F., Romeo, A. M., and Kosman, D. J. (1998) Regulation of high affinity iron uptake in the yeast *Saccharomyces cerevisiae* - Role of dioxygen and Fe(II), *J Biol Chem 273*, 7628-7636.

98. Waters, B. M., and Eide, D. J. (2002) Combinatorial control of yeast FET4 gene expression by iron, zinc, and oxygen, *J Biol Chem 277*, 33749-33757.

99. Cavadini, P., Biasiotto, G., Poli, M., Levi, S., Verardi, R., Zanella, I., Derosas, M., Ingrassia, R., Corrado, M., and Arosio, P. (2007) RNA silencing of the mitochondrial ABCB7 transporter in HeLa cells causes an iron-deficient phenotype with mitochondrial iron overload, *Blood 109*, 3552-3559.

100. Halliwell, B. (2009) The wanderings of a free radical, *Free Radic Biol Med 46*, 531-542.

101. Imlay, J. A. (2006) Iron-sulphur clusters and the problem with oxygen, *Mol Microbiol 59*, 1073-1082.

102. Mühlenhoff, U., Richhardt, N., Gerber, J., and Lill, R. (2002) Characterization of iron-sulfur protein assembly in isolated mitochondria - A requirement for ATP, NADH, and reduced iron, *J Biol Chem 277*, 29810-29816.

103. Cambridge Structural Database. *http://www.ccdc.cam.ac.uk/products/csd/*.

104. Wilkinson, E. C., Dong, Y. H., and Que, L. (1994) Modeling hydrolysis at dinuclear iron centers, *J Am Chem Soc 116*, 8394-8395.

105. Schueck, N. D., Woontner, M., and Koeller, D. M. (2001) The role of the mitochondrion in cellular iron homeostasis, *Mitochondrion 1*, 51-60.

106. Burke, M. A., and Ardehali, H. (2007) Mitochondrial ATP-binding cassette proteins, *Transl Res 150*, 73-80.

107. Chen, S., Sanchez-Fernandez, R., Lyver, E. R., Dancis, A., and Rea, P. A. (2007) Functional characterization of AtATM1, AtATM2, and AtATM3, a subfamily of *Arabidopsis* half-molecule ATP-binding cassette transporters implicated in iron homeostasis, *J Biol Chem 282*, 21561-21571.

108. Eide, D., Daviskaplan, S., Jordan, I., Sipe, D., and Kaplan, J. (1992) Regulation of iron uptake in *Saccharomyces cerevisiae* - the ferrireductase and Fe(II) transporter are regulated independently, *J Biol Chem 267*, 20774-20781.

109. Yamaguchi-Iwai, Y., Ueta, R., Fukunaka, A., and Sasaki, R. (2002) Subcellular localization of Aft1 transcription factor responds to iron status in *Saccharomyces cerevisiae*, *J Biol Chem 277*, 18914-18918.

110. Yamaguchiiwai, Y., Dancis, A., and Klausner, R. D. (1995) Aft1 - a mediator of iron-regulated transcriptional control in *Saccharomyces cerevisiae*, *EMBO J 14*, 1231-1239.

111. Li, H. R., Mapolelo, D. T., Dingra, N. N., Naik, S. G., Lees, N. S., Hoffman, B. M., Riggs-Gelasco, P. J., Huynh, B. H., Johnson, M. K., and Outten, C. E. (2009) The yeast iron regulatory proteins Grx3/4 and Fra2 form heterodimeric complexes containing a [2Fe-2S] cluster with cysteinyl and histidyl ligation, *Biochemistry 48*, 9569-9581.

112. Morales, J. G., Holmes-Hampton, G. P., Miao, R., Guo, Y. S., Munck, E., and Lindahl, P. A. (2010) Biophysical characterization of iron in mitochondria isolated from respiring and fermenting yeast, *Biochemistry 49*, 5436-5444.

113. Singh, A., Kaur, N., and Kosman, D. J. (2007) The metalloreductase Fre6p in Fe-Efflux from the yeast vacuole, *J Biol Chem 282*, 28619-28626.

114. Li, L. T., and Kaplan, J. (2004) A mitochondrial-vacuolar signaling pathway in yeast that affects iron and copper metabolism, *J Biol Chem 279*, 33653-33661.

115. Foury, F., and Roganti, T. (2002) Deletion of the mitochondrial carrier genes MRS3 and MRS4 suppresses mitochondrial iron accumulation in a yeast frataxin-deficient strain, *J Biol Chem 277*, 24475-24483.

116. Miao, R., Kim, H., Koppolu, U. M. K., Ellis, E. A., Scott, R. A., and Lindahl, P. A. (2009) Biophysical characterization of the iron in mitochondria from Atm1p-depleted *Saccharomyces cerevisiae*, *Biochemistry 48*, 9556-9568.

117. Rutherford, J. C., Jaron, S., and Winge, D. R. (2003) Aft1p and Aft2p mediate iron-responsive gene expression in yeast through related promoter elements, *J Biol Chem 278*, 27636-27643.

APPENDIX I

Table S1: Mössbauer parameters of various Fe(II) complexes

Component	δ (mm/s)	ΔE_Q (mm/s)	Linewidth (mm/s)
1ST+EGTA (buffer used for reducing mitochondria) 100mM Tris, 0.6 M Sorbitol, 1mM EGTA, 10 mM dithionite, 1 mM ^{57}Fe, pH 8.5	1.34	3.60	0.48
1ST+EGTA without sorbitol 100 mM Tris, 1 mM EGTA, 10 mM dithionite, 1 mM ^{57}Fe, pH 8.5	1.35	3.61	0.38
Fe(II)-phosphate complex 100 mM KH_2PO_4, 10 mM dithionite, 1 mM ^{57}Fe, pH 7.4	1.40	3.00	0.64
Fe(II)-ATP complex 100 mM MOPS[a], 20 mM ATP, 10 mM dithionite, 1 mM ^{57}Fe, pH 7.4	1.39	2.92	0.52
Fe(II)-Tris complex 50 mM Tris, 10 mM dithionite, 1.2 mM Fe^{57}, pH 8.5	1.34	3.05	0.59

[a] MOPS is non-complexing and should not interfere with ATP-Fe(II) binding.

APPENDIX II

Curve fittings of Fe K edge EXAFS to different models.

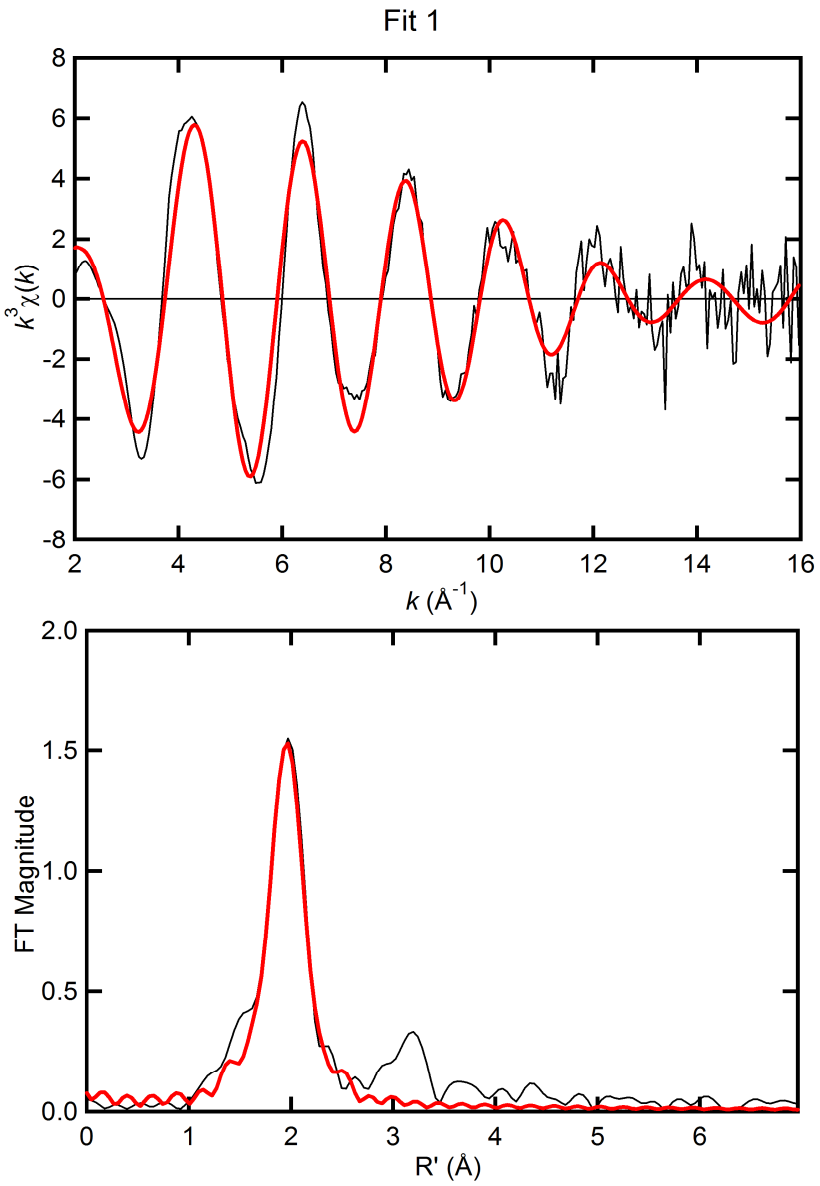

Sample, filename (k range) $\Delta k^3\chi$	Fit	Shell	R_{as} (Å)	σ_{as}^2 (Å^2)	ΔE_0 (eV)	f'[b]	BVS[c]
FMG0B (k = 2 – 16 Å^{-1}) $\Delta k^3\chi$ = 12.64	1	Fe-O_5	1.973	0.0055	-2.92	0.070	2.804

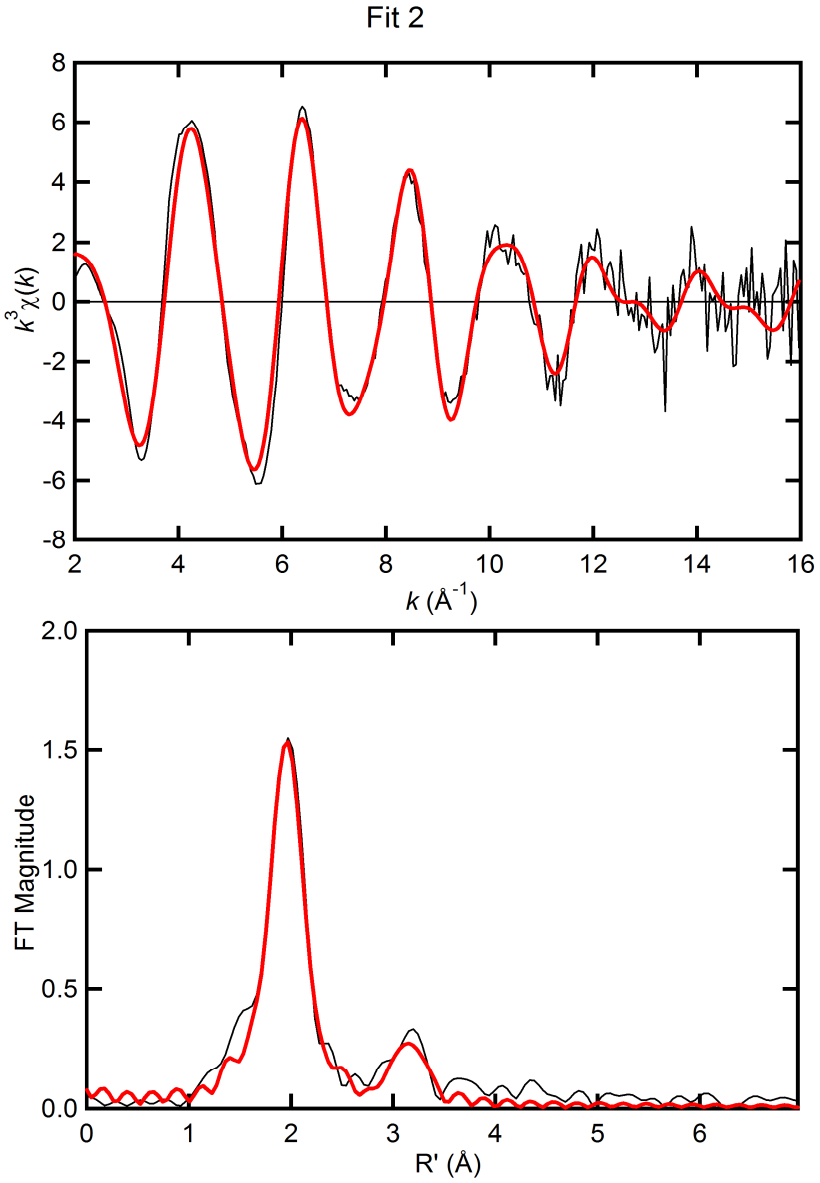

Sample, filename (k range) $\Delta k^3\chi$	Fit	Shell	R_{as} (Å)	σ_{as}^2 (Å^2)	ΔE_0 (eV)	f'[b]	BVS[c]
FMG0B (k = 2 – 16 Å^{-1})	2	Fe-O_5	1.973	0.0055	-2.92	0.058	2.804
$\Delta k^3\chi$ = 12.64		Fe-P_1	3.210	0.0025	[-2.92]		

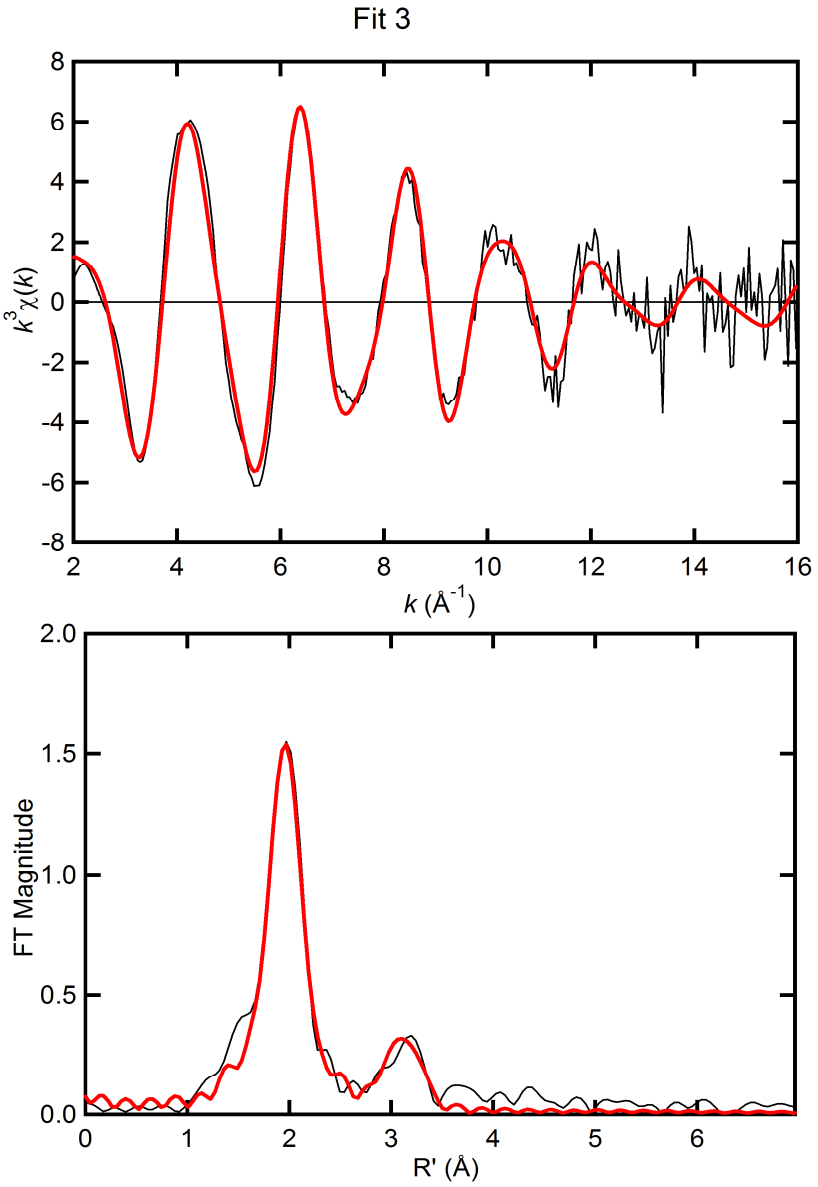

Sample, filename (k range) $\Delta k^3\chi$	Fit	Shell	R_{as} (Å)	σ_{as}^2 (Å^2)	ΔE_0 (eV)	f'[b]	BVS[c]
FMG0B (k = 2 – 16 Å^{-1})	3	Fe-O_5	1.973	0.0055	-2.84	0.057	2.804
$\Delta k^3\chi$ = 12.64		Fe-P_2	3.210	0.0067	[-2.84]		

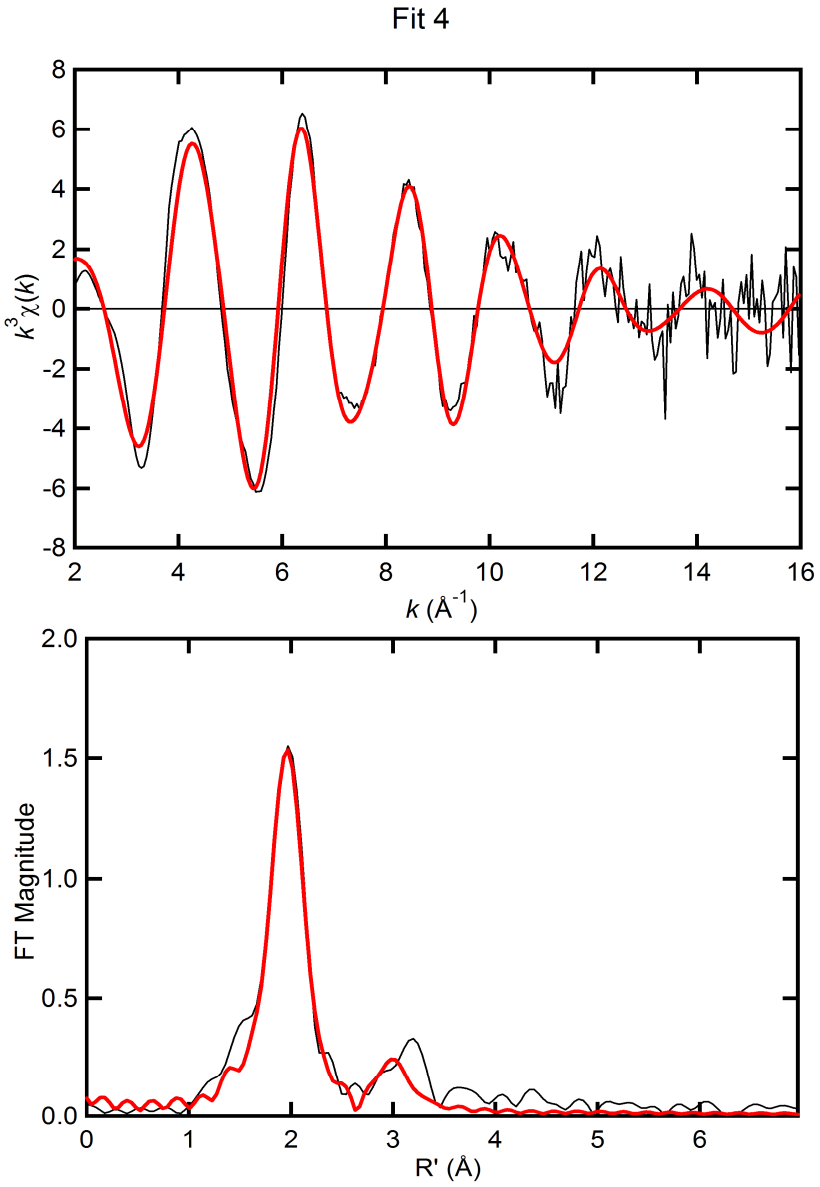

Sample, filename (k range) $\Delta k^3\chi$	Fit	Shell	R_{as} (Å)	σ_{as}^2 (Å^2)	ΔE_0 (eV)	f'[b]	BVS[c]
FMG0B (k = 2 – 16 Å^{-1})	4	Fe-O_5	1.973	0.0055	-2.80	0.064	2.804
$\Delta k^3\chi$ = 12.64		Fe-Fe_1	3.020	0.0105	[-2.80]		

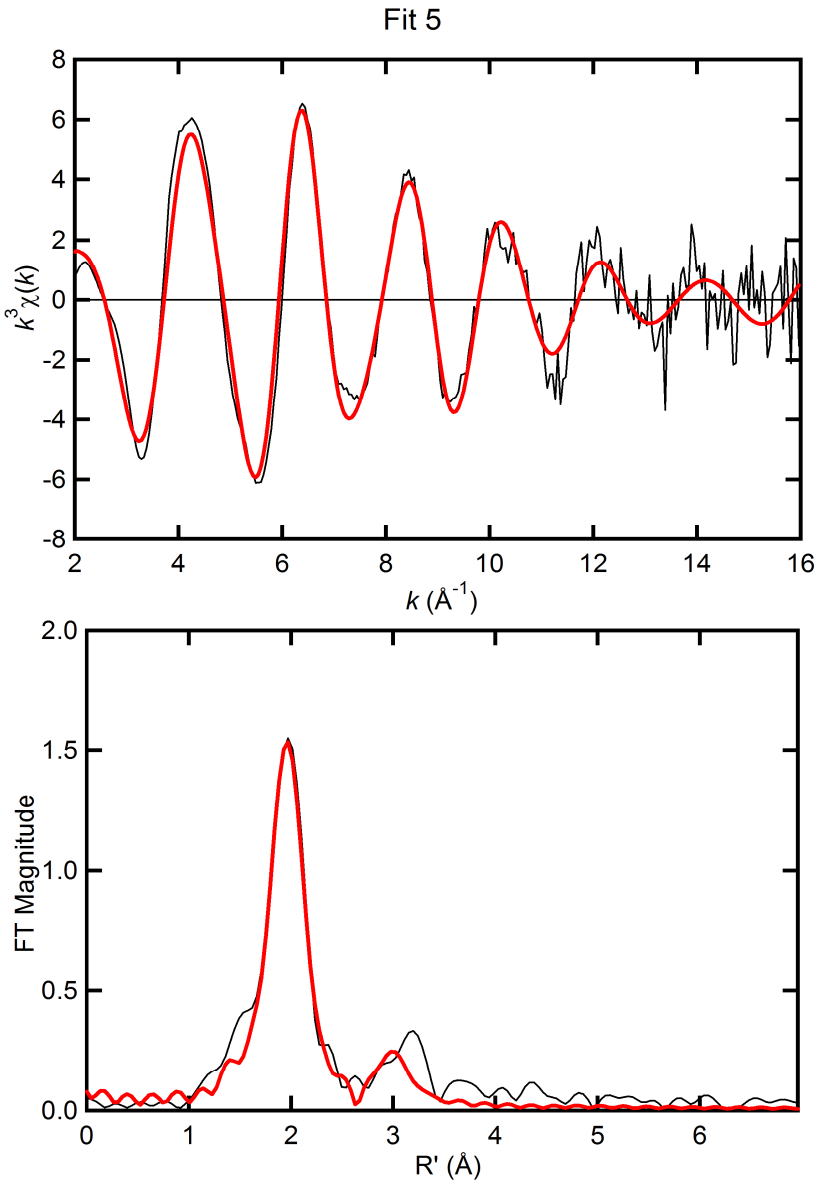

Sample, filename (k range) $\Delta k^3\chi$	Fit	Shell	R_{as} (Å)	σ_{as}^2 (Å^2)	ΔE_0 (eV)	f'[b]	BVS[c]
FMG0B (k = 2 – 16 Å^{-1})	5	Fe-O_5	1.974	0.0055	-2.74	0.062	2.796
$\Delta k^3\chi$ = 12.64		Fe-Fe_2	3.003	0.0163	[-2.74]		

VITA

Ren Miao
c/o Department of Chemistry
Texas A&M University
PO Box 30012
College Station, TX, 77842-3012

EDUCATIONAL BACKGROUND:

2005-2010 Texas A&M University, Ph.D., Chemistry
2002-2005 Nanjing University, M.S., Chemistry
1998-2002 Nanjing University, B.Sc., Chemistry

SELECTED PUBLICATIONS:

1 Miao, R., Kim, H., Koppolu, U. M. K., Ellis, E. A., Scott, R. A., and Lindahl, P. A. (2009) Biophysical characterization of the iron in mitochondria from Atm1p-depleted *Saccharomyces cerevisiae*, *Biochemistry 48*, 9556-9568

2 Miao, R., Martinho, M., Garber-Morales, J., Kim, H., Ellis, E. A., Lill, R., Hendrich, M. P., Münck, E., and Lindahl, P. A. (2008) EPR and Mössbauer spectroscopy of intact mitochondria isolated from Yah1p-depleted *Saccharomyces cerevisiae*, *Biochemistry 47*, 9888-9899

3 Holmes-Hampton, G. P., Miao, R., Garber-Morales, J., Guo, Y., Münck, E., and Lindahl, P. A. (2010) A nonheme high-spin ferrous pool in mitochondria isolated from fermenting *Saccharomyces cerevisiae*, *Biochemistry 49*, 4227-4234

4 Lindahl, P. A., Garber-Morales, J., Miao, R., Holmes-Hampton, G. P. (2009) Isolation of *Saccharomyces cerevisiae* mitochondria for Mössbauer, EPR and electronic absorption spectroscopic analysis, *Methods in Enzymology 456*, 267-285

5 Garber-Morales, J., Holmes-Hampton, G. P., Miao, R., Guo, Y., Münck, E., and Lindahl, P. A. (2010) Characterization of iron in mitochondria isolated from respiring and fermenting yeast, *Biochemistry 49*, 5436-5444